5-2013

The Effects of Physicochemical Properties of CeO2 Nanoparticles on Toxicity to Soil Denitrification Processes

Jessica Dahle
Clemson University, jdahle@clemson.edu

THE EFFECTS OF PHYSICOCHEMICAL PROPERTIES OF CeO_2 NANOPARTICLES ON TOXICITY TO SOIL DENITRIFICATION PROCESSES

A Thesis
Presented to
the Graduate School of
Clemson University

In Partial Fulfillment
of the Requirements for the Degree
Master of Science
Environmental Toxicology

---

by
Jessica Teague Dahle
May 2013

Accepted by:
Dr. Yuji Arai, Committee Chair
Dr. Elizabeth Carraway
Dr. Lisa Bain

ABSTRACT

Due to the rise of nanotechnology in industry, the concentrations of engineered metal oxide nanoparticles being released to the environment are increasing daily. Cerium-based compounds such as nanoparticulate ceria (NP CeO_2) have received much attention in the last several years due to their popular applications (e.g., mischmetal, pharmaceuticals, nanotechnology) in industrial and commercial uses. Like many emerging pollutants, NP CeO_2 is often released to the environment, where its toxicological effects are not well known. Though several environmental exposure pathways have been identified for CeO_2 NPs, a major route of NP introduction to the environment is via biosolids application to agricultural lands. Thus, concerns about the release of NP CeO_2 and its impact on ecosystem health have stimulated many recent toxicological studies. Recent investigations have uncovered the effect of NP CeO_2 at cellular levels showing both protection of cells and severe cellular damage depending on pH, particle size, concentration, and aggregation state. Yet, the toxicological information of NP CeO_2 to aquatic and terrestrial biota remains largely unknown. The studies presented in this thesis identify the impact of NP CeO_2 on soil denitrifying microbial communities and reveal that physical and chemical characteristics including particle size, speciation, concentration, pH, and presence of ligands are key to predicting environmental fate and reactivity of NP CeO_2 in the soil.

A review of the literature in Chapter 1 revealed a widespread lack of toxicological information for soil exposures to NP CeO_2. Soil denitrifying bacteria are a keystone species because they serve an important role in the global nitrogen cycle controlling the atmospheric nitrogen input. Soil denitrifiers are important to this study because the reducing conditions during denitrification could induce phase transformation of Ce(IV) to Ce(III), potentially influencing the toxicity of Ce. Cerium is well known for being the only lanthanide that is thermodynamically stable in both the trivalent and tetravalent state in low temperature geochemical environments. Using well characterized NP $Ce(IV)O_2$ as well as bulk soluble Ce(III), batch denitrification experiments were conducted to evaluate the toxicity of Ce species to the denitrifying community in a Toccoa sandy loam soil. The statistical analysis on the antimicrobial effect on soil denitrifiers was conducted using both steady-state evaluation and zero-order kinetic models in order to compare the toxicity of the Ce(III) species to the NPs. These studies, presented in Chapter 3, show that soluble Ce(III) is far more toxic than $Ce(IV)O_2$ NPs when an equal total concentration of Ce is used, though both species exhibit toxicity to the denitrifiers via statistically significant inhibition of soil denitrification processes. Particle-size dependent toxicity, species-dependent toxicity, and concentration-dependent toxicity were all observed in this study for both the steady-state and the kinetic evaluations.

The possibility of toxicity enhancement and diminishment via dissolution and ligand complexation pathways was investigated thoroughly in Chapter 2. In addition to the

equilibrium and kinetic-based toxicological assessments presented in Chapter 1, dissolution and sorption experiments were performed to gain an overall understanding of Ce biogeochemistry in the terrestrial environment post-release and reveal possible geochemical controls on toxicity. It was shown that dissolution of bioavailable Ce is pH-dependent; dissolution is only detectable at acidic pH values (< pH 5) and increases with increasing acidity. Dissolution of Ce from NP CeO_2 was identified to be almost 100% Ce(III). It was also demonstrated that this dissolution is suppressed by the addition of phosphate ligand, which is largely bioavailable in soils, especially in agricultural lands. This suppression was explained by the strong sorption of phosphate ligand to NP CeO_2. The elimination of bioavailable Ce(III) release from NP CeO_2 by phosphate ligand is likely one of the most important controls on toxicity effects and should be a large consideration in determining the fate and transport of NP CeO_2 in the aquatic and terrestrial environment. It was also demonstrated that both Ce(III) and NP CeO_2 have extremely strong affinity for sorption to soil matter, which could serve as another controlling pathway. Experiments indicated that factors such as reductive transformation of NP CeO_2 in soils and exchangeable Ce(III) impurity in the NPs could contribute to controls on toxicity as well.

In conclusion, the studies presented in this thesis indicate that the toxicity effects of the studied Ce species to soil denitrifiers are strongly affected by physical and chemical characteristics such as speciation, pH, and bioavailable ligands. As the global market for

nanomaterials rapidly expands, so does the need of the scientific community for an understanding of how these influences in environmental fate and reactivity may be key in assessing toxicological risks associated with environmental exposures to NP CeO_2 as well as other engineered metal oxide nanoparticles.

DEDICATION

To my teacher James Alverson, who introduced me to chemistry and the physical sciences; and whose infectious passion for the subjects forever changed my life.

ACKNOWLEDGEMENTS

I would like to express my deep appreciation and gratitude to several people for the contributions and support given to me during my educational journey. First, I would like to thank my advisor, Dr. Yuji Arai, for his encouragement, guidance, and mentorship throughout my studies. His dedication to his students and most of all his patience has inspired and shaped my intellectual growth as a researcher. I also wish to thank my committee members, Dr. Elizabeth Carraway and Dr. Lisa Bain, for their guidance, suggestions, and support.

I would like to thank the people whose experimental assistance helped make my research possible; particularly Dr. Ryan Tappero of the National Synchroton Light Source at Brookhaven National Laboratory and Dr. Brian Powell of the Rich Lab of Environmental Engineering and Earth Sciences at Clemson University. In addition, I would like to thank my lab mates for the impact their continual support and encouragement has made on me.

I wish to thank my family, most especially my parents Bobby and Gina Humphreys, for their unconditional love, support, and patience. I am deeply thankful to them for always pushing me to advance myself personally and academically.

Finally, I must thank my teacher, James Alverson, who is solely responsible for sparking the love of math and science that serves as my driving force. His encouragement and

influence has greatly shaped my life, and without it I would not be the person I am today. My gratitude to him for inspiring my passion for chemistry and deep curiosity about the universe is unending.

TABLE OF CONTENTS

Table of Contents (Continued)

Page

LIST OF TABLES

List of Tables (Continued)

Page

LIST OF FIGURES

List of Figures (Continued)

Page

List of Figures (Continued)

Page

CHAPTER ONE

INTRODUCTION AND LITERATURE REVIEW

1.1 Introduction to Cerium

The Discovery of Cerium

Cerium (Ce), a member of the lanthanide series of metals on the periodic table, is the most abundant of the rare-earth metals found in the earth's crust (Hedrick, 2004). Cerium comprises about 0.0046% of the earth's crust by weight, occurring at average concentrations of around 50 mg kg^{-1}. Cerium and other lanthanide metals naturally occur in an array of minerals in the environment including allanite ($(Ca,Ce)(Al_2Fe^{2+})(Si_2O_7)(SiO_4)O(OH)$), bastnäsite ($(Ce,La)(CO_3)F$), cerite ($(Ce,Ca)_9(Fe,Mg)(SiO_4)_3(HSiO_4)_4(OH)_3$), monazite ($(Ce,La,Nd,Th)(PO_4)$), and euxenite ($(Y,Ca,Ce,U,Th)(Nb,Ti,Ta)_2O_6$); however, of these minerals, only bastnäsite and monazite serve as important sources commercially. The discovery of cerium in the form of its oxide (CeO_2) was first reported in 1803 by scientists in both Sweden and Germany. This oxide was given the name "ceria" by discoverer Jons Jacob Berzelius in Sweden; this name is still used today (Weeks, 1932). Berzelius named the compound after the dwarf planet Ceres, which itself was named for the Roman goddess of agriculture.

In the last several years, Ce based compounds have received much attention because of their popular applications (e.g., mischmetal, pharmaceuticals, nanotechnology) in

industrial and commercial uses. This review chapter summarizes an overview of cerium chemistry, geologic occurrence, current and historic uses, toxicological data, and environmental fate.

1.2 Cerium Chemistry

Chemical and Physical Properties

Elemental cerium is a soft, ductile metal that is silver in color and a strong oxidizer in the presence of air (O'Neil, 2001). It exhibits a melting point of 798 °C and a boiling point of 3443 °C. The density of cerium is 6.770 g cm^{-3} and it is found to decompose slowly in cold water and rapidly in hot water. Cerium is also soluble in dilute, mineral acids. The atomic weight of cerium is 140.116 g mol^{-1}. Elemental cerium exhibits paramagnetism and a face-centered cubic crystal structure. Cerium metal tarnishes slowly in air and burns readily at 150 °C to form CeO_2 (Lide, 2005).

Elemental cerium exhibits complex low temperature behavior. Four allotropic modifications are thought to exist: γ cerium, β cerium, α cerium, and δ cerium. Cerium existing at room temperature and atmospheric pressure is known as γ cerium. Upon cooling to -16 °C, γ cerium begins to change to β cerium. The remaining γ cerium begins to change to α cerium when cooled to -172 °C, and the transformation is complete at a temperature of -269 °C. The transformation from γ cerium α cerium results in a 17% volume collapse of the face-centered cubic cerium structure (Moore, Belhadi, et al.,

2011). The δ form of cerium exists above 726 °C. At atmospheric pressure, liquid cerium is more dense than its solid form at the melting point (Stassis, Gould, et al., 1979).

Nearly 89% of naturally occurring Ce consists of four observationally stable isotopes (^{136}Ce, ^{138}Ce, ^{140}Ce, ^{142}Ce). With the exception of ^{140}Ce (the most abundant isotope at 88.5% natural occurrence), these isotopes are expected to undergo double beta decay. Radioisotopes of Ce also occur; three radioisotopes exist with considerable half-lives (^{144}Ce, $t_{1/2}$ ~ 285 d, ^{139}Ce, $t_{1/2}$ ~ 138 d, ^{141}Ce, $t_{1/2}$ ~ 33 d). Other radioisotopes of Ce consist of species with half-lives of less than 4 d; these radioisotopes are largely comprised of species with half-lives under 10 min. Thirty-five isotopes of cerium are currently known; less than half of all possible isotopes have been observed (Ginepro, Snyder, et al., 2009). The first isotopes of cerium discovered were found concurrently in 1925 in Cambridge, England by Francis William Aston. The isotopes ^{140}Ce and ^{142}Ce were discovered together via mass spectroscopy of cerium bromide (Aston, 1925).

Cerium (electronic configuration: [Xe] $4f^1$ $5d^1$ $6s^2$) exhibits a variable electronic structure which sets it apart from other lanthanides. The energy of the inner 4f level is nearly equal to the energy of outer or valence electrons. Since a very small amount of energy is necessary to change the relative occupancy (of these electronic levels), dual valence states of 3^+ and 4^+ occur in cerium (Patnaik, 2003).

In low temperature geochemical environments, cerium commonly exists in both the trivalent cerous state (Ce^{3+}) and the tetravalent ceric state (Ce^{4+}). (Cerium also occasionally exhibits a 2^+ oxidation state; this rare valency is found in CeH_2, CeI_2, and CeS.) Cerium exhibits a unique stability in the tetravalent state; other lanthanides are only stable in the trivalent state. This feature allows for easy separation of cerium from other rare-earth elements through oxidation (forming CeO_2) followed by variable solubility filtration. Cerium salts can be extracted via liquid-liquid extraction of rare-earth cerium-containing solutions; cerium metal can be obtained via the reaction of CeF_3 with excess air at approximately 900 °C or via fused-salt electrolysis of a mixture of cerium chlorides and fluorides (Stassis, Gould, et al., 1979). Two common methods exist for the preparation of metallic cerium. Metallothermic reduction of CeF_3 with calcium is used to produce high-purity cerium; electrolysis of molten $CeCl_3$ or other cerous halides yields a less pure product (Oxford, 2011).

Aqueous Chemistry of Cerium

The formation of Ce aqueous complexes and solubility products involve the binding of a metal center (like Ce^{3+} or Ce^{4+}) to a ligand to form a coordination complex. These interactions are normally soft-soft or hard-hard as described below by the hard and soft acid and base (HSAB) theory. Hard-hard affinity can be described as mostly ionic while soft-soft affinity is covalency-driven. Characterizing the electronegativity, size, and charge properties of cerium is key to understanding its association chemistry since the affinity of metals for ligands is controlled by these three factors.

The HSAB theory can be used to explain the tendency of Ce to quickly and strongly bond with ligands such as phosphates and hydroxides over species like sulfates and hydrides. Using HSAB, species are first characterized as a Lewis acid or Lewis base, then identified as a "hard" or "soft" species. Hard species exhibit a small atomic/ionic radius, high oxidation state, and are only weakly polarizable while soft species are large in size, have low oxidation states, and are strongly polarizable. Common examples of hard ions include Fe^{3+} and OH^-; Ag^+ and SH^- are some well-known soft ions. Hard acids have a strong affinity for hard bases while soft acids "prefer" to bond with soft bases. Intermediate ions (such as Pb^{2+}) that have no strong preference for hard over soft bonding partners also exist.

While HSAB theory serves mainly as a qualitative identification system, a quantitative definition for chemical hardness has also been developed such that the chemical hardness of an acid or base can be described in electron volts (eV). The harder the acid or base, the higher the eV value; values tend to be much higher for acids than for bases. Cerium is classified as a hard acid based on its small size, high oxidation state (most commonly 3^+ or 4^+) and weak polarizability; thus, it is most likely to bond with hard bases such as phosphate, hydroxide, and carbonate.

Cerium oxide nanoparticles are most often noted for their catalytic ability, which is largely affected by redox behavior and is known to be directly dependent on cerium's redox state. The nanoparticles are often largely composed of Ce(III) (up to 60% in some

cases) as well as Ce(IV); the more Ce(IV) in the nanoparticles, the stronger the catalase mimetic activity (Pirmohamed, Dowding, et al., 2010). Another study has shown that a decrease in the $3^+/4^+$ ratio directly correlates with a loss of superoxide dismutase (SOD)mimetic activity (Heckert, Karakoti, et al., 2008). Clearly, redox state plays a large role in determining the characteristics and behavior of cerium oxide nanoparticles.

To better understand the aqueous chemistry of Ce, it is also important to discuss the chemistry of 4^+, 3^+, and 2^+ lanthanides in aqueous systems. The primary hydration numbers of most lanthanides are 8 and 9; salts with common anions frequently contain $Ln(H_2O)_9^{3+}$ with tri-capped trigonal prismatic geometry. Cerium's normal coordination/ hydration number of 6 is quite uncommon among lanthanides. However, as previously stated, cerium does exhibit other coordination numbers as well; for example, in the case of nitrates, $Ce(NO_3)_5^{2-}$ features a 10-coordinate bicapped dodecahedron structure and $Ce(NO_3)_6^{3-}$ features a 12-coordinate icosahedron structure. Other common O-donor chelating ligands that form complexes with Ce and other lanthanides include oxalate, citrate, tartrate, and beta-diketonates. Classic bidentate complexes, macrocyclic ligands (crown ethers), and weak coordination by halides are also key to the solution chemistry of 3^+ lanthanides (Evans, 2000).

In terms of 4^+ lanthanides, cerium is the only tetravalent lanthanide with significant coordination and/or aqueous chemistry. Lower oxidation states occur in bromides and iodides while higher oxidation states of lanthanides tend to occur in fluorides and oxides.

The E° value of Ce(IV)aq/Ce(III)aq = 1.72 V; the E° value of other lanthanides is ~ 2.9 V. This value is largely dependent on hydrolysis and complexation properties of Ce including pH. In solution, hydrolysis to $Ce(OH)^{3+}$ occurs, then polymerization which leads to precipitation of yellow gelatinous hydrated cerium(IV) oxide (Evans, 2000). Values for $3^+/2^+$ lanthanide reduction potentials can be found in Table 1.1.

Properties of the 2^+ lanthanides are very closely related to the electronic properties of the alkaline earths. In particular, Eu is often linked to barium(II); the two species exhibit similar salt solubilities (insoluble sulfates, soluble hydroxides), similar behavior in ammonia, similar coordination chemistry (not extensive, hard ligands), but extremely different redox chemistry. The solution chemistry of 2^+ lanthanides is essentially confined to samarium(II) (Sm(II)), Eu(II), and ytterbium(II) (Yb(II)). All three are prepared via electrolytic reduction of the 3^+ form. The colors of the 2^+ products vary largely; Sm(II) features a blood red hue, Eu(II) is colorless, and Yb(II) appears yellow. The 2^+ states are readily oxidized by air but $Eu(II)_{(aq)}$ is easily handled. Sm(II) and Yb(II) reduce water and are susceptible to oxidation by their water of crystallization. More characteristics of these 2^+ lanthanides include Eu(II)'s stability in the dark and the dissolution of Eu(II) and Yb(II) in liquid ammonia to give intense blue, highly reducing solutions which decompose on standing, precipitating the amide (Eu- or Yb-$(NH_2)_2$) (Evans, 2000).

Solubility and Redox Properties of Ce Compounds

The solubility properties of cerium compounds such as these listed above vary greatly. Solubility constants for Ce(III) and Ce(IV) bound to common ligands including hard bases like phosphate are listed in Table 1.2**.** Cerium phosphate forms quickly and is extremely insoluble; the species will precipitate out of solution almost immediately upon formation. Cerium(IV) hydroxide exhibits similar properties. However, cerium(III) hydroxide is many orders of magnitude more soluble than cerium(IV) hydroxide. Among cerium species, even cerium(III) hydroxide is not regarded as particularly soluble. Among the most soluble species are cerium(III) chloride and cerium(III) nitrate. Cerium(III) selenite and cerium(III) sulfate are also relatively soluble.

Analogues of Ce, or lanthanides and possibly actinides that react similarly and become more soluble as the valence state becomes more reduced, are difficult to identify since the tetravalent state is only characteristic of cerium. Since it is not possible to identify "true" analogues, instead comparisons must be made across systems with $3^+/2^+$ systems (such as that of europium) instead of cerium's $4^+/3^+$ system. Cerium has the notable characteristic of becoming more soluble as its coordination state becomes more reduced. Other lanthanides are only stable at 3^+ with the exception of europium (Eu), which may be the only "good" analogue of Ce in the lanthanides. Eu usually assumes a 3^+ oxidation state, but 2^+ is also very common. The solubility constant of Eu(III) hydroxide at 20 °C is 1.538×10^{-5}, which is similar in magnitude but overall less soluble than Ce(III) hydroxide. The solubility constant of Eu(III) sulfate at 20 °C is 2.56, which is also much less soluble than

Ce(III) sulfate. The sulfate of Eu(II) is highly insoluble in water. Other compounds of Eu(III) exhibit similar properties such that the compounds of Eu(III) tend to be far less soluble than the same compounds of Ce(III). Like the Eu(III) compounds discussed above, most lanthanides existing in the 3^+ state are not very soluble in water. The lighter lanthanides are more soluble when paired with oxalates, double sulfates, or double nitrates, while the heavier lanthanides are more soluble with basic nitrates.

The HSAB theory discussed earlier is key in understanding how the redox properties of CeO_2 NPs come into play when metals such as cerium are introduced to the soil. Metals in the soil are Lewis acids and ligands in the soil are Lewis bases. Each of the ligands important to soil geochemistry can be classified using the HSAB theory. Distribution of hardness and softness for potential donor atoms for ligands in the periodic table is illustrated in Figure 1.1. Hard bases commonly found in soil and soil minerals include water, OH^-, F^-, PO_4^{3-}, SO_4^{2-}, Cl^-, CO_3^{2-}, ClO_4^-, and NO_3^-. Several soft bases include I^-, CN-, CO, S^{2-}, sulfhydryl (R-SH), and $R\text{-}S^-$. Likewise, the soil also include hard acids such as H^+, Li^+, Na^+, K^+, Be^{2+}, Mg^{2+}, Ca^{2+}, Sr^{2+}, Fe^{3+}, Al^{3+}, and Se^{3+}, as well as soft acids such as Ag^+, Au^+, Tl^+, Cu^+, Zn^{2+}, Cd^{2+}, Hg^{2+}, and Sn^{2+}. Hard acids associate with hard bases through ionic (electrostatic) bonds and soft acids associate with soft bases through covalent bonds. The preference of hard metals (acids) for ligands falls from the strongest preference for the hardest donors (like nitrate, water, and hydroxide) to the softest donors (like sulfide, bromide, and iodide). In additional to simple inorganic ligands, natural

organic matter in the soil also has hard (carboxylic and phenolic) and soft (sulfur-containing) sites (Sparks, 2003).

As noted earlier, the variable electronic structure of cerium (electronic configuration: [Xe] $4f^1$ $5d^1$ $6s^2$) truly sets it apart from other lanthanides. The energy of the inner 4f level is nearly equal to the energy of outer (valence) electrons. Since a very small amount of energy is necessary to change the relative occupancy (of these electronic levels), dual valence states of +3 and +4 occur in cerium (Patnaik, 2003). As previously stated, in low temperature geochemical environments, cerium commonly exists in both the trivalent cerous state (Ce^{3+}) and the tetravalent ceric state (Ce^{4+}). The electronegativity value of Ce is 1.12 on the Pauling scale; the electronegativity values of other common species found in soils are shown in Table 1.3. Cerium has three ionization energies. Its first ionization energy is 534.4 kJ mol^{-1} (Ce^{4+}), its second ionization energy is 1050 kJ mol^{-1} (Ce^{3+}), and its third ionization energy is 1949 kJ mol^{-1} (Ce^{2+}).

As mentioned previously, the electronegativity values identified in Table 1.3 are on the Pauling scale. Pauling's rules are a set of steps that allow identification of coordination properties of any compound. The first of Pauling's five rules can be used to calculate the coordination number of compounds by dividing the cationic radius by the anionic radius of the compound and then classifying that ratio into a distinct interval identifying it's coordination number and crystal structure (Sparks, 2003). The coordination number of cerium(IV) oxide (perhaps the most environmentally relevant Ce species) is 6, so the

crystal exhibits an octahedron structure (such as the Al-O octahedral sheets well known in clay minerals). Cerium(III) oxide also features a coordination number of 6 and the same octahedron crystal structure. However, cerium compounds are not always coordinated octahedrally; for the compounds CeF_6^{2-} (via fluoride bridging) and $CeCl_6^{2-}$, the coordination number is 8. The 4^+ charge also stabilizes halogeno-complexes like CeF_8^{4-} (Evans, 2000).

1.3. Geochemical Occurrence

Cerium is found in a variety of mineral classes, primarily including carbonates, phosphates, silicates, oxides and hydroxides. Main sources of industrial cerium include the carbonate mineral bastnäsite and the phosphate mineral monazite. These key cerium minerals and other lanthanide associated minerals are discussed in detail below and tables documenting members of the rare earth carbonates (Table 1.4), phosphates (Table 1.5), silicates (Table 1.6), oxides and hydroxides (Table 1.7) can be found at the end of this chapter.

Carbonates

Carbonates, the largest group of Ce-containing minerals, feature three oxygen atoms in a triangular arrangement about a central carbon. This CO_3 group exhibits a 2^- overall charge and is the essential featured structure of carbonate minerals. The oxygen ions are much more strongly bonded to the central C^{4+} cation than to any other cations in the

structure and an oxygen ion in one CO_3^{2-} group cannot be shared with another CO_3^{2-} group. Therefore, the structure of all carbonates is based on CO_3^{2-} groups that are laterally bonded through various cations. Additional OH^- or other anionic components may also appear in carbonate minerals.(Nesse, 2000).

As stated earlier, monazite and bastnäsite are presently the two most important sources of cerium and other rare-earth metals (such as thorium). Bastnäsite is of particular importance to the discovery of cerium. Bastnäsite is a carbonate-fluoride mineral which was first described by Hisinger in 1838 when ore samples from the Bastnäs mine in Vastmanland, Sweden were analyzed, leading to the discovery of multiple minerals and chemical elements by Berzelius, Hisinger, and Carl Gustav Mosander. It was many years before the chemistry of these ores was fully understood; while cerium was discovered in 1803, lanthanum was not described until 1839. Bastnäsite was one of the new minerals discovered from the ore; Hisinger, who owned the Bastnäs mine, gave the mineral its name (bastnäsit) when he described it in 1838.

Mining for bastnäsite began at the Mountain Pass rare earth mine in San Bernardino, California with the discovery of a new class of rare earth deposit: a large carbonaceous mineral deposit containing significant amounts of bastnäsite. The major composition of bastnäsite consisted of approximately 49% cerium, 33% lanthanum, 12% neodymium with some praseodymium, samarium and gadolinium. Bastnäsite minerals also exhibited at least twice the europium concentrations of a typical monazite. As more carbonatite

deposits were discovered in Africa and China, mining processes were developed and these deposits became vital to the global lanthanide supply. From 1965 to the mid 1980s, the Mountain Pass site emerged as the world's major source of lanthanides. Currently China plays a leading role in the global rare earth supply (as high as 97%); the Bayan Obo Mining District is the source of the majority of the world's lanthanides (Lide, 2005).

Phosphates

Though relatively few cerium phosphate minerals exist, they are very important to consider when identifying sources of cerium. The key structural element of phosphate minerals is the tetrahedral PO_4^{3-} groups. These anionic tetrahedron groups feature a cationic P^{5+} center surrounded by oxygen anions at the corners of a tetrahedron. As with carbonate groups, the oxygen anions are more strongly bonded to the central atom, P^{5+}, than to other cations in the mineral, so the PO_4^{3-} groups are the fundamental structural units of phosphate minerals. Phosphate minerals are not as widespread and well-known as silicate or carbonate minerals; only a few phosphate minerals are common. Turquoise is perhaps the best-known phosphate mineral, often used in jewelry; however, it is actually a fairly rare mineral. (Nesse, 2000).

Until bastnäsite began to be processed around 1965, the phosphate mineral monazite, which usually forms small reddish-brown crystals, was the only significant commercial source of lanthanides such as cerium and thorium. Monazite is most often found in placer deposits, which are mineral accumulations often in the form of black sedimentary

rocks. Monazite is fairly dense (about 4.6 to 5.7 g cm^{-3}), a property consistent with that of most black sand mineral constituents (such as zircon and cassiterite). Monazite exhibits a range of hardness of 5.0 to 5.5 Mohs. Placer deposits in India are particularly rich in monazite as well as deposits in Australia, Madagascar and South Africa (Anthony)

One of the major reasons that bastnäsite came to replace monazite in lanthanide production in the 1960's is the radioactive nature of monazite, which contains thorium and produces radioactive daughter products. This radioactive character is useful because it allows monazite to be used as a geological dating tool; thorium was also considered as a potential nuclear fuel in the 1960s. When this interest began to decline, bastnäsite was an attractive replacement option because it contained much lower concentrations of thorium than were found in monazite. Monazite is also more difficult to store than bastnäsite since it must be kept away from any mineral samples that are sensitive to radiation.

Monazite and bastnäsite minerals are both broken down into further classifications based on relative elemental composition. Four types of monazite and three types of bastnäsite are commonly referred to in geological literature. Monazite occurs in monazite-(Ce) (meaning cerium is the most predominant rare earth metal in monazite-(Ce)), monazite-(La), monazite-(Nd), and monazite-(Pr); bastnäsite occurs in bastnäsite-(Ce), bastnäsite-(La), and bastnäsite-(Y). The –(Ce) compositions constitute most of the bastnäsite and monazite minerals in existence (Anthony).

Silicates

Silicates comprise the most abundant group of minerals in the earth's crust. Silicates play an extremely important role in soils. They are the basic building block of all silicate minerals in the silicon tetrahedral which exhibits Si^{4+} with a net tetrahedron charge of 4^-. Minerals in this class can be categorized as orthosilicates, disilicates, ring silicates, chain silicates, sheet silicates, and framework silicates (Nesse, 2000).

Though bastnäsite and monazite serve as the two largest commercial sources of cerium, a significant amount of cerium (as well as thorium, uranium, and chromium) is also found in the silicate mineral allanite. Like bastnäsite and monazite, allanite can be broken down into three further classifications: allanite-(Ce), allanite-(La), and allanite-(Y). Allanite is a useful source of rare earth elements because it can contain up to 20% rare earths by composition. The high concentrations of thorium and other radioactive elements in the mineral lead to radiative degradation and structure disruption of allanite and surrounding minerals. The distribution of allanite minerals is widespread with large, high-quality deposits occurring in Greenland (where allanite was discovered), Sweden, Norway, Finland, and Russia. Allanite has hardness values ranging from 5.5 – 6 Mohs and is found mainly in metamorphic sedimentary and felsic igneous rocks. Allanite is also commonly referred to as orthite.

Oxides and Hydroxides

Oxide minerals feature one or more metal cations combined with oxygen. Since oxide structures are normally based on systematic oxygen anion packing (often cubic or hexagonal close packed), most oxide minerals exhibit very high symmetry. The tetrahedral and octahedral sites between regularly packed anions are occupied by metal cations. Although it may seem counterintuitive, most oxygen in the geological environment does not occur in oxide minerals; the abundance of silicon in the environment for most geographical areas keeps most oxygen tied up in silicate minerals. Oxide minerals exhibit a wide variety of structural forms, including X_2O (cuprite, ice), XO (periclase, zincite), XY_2O_4 (magnetite, chromite, spinel, chrysoberyl), X_2O_3 (hematite, corundum, ilmenite), and XO_2 (rutile, cassiterite, pyrolusite, uraninite), where X is a metal cation (Nesse, 2000).

The hydroxides are another class of very common minerals. Many hydroxide minerals are formed by weathering and hydration of other minerals. For this reason, hydroxides normally occur as fine-grained aggregates mixed with other minerals (including clays) produced by the same processes rather than alone. Hydroxide minerals are used to describe other minerals in this way; brucite and gibbsite are significant hydroxides that are commonly used as a starting point for describing layer silicates. Their structures (OH^- anions arranged in planes) allow for useful classification of other, co-occurring materials (Nesse, 2000).

Of the few oxides and hydroxides that contribute to commercial cerium sources, euxenite is the most significant despite its low composition percent of cerium (around 4%). Unlike allanite, monazite, and bastnäsite, euxenite exists almost entirely in the euxenite-(Y) form, featuring yttrium as its major component instead of cerium. Like allanite, euxite also exhibits radiation damage to itself and nearby minerals due to high radioactive content. With hardness values varying between 5.5 and 6.5 Mohs, euxenite features comparable to slightly higher hardness than its other cerium-containing counterparts, allanite, monazite, and bastnäsite. Euxenite occurs along with monazite in black sands as well as in granite pegmatites. Euxenite is found primarily in Norway, where it was discovered, as well as in Russia, Brazil, Madagascar, Canada, and the US. Euxenite functions as an ore for many of the other rare earth elements contained in the mineral as well (Anthony)

As discussed earlier, Ce is commonly present with other lanthanides and metals forming phosphate and carbonate minerals. The heterogeneity of natural minerals makes the isolation process of pure Ce extremely difficult. Some ores are directly used for metallurgical purposes. Other Ce enriched ores undergo the purification process prior to industrial and commercial uses. The separation of Ce from natural minerals is conducted via oxidation and variable solubility based filtration steps.

In general, the mineral ores are leached with sulfuric acid and then titrated with sodium hydroxide to remove thorium precipitates. This step is followed by precipitation with

oxalate to remove to most of rare earth elements (e.g., Ce, La, Th, Nd) as insoluble oxalate forms. These oxalates undergo annealing/oxidation process to produce lanthanide (tri-and tetra-valent state) oxides. Acidification of these mixed oxides by nitric acid makes all of the lanthanide (III) oxides soluble except for $Ce(IV)(OH)_4$. Insoluble cerium(IV) hydroxides are separated through the filtration process (Abreu and Morais, 2010, Patnaik, 2003). Once the purity of Ce is improved from the mixed lanthanide/metal oars, a variety of Ce compounds are synthesized for commercial and industrial applications. The historic and current uses of Ce compounds are discussed below.

1.4. Historical and Current Uses

Drugs and Pharmaceuticals

Cerium compounds have recorded uses in drugs and pharmaceuticals as early as the mid nineteenth century. In 1854, cerium nitrate was first reported to relieve vomiting. Cerium(III) oxalate was administered for many following decades for anti-vomiting effects in cases of sea sickness, gastrointestinal and neurological disorders, and especially in pregnant women. Cerium(III) oxalate was used as an antiemetic until the mid 1950s when it was replaced by the antihistamine meclizine which is still in use today (Jakupec, Unfried, et al., 2005).

Trivalent cerium exhibits similar size and bonding properties to Ca^{2+}, an extremely biologically important cation. Ce^{3+} can replace Ca^{2+} in biomolecules due to their similar

ionic radius, thus Ce^{3+} compounds strongly exhibit the ability to act as anticoagulant, or anti-clotting, agents. Several of the lanthanides, including cerium, are well-known for their anticoagulant properties and have been employed as antithrombic drugs (Jakupec, Unfried, et al., 2005).

Cerium compounds are also known in particular for their uses in topical burn treatments due to their bacteriostatic and bactericidal effects. By the end of the nineteenth century, cerium compounds were used in both human and veterinary medicine; most commonly used were cerium(III) acetate and cerium(III) stearate treatments. Later, studies confirmed the antiseptic effects of cerium(III) chloride, cerium(III) nitrate, and cerium(IV) sulfate and demonstrated particular subsceptibility of both gram-negative and gram-positive bacteria (which tend to coat burn wounds) to their effects (Jakupec, Unfried, et al., 2005). Cerium(III) nitrate in particular is a widely used treatment for burn wounds, exhibiting nearly a 50% reduction in death rate for patients with life-threatening burns when compared to patients who were administered silver nitrate treatments (Monafo, Tandon, et al., 1976).

Mischmetal

While commercial applications of cerium are numerous, it is most commonly used in the form of mischmetal for metallurgical purposes. Mischmetal is an alloy of rare earth metals in various naturally occurring proportions; a typical composition includes approximately 50% cerium and 25% lanthanum, as well as small amounts of neodymium

and praseodymium. Mischmetal reacts with impurities found in metals to form solid compounds, thereby reducing the effect of these impurities on the properties of the metal. Mischmetal is used in steel manufacturing to improve shape control, reduce hot shortness, and increase heat and oxidation resistance. The addition of mischmetal to cast iron improves ductility, toughness, and microstructure. Mischmetal is also commonly used in the "flint" ignition devices of lighters and torches; it is blended with iron oxide and magnesium oxide to form ferrocerium, a hard enough material to give good sparks (Kilbourn, 2003).

The high scavenging capacity of cerium with respect to oxygen and sulfur can be used to improve oxidative resistance of alloys; however, apart from mischmetal, elemental cerium is not used for a wide variety of applications due to its high reactivity and immediate oxidation potential. However, a wide array of applications arises from the combination of cerium with other materials to produce assorted cerium compounds. Chemical companies began selling cerium compounds in the late 1950s for use primarily in mischmetal; since then, the use of cerium compounds for multiple applications has become widespread. Many of these applications are discussed below.

Organic Synthesis Starting Materials

Cerous chloride ($CeCl_3$) is used as a catalyst in Friedel-Crafts alkylation reactions as well as a starting material for the preparation of other cerium salts. Anhydrous cerous chloride is generally prepared via thermal treatment of heptahydrate $CeCl_3 \cdot 7H_2O$ under

vacuum (Dimitrov, Kostova, et al., 1996, Edelmann, 1997). This hydroscopic solid is mostly important in organic syntheses such as Luche reduction and alkylation of ketones for which organolithium reagents cannot be used (Johnson and Tait, 1987, Paquette, 1999).

Scintillation Counters

Cerous bromide is a component of interest in scintillation counters, which measure ionizing radiation. Aqueous solutions of cerous bromide ($CeBr_3 \cdot H_2O$) can be prepared by reacting $Ce_2(CO_3)_3 \cdot H_2O$ with HBr. Heating the product with NH_4Br followed by sublimation of residual NH_4Br will allow dehydration, yielding in white hygroscopic cerous bromide ($CeBr_3$) solids. Well-ordered single crystals may be produced using standard crystal growth methods such as the Bridgman or Czochralski methods (Higgins, Churilov, et al., 2008). Cerous bromide-doped lanthanum bromide single crystals exhibit superior scintillation properties; applications for $CeBr_3$ include security, medical imaging, and geophysics detectors (van Loef, Dorenbos, et al., 2001). Undoped single crystals of $CeBr_3$ have also shown promise as gamma ray scintillation detectors in similar fields as well as oil exploration and environmental remediation.

Other

Other selected cerium compounds also have many applications of interest. Hydrated cerium oxide is used in the production of cerium salts and cerium oxide (Kilbourn, 2003).

Cerous fluoride (CeF_3) is used in the preparation of cerium metals as well as in arc carbons to increase brilliance (Kilbourn, 2003).

Nanoparticles: Catalysts, Glass Additives, and Fuel Additives

Cerium in its nanoparticulate form is especially important when considering applications of cerium. Nanoparticles (NPs) are substances that are less than 100 nm in all three dimensions. Although the applications of compounds such as $CeCl_3$ and $CeBr_3$ discussed above are important, cerium compounds are best known for their uses in catalysts, fuel cells, glass (de)pigmentations, and fuel additives. All of these applications are based on the same compound: cerium dioxide (CeO_2), or ceria. Ceria, which can be in the form of a white, pale-yellow, or brownish power depending on its purity, is by far the most widely commercially used cerium compound.

Ceria exhibits cubic crystal structure akin to a fluorite type structure. The fluorite structure of CeO_2 allows for rapid diffusion of oxygen as a function of the number of oxygen vacancies since the oxygen atoms in the crystal are all in plane with one another. As the number of vacancies increases, the oxygen is more easily able to move around in the crystal, allowing reduction and oxidation of molecules or co-catalysts on the crystal's surface. Ceria is used as a co-catalyst in a number of reactions, including the water-gas shift and steam reforming of ethanol or diesel fuel into hydrogen gas and carbon dioxide. It is useful in the Fischer-Tropsch reactions and in selected oxidations (Reinhardt and Winkler, 2002).

Gadolinium, samarium, or platinum doped CeO_2 are useful materials for solid oxide fuel cells due to relatively high oxygen ion conductivity at intermediate temperatures (Kilbourn, 2003). Substituting a fraction of the CeO_2 with these elements is a way to increase ionic conductivity and create a better electrolyte since this introduces oxygen vacancies in the crystal without adding electronic charge carriers. A large amount of oxygen vacancies within the electrolyte will form on the anode (reducing) side of the fuel cell. Some of the ceric oxide is reduced to cerous oxide under these conditions; this transformation increases the electronic conductivity of the material. The lattice constant of CeO_2 increases under reducing conditions as well as with decreasing nanocrystal size as a result of this reduction of the cerium cation from Ce(IV) to Ce(III). This increase compensates for the formation of oxygen vacancies, resulting in an increase in the fuel cell efficiency.

Nanoparticulate CeO_2 has a particularly high oxygen storage capacity which, when coupled with its ease of transition between trivalent and tetravalent states and its high natural abundance, makes it an excellent choice as a catalyst. Nanoparticulate CeO_2 is most often used in catalytic converters in automobiles due to its non-stoichiometric ability to give up oxygen without decomposing. Ceria can release or take in oxygen in the exhaust stream of a combustion engine depending on its ambient partial pressure of oxygen. Via this mechanism, NO_x emissions are reduced and carbon monoxide is converted to carbon dioxide. Ceria is relatively inexpensive but its addition has been

shown to provide substantial reductions in the amount of platinum catalyst needed for complete oxidation of NO_x and other harmful incomplete combustion products (Reinhardt and Winkler, 2002). Fuel burns more cleanly upon addition of CeO_2, resulting in less air pollution. It has also been characterized as a useful catalyst in systems including oxidation of volatile organic carbon (Abbasi, Haghighi, et al., 2011) and toluene (Abbasi, Haghighi, et al., 2011), ozonation of organic compounds (Orge, Orfao, et al., 2011), and water-gas shift reactions(Yuan, Idakiev, et al., 2008). More properties and applications of nanoparticulate CeO_2 are discussed below at length.

Because CeO_2 is remarkably insoluble in water and in dilute acid (Kilbourn, 2003) it is commonly used as an abrasive; the powder is used in the grinding/polishing of other materials. For many years, it was used for polishing specialized glass (telescope mirrors, for example) (Hedrick and Sinha, 1994). It is also used in heat-resistant alloy coatings and in ceramic coatings.

Potential Future Applications of Cerium (III) Oxides: the Ceria Cycle for Hydrogen Production and Catalysts

While cerium dioxide exhibits a particularly large wide variety of uses, another useful oxide of cerium must be mentioned as well: cerium(III) oxide. Cerium dioxide and cerium(III) oxide (or cerous oxide) are combined in an extremely useful process known as the ceria cycle. The ceria cycle serves as a pathway of great interest for hydrogen production. This thermochemical process splits water into hydrogen and oxygen and is

carried out in two steps: the endothermic dissolution of CeO_2 followed by the exothermic hydrolysis of Ce_2O_3. In the first step, CeO_2 is thermally dissociated in an inert gas atmosphere into Ce_2O_3 and $0.5O_2$. This reaction takes place at 2000 °C and 100-200 mbar of pressure. During the second step, Ce_2O_3 is reduced at 400-600 °C in a fixed-bed reactor with water to produce $2CeO_2$ and H_2. The high reactivity of Ce_2O_3 with steam draws the main interest in this cycle; however, a major drawback lies in the partial vaporization of CeO_2 during the reduction step at reduced pressure. Water is the only material input to the ceria cycle and heat is the only energy input, making the ceria thermochemical cycle "a promising process for hydrogen production." The ceria cycle is also sometimes referred to as the cerium oxide cycle (Chueh, Falter, et al., 2010).

Cerium(III) oxide has several uses in addition to water splitting. The compound is used mainly in cooking appliances; it is incorporated into the walls of modern ovens to prevent the build-up of cooking residues and act as a catalyst for the oven's self-cleaning mode. Ce_2O_3 has also shown promise as a new petroleum-cracking catalyst (Abanades and Flamant, 2006).

1.5. Toxicity of Cerium

Nanoparticle Toxicity

Nanoparticle toxicity is only well-understood for a small range of nanomaterials since the field is relatively new. Nanoparticles tend to sorb more than their bulk counterparts and

exhibit multiple exposure routes for biological organisms including ingestion, inhalation, absorption/ adsorption onto surfaces, uptake across epithelia, and multiple other pathways. Multiple toxicity mechanisms have been reported for a variety of NPs, from physical damage to ROS generation to dissolution of toxic ions/species.

Two major considerations for NP toxicity are size effects and capping agents. Nanoparticle toxicity characteristically exhibits size-dependent effects. For a large variety of NPs including species such as NP silver, silicon dioxide, and titanium dioxide it has been demonstrated that smaller sizes (and thus larger reactivities) lead to heightened toxicity effects across biological systems. Nanoparticles tend to exhibit much higher toxicities than their bulk counterparts; this tendency is especially exaggerated in bacteria due to the NP's higher affinity for attachment to bacterial cell walls (Jiang, Mashayekhi, et al., 2009) that could potentially perturb the electron transfer reaction and respiration. Capping agents (or lack thereof) also play a large part in NP toxicity. Capping agents stabilize NPs by covering a large portion of their surface area and preventing aggregation as well as introducing multiple functionalities such as enhanced solubility effects. Polymers are popular capping agents along with other organic materials (Lead and Smith, 2009).

As mentioned previously, the large surface area of NPs results in their ability to often exhibit much higher reactivity and interaction potential with biological systems. Several potential risks are postulated: 1) the production of reactive oxygen species (ROS) and 2)

the release of reaction products (e.g., ionic metal(loid)s via dissolution). A primary mechanism of NP toxicity is the ability to generate ROS such as free radicals (Lead and Smith, 2009). Reactive oxygen species contain unpaired valence electrons which yield extremely high chemical reactivity and the ability to induce severe damage to cells, including DNA and RNA damage, oxidations of lipids and proteins, and enzyme (cytochrome P) deactivation. A wide array of NPs has been found to induce ROS production; among these are carbon nanotubes (CNTs), fullerenes (C_{60}), and titanium dioxide NPs (TiO_2). The release of metal ions from quantum dots (e.g., CdSe) and nanosilver can be highly toxic to bacterial cells, (Liu, Sonshine, et al., 2010, Lubick, 2008) as well as organic coatings of NPs (Hoshino, Fujioka, et al., 2004, Mahendra, Zhu, et al., 2008).

Conflicting Views: Are CeO_2 NPs Harmful or Helpful?

Recent research on NP CeO_2 has reported conflicting results regarding toxic effects: NP CeO_2 has been reported to act as both an antioxidant and a ROS production-inducing agent across multiple biological pathways.

Many researchers have reported that CeO_2 NPs utilize their ability to scavenge free radical species in order to act as an antioxidant. Ceria NPs have been reported by multiple researchers to act as a mimetic of superoxide dismutase, the main catalyst that reduces the production of and damage caused by ROS to mammalian cells by transforming superoxide into oxygen and hydrogen peroxide. They have been shown to inhibit cellular

aging (Karakoti, Singh, et al., 2010) and have even demonstrated the ability to increase the lifespan of brain cell cultures (Rzigalinski, Bailey, et al., 2003). Their properties have been implied in the prevention of retinal disorders leading to blindness (Chen, Patil, et al., 2008). However, other research seems to tell a different story about CeO_2 NPs. Multiple researchers report strikingly opposite effects. Ceria NPs have been reported to induce and catalyze the generation of ROS across multiple biological systems. Nanoceria has been reported to lead to decreased lifespans in roundworms (Zhang, He, et al., 2011), cause liver damage in rats (Nalabotu, Kolli, et al., 2011), and exhibit moderate toxicity to various human muscle tissues including lung tissue (Park, Choi, et al., 2008).

An important consideration is the tendency of NP toxicity to exhibit size dependent effects. The effects of pH and ionic strength of systems also play a large role in the contrasting reported effects of nanoparticulate CeO_2. These toxicity factors will be discussed in detail in further sections.

Introduction to the Environment

The environmental fate of cerium is dependent on its applications and uses. As previously stated, the use of cerium as a diesel fuel additive coupled with a particulate filter drastically decreases particulate matter emissions in automobile exhaust, up to 90% by weight (Institute, 2001). Some cerium escaping in the emissions could accumulate in the soil. Cerium is also introduced to the environment via wastewater discharge from ceramic manufacturing plants and recycling of sewage sludge to soils. Most notably, cerium

levels in the soil can be attributed to agricultural amendments via application of biosolids from wastewater treatment plants.

When particles are not efficiently removed from wastewater streams, they can become a long-term problem for the environment. A study by Limbach, et al. has shown that, for a model wastewater treatment plant, a significant fraction of cerium oxide nanoparticles were able to escape the clearing system and avoid adsorption to clearing sludge. The surface charge of the NPs was found to play a key role in the stabilization against clearance, leading to detectable concentrations of CeO_2 NPs up to 6 wt % in the model plant's exit stream (Limbach, Bereiter, et al., 2008). Thus, industrial wastewaters serve as a significant environmental source of CeO_2 NP exposure.

Another notable source of exposure is road runoff after CeO_2 NPs are deposited in soils from exhaust catalysts. Since about 95% of CeO_2 NPs undergo biosolid accumulation in wastewater treatment plants, CeO_2 discharge into the aquatic environment is fairly limited as compared to accumulation levels in the soil (Limbach, Bereiter, et al., 2008). Exhaust particulate matter exists as very fine particles, normally < 1 μm, leading to extremely diffuse pollution through air exposure (Moller, Morteani, et al., 2003). Since CeO_2 NP partitioning is the most significant in wastewater treatment plant biosolids, it follows that Ce pollution largely occurs after the amendment of agricultural soil via application of wastewater biosolids. As in the case of many other metal NPs such as TiO_2, ZnO, and Ag NPs (Gottschalk, Sonderer, et al., 2009), it is believed that biosolids

application to agricultural soils serves as one of the largest environmental exposure pathways for CeO_2 NPs (Cornelis, Ryan, et al., 2011); thus, this pathway needs to be studied extensively and monitored in order to control Ce enrichment and transformation in natural soils and waters.

Unfortunately, due to the relativeness newness of discovery of NP chemistry as a field, the fate and transport of NPs in general are not well-understood. Much work has been done with TiO_2 and silver NPs but most NPs have not been studied as extensively. Nanoparticulate CeO_2, while greatly useful for a wide variety of applications, is not without the risks and hazards associated with NPs in general. The toxicity of cerium NPs and cerium in general is discussed in depth in Chapter 3.

Cerium oxide NPs are of great interest biologically for many reasons, including their many starkly contrasting toxicity effects in different conditions. As previously mentioned, increased Ce(III):Ce(IV) ratios result in increased SOD mimetic activity and thus further inactivation of superoxide free radicals(Heckert, Karakoti, et al., 2008). Unlike SOD, CeO_2 NPs can directly react with hydroxyl radicals (Karakoti, Monteiro-Riviere, et al., 2008) as well as superoxide radicals in order to inactivate both short-lived and stable radicals (Babu, Velez, et al., 2007). A study by Ivanov, et al. showed that the rate of inactivation of stable radicals by CeO_2 NPs is dependent directly upon particle size and that smaller particle sizes result in increased rates of radical inactivation (Ivanov, Shcherbakov, et al., 2010). Discussed below are effects of CeO_2 NP exposure to

biological organisms including plants, bacteria/aquatic organisms, and mammals, as well as the recorded and possible effects of these exposures.

Exposure to Biological Organisms and Effects: Plants

Once in the soil, $CeO_{2(s)}$ tends to accumulate in suspensions due to natural organic matter reducing its aggregation capability. Cerium in the soil may be absorbed into vegetation or contaminate water. Cerium has been shown to be likely to enter the produce food chain through take-up by alfalfa, corn, tomato, and cucumber (Lopez-Moreno, de la Rosa, et al., 2010). Nanoparticles tend to accumulate on root surface of plants, decreasing hydraulic conductivity and often inhibiting root growth. Nanoceria has been reported to significantly reduce germination rates in corn, tomato, and cucumber; the same study reported enhanced root growth in cucumber and corn species after introduction of CeO_2 NPs, but reduced root growth in tomato and alfalfa plants. Shoot elongation was also found to be enhanced in all four species (Lopez-Moreno, de la Rosa, et al., 2010). Another study displayed differing effects, finding that CeO_2 NPs did not affect root growth in radish, tomato, lettuce, wheat, rape, cabbage, and cucumber plants (Ma, Kuang, et al., 2010). Concentration-dependent absorption by plant roots has been observed, but most of the NPs are instead adsorbed to the surface of the root; entry into the roots is limited and very difficult (Zhang, He, et al., 2011).

Nanoceria particles have also been shown to protect anthocyanins in grapes from ROS by inhibiting oxidative degradation in neutral and alkaline solutions. However, in acidic

solutions, no inhibitory effects were observed after exposure of the anthocyanins to NP CeO_2 (Ivanov, Usatenko, et al., 2009). Similar pH-dependent effects have been demonstrated across a variety of plants and other organisms.

Nanoceria particles have also shown translocation ability; that is, the capability to cross biological barriers such as the blood-brain barrier. When applied to maize leaves, NP CeO_2 was demonstrated to either adsorb to the leaf surface in agglomerated form (larger particles) or penetrate the leaf and become incorporated into the leaf structure (smaller particles). However, in plants cultivated after airborne exposure to NP CeO_2, newly grown leaves exhibited no translocation. This lack of evidence for translocation is important since maize is a major agricultural crop and knowledge of NP ability to translocate into newly grown, non-exposed plants is needed. Nanoparticles most commonly enter plants via root uptake or air exchange into the leaves. Nanoparticles larger than 1.1 μm were found by the study to be unable to penetrate the leaf surface and enter the leaves (Birbaum, Brogioli, et al., 2010).

Bacteria and Aquatic Organisms

Nanoparticle effects on both gram-positive and gram-negative bacteria have been studied extensively. Nanoceria was shown to exhibit size-dependent and concentration-dependent inhibition of both *Escherichia coli* and *Bacillus subtilis*; it is suggested that the NPs do not penetrate the bacterial cells, but rather adsorb to them, inducing deleterious effects. The same study found that NP CeO_2 induced no inhibitory effects on the growth

of *Shewanella oneidensis*, demonstrating that bacterial responses to NPs and interactions between the two vary greatly among bacterial species (Pelletier, Suresh, et al., 2010).

After exposure to NP CeO_2 in pure water for 24 hours, the aquatic cyanobacteria *Anabaena* CPB4337 exhibited toxicity values ranging from 0.27 to 6.3 mg L^{-1} and the aquatic green alga *Pseudokirchneriella subcapitata* exhibited values from 2.4 – 29.6 mg L^{-1}. Ceria NPs were shown to cause membrane disruption and severe damage to the cells of both organisms though uptake of the NPs by the cells was not indicated. As in the case of *E. coli* and *B. subtilis* mentioned above, the *Anabaena* cells became coated with adsorbed NP CeO_2. It is suspected that cell wall and membrane disruption was likely the cause of cell damage rather than oxidative activity (Rodea-Palomares, Boltes, et al., 2011). From these and other similar studies, it remains unclear whether nanoceria toxicity can be largely attributed to cellular adsorption or if uptake of the particles lends to intracellular effects, especially because negatively charged particles should be repelled by the large negatively charged domains of cell membranes. Importantly, it has been demonstrated that CeO_2 NP toxicity in *P. subcapitata* is largely influenced by pH, ionic strength and amounts of natural organic matter. Increasing pH and ionic strength levels result in increased NP aggregation (and therefore increased toxicity), while higher levels of natural organic matter sharply lowered average NP aggregate sizes, severely decreasing aggregation from particle sizes of ~ 4,500 nm to sizes of 100-200 nm. Adsorption of the particles to natural organic matter reduced their bioavailability and thus

the resultant toxicity of the particles to *P. subcapitata* (Van Hoecke, De Schamphelaere, et al., 2011).

Aquatic organisms are perhaps some of the least well-studied systems for NP CeO_2 toxicity, largely due to the undocumented nature of nanoparticulate species presence in waterways. In a study on the effect of NPs on microbial communities in wastewater treatment plants, it was found that CeO_2 NPs exhibited stronger inhibitory effects on biogas production by the microbes than TiO_2, gold, or silver NPs (Garcia, Delgado, et al., 2012). After release into the waterway, NP CeO_2 is far more likely to partition into aquatic plants and sediment than to stay in the water, but some aquatic species such as algae and fish are still at risk and the possible toxicity and effects of NP CeO_2 uptake in these organisms must be investigated (Lu, Zhang, et al., 2010). When CeO_2 NPs do stay in the sediment, concentrations tend to be locally high due to the adsorption and aggregation tendencies of NPs, as stated earlier.

Caenorhabditis elegans is a commonly-studied soil nematode that serves as an important aquatic indicator. Ceria NPs have been shown to induce size-dependent toxicity effect on the survival and fertility of *C. elegans*; while all CeO_2 NP exposure sizes in one study led to decreased reproductive ability and increased fatality, the smaller NPs had a markedly more toxic effect than the larger NPs. This effect was also observed for TiO_2 NPs (Roh, Park, et al., 2010). Another study on nanoceria exposure in *C. elegans* indicated that NP CeO_2 could lead to reduced lifespans via catalysis of ROS generation and subsequent

oxidative damage. The study observed a 12% reduction in mean lifespan even at the lowest NP CeO_2 exposure level of 1 nM (Zhang, He, et al., 2011). Cellular function was inhibited in another study on *P. subcapitata* by 10.3 mg L^{-1} of NP CeO_2, leading to damaged cell membranes and growth inhibition (Rogers, Franklin, et al., 2010). Yet another study found that only 7.6 mg L^{-1} NP CeO_2 was required to inhibit algal growth in *P. subcapitata*, while the two crustaceans *Daphnia magna* and *Thamnocephalus platyurus* suffered no acute toxicity effects from NP CeO_2 concentrations, even ranging up to 5,000 mg L^{-1} (Hoecke, Quik, et al., 2009).

Another study on cytotoxicity of CeO_2 NPs to gram-negative *E. coli* confirmed that the NPs were adsorbed in large amounts on the outer membrane. The NPs are positively charged at neutral pH values, meaning they are subject to a strong electrostatic attractive force toward bacterial outer membranes such as that of *E. coli*. Close contact was reported between the NPs and *E. coli*, indicating that oxidative response may have been responsible for the observed toxicity, which was significant after the adsorption of the NPs and their reduction from Ce(IV) to Ce(III). The survival rate of *E. coli* was reduced to half for a 5 ppm exposure to CeO_2 (Thill, Zeyons, et al., 2006). This study as well as other investigations have found that cytotoxicity of CeO_2 NPs for *E. coli* can be reversed by changing the exposure media, indicating that surface charge density is largely responsible for NP CeO_2 cytotoxic effects (He, Kuang, et al., 2012).

It is known that CeO_2 nanocrystals are positively charged under acidic and neutral conditions (below pzc at pH = 8.0) while negatively charged under more basic conditions (above pH = 8.0). Nanoceria crystals aggregate strongly at pH values near the pzc across multiple medias, resulting in increased hydrodynamic radii; decreases in hydrodynamic radii occur at higher pH values when the surface charge of the crystals becomes reversed. Since the pzc is around neutral pH values, NP CeO_2 crystals aggregate at the same pH values that optimize the growth of bacteria.

Larger-scale organisms should also be considered when evaluating the ecotoxicological effects of CeO_2 NPs. In a study exposing multiple nanoscale metal oxides (zinc oxide, cerium dioxide, and titanium dioxide) to zebrafish (*Danio rerio*) and rainbow trout (*Oncorhynchus mykiss*) both via water and via diet, the oxide NPs were largely not found to be able to penetrate the fish cell barriers. The zinc, cerium, and titanium content was measured in the gill, liver, skin, brain, but, blood, and kidneys of the two fish species and only two areas of significant NP uptake were observed. Ceria NP uptake was discovered in the liver of the zebrafish exposed via water and ionic titanium was detected in the gut of the trout exposed via diet. It is likely that this inability of the metal oxide NPs, including CeO_2, was due to limited bioavailability caused by accumulation of large aggregates (up to 3 μm) in the aqueous exposure route (Johnston, Scown, et al., 2010).

Mammals

Mammals are among the lesser-studied organisms for CeO_2 NP toxicity effects; unlike the widespread variety of plants, bacteria, and aquatic organisms investigated, the only mammal cell lines that have been evaluated for NP CeO_2 toxicity currently include those of rodents and humans. Ceria NPs have been demonstrated to be neuroprotective in mouse hippocampal brain slices, indicating that the NPs could be useful as therapeutic agents for strokes due to reduced ischemic cell death (Estevez, Pritchard, et al., 2011). Another study of rodent cell line HT22 verified that CeO_2 NPs (as well as yttrium NPs) prevent oxidative stress to cells and are neuroprotective (Schubert, Dargusch, et al., 2006). However, it has also been shown that a single CeO_2 NP exposure leads to reduced liver weight, hepatocyte enlargement, reduced albumin levels, and diminished sodium-potassium ratios in male Sprague-Dawley rats (Nalabotu, Kolli, et al., 2011).

Ceria NPs have demonstrated a range of activity in human cells as well. Unlike bacterial and algal cells, effective uptake of CeO_2 NPs by human cells has been demonstrated repeatedly. It has been shown that CeO_2 NPs modulate the brain-derived neurotrophic factor (BDNF) pathway in human Alzheimer's disease models in order to trigger neuronal survival (D'Angelo, Santucci, et al., 2009). The NPs have been shown to exhibit toxicity to bronchial epithelial cells due to ROS production (Xia, Kovochich, et al., 2008), although another study showing the same results for bronchial epithelial cells also found no toxic effects for human brain cells and rat cardiomyocytes (Park, Choi, et al., 2008). Another study exhibited low to moderate toxicity of CeO_2 NPs to human

alveolar epithelial and macrophage cell lines (Lanone, Rogerieux, et al., 2009). In a study comparing CeO_2 to Al_2O_3 and ZnO NPs, CeO_2 NPs were found to induce membrane damage and inhibit colony formation to differing degrees across human lung epithelial cells, carcinoma cells, and normal cell lines. The CeO_2 NPs did not demonstrate notable adverse effects on cell proliferation and viability; they were shown to be much less toxic than ZnO in terms of cell viability, proliferation, colony formation, and membrane integrity, but more toxic than Al_2O_3 even after long-term exposure (Kim, Baek, et al., 2010).

As previously stated, the results of studies across similar cell lines are not always in agreement. Ceria NPs have been reported to both induce and prevent oxidative stress in a variety of organisms. Studies have shown that existing levels of CeO_2 in the environment are far "lower than the estimated no effect dose for chronic human exposure" (Park, Choi, et al., 2008), leading to the assertion by some that NP CeO_2, along with a variety of other NPs, may not exhibit any environmental effects at all (Rodea-Palomares, Boltes, et al., 2011). However, until the ecotoxicological effects of NP CeO_2 are well-known, studies must continue to investigate the generation, transport, uptake, and toxicity mechanisms of these potentially harmful materials.

Mechanisms of Toxicity

Unfortunately, little literature exists revealing possible toxicity mechanisms of CeO_2 NPs (or their large amounts of Ce^{3+} impurity) to denitrifying bacteria. However, many studies

exist detailing the effects of the NPs on other bacteria; from these studies, conclusions can be drawn about several likely toxico-mechanistic pathways of CeO_2 NPs in denitrifiers.

As previously mentioned, ceria NPs have best been studied for *E. coli* cells. A study by Thill, et al. found that large amounts of CeO_2 NPs are able to be adsorbed to the outer membrane of *E. coli* and that the speciation of the Ce following adsorption was significantly different. Post-adsorption, the ratio of Ce(IV):Ce(III) decreased sharply, indicating reduction of the Ce species was taking place at the cell surface. They also found significant cytotoxicity was associated with the adsorption of the NPs and their concurrent reduction at the cell surface. When coupled with the resulting cytotoxic effects, the fact that the reduction of the NPs always occurred at the cell surface revealed that surface adsorption of the NPs is associated with oxidative stress in the bacterial cells. Furthermore, they observed a lack of difference in toxicity after 1 h and 5 h of exposure, which supports rapid biological reductive mechanisms after NP adsorption to the cell membrane (Thill, Zeyons, et al., 2006).

Ceria nanoparticles have also been shown to exhibit surface-charge dependent cytotoxicity in *E. coli*. In normal saline media, the (positively-charged) NPs caused destabilization upon contact with the outer membrane as well as loss of viability and increased ROS production. However, in the presence of phosphate-buffered saline, the amount of contact with the outer membrane was greatly reduced; thus, the destabilization

was far less and no cytotoxic effects or ROS production was observed (He, Kuang, et al., 2012). The surface charge density is extremely closely related to the cytotoxic effects of CeO_2 NPs and is perhaps one of the most important considerations when evaluating the NPs for cytotoxicity to other organisms as well. It was also demonstrated that CeO_2 NPs exhibit more antibacterial activity than bulk CeO_2. In another similar study, it was confirmed that direct contact of the NPs with the surface (outer membrane) of the *E. coli* bacterial cells induced an increase in intracellular ROS levels (Kuang, He, et al., 2011). Other studies have also supported the idea that adsorption of CeO_2 NPs to bacterial cells is the cause of cytotoxic effects, rather than penetration of the cells. In another study demonstrating inhibited cell growth of *E. coli* and *B. subtilis* by CeO_2 NPs, STEM imaging was used to find that the NPs quickly adsorb to the bacterial cells but are unlikely to actually penetrate them. The study also found that the NPs aggregated fairly strongly (Pelletier, Suresh, et al., 2010). The results of the imaging from this study are in agreement with the earlier mentioned study suggesting that NP adsorption was responsible for cytotoxic effects, rather than penetration (Thill, Zeyons, et al., 2006).

Though extensive literature is not available on the mechanism of CeO_2 NP toxicity to denitrifying bacteria, it is likely that the mechanism is similar to those discussed for *E. coli* and other bacteria: the NPs undergo aggregation and adsorb to the surface of the bacterial cells, but do not penetrate the cells. The direct contact between the cell surface and the NPs results in reduction of Ce species, thus inducing oxidative stress in the bacterial cells, leading to increased ROS production. This is the best mechanism that can

currently be postulated for cytotoxicity of CeO_2 NPs. However, a discussion of ceria cytotoxicity would not be complete without also considering the large amount of Ce^{3+} impurity that is also inherent in the NPs (some manufacturers have reported up to 55% Ce^{3+} impurity). It is likely that the Ce^{3+} impurities in the NP could also play a large role in any observed cytotoxic effects. Another possible pathway of cytotoxicity that has been far less studied is that of Ce^{3+} as an ATPase inhibitor. Several of the lanthanides have been identified as ATPase inhibitors (Gruner, Sehrt, et al., 1992, Palasz and Czekaj, 2000) that are capable of inhibiting phagocytosis in neutrophil granulocytes (white blood cells) (Gruner, Sehrt, et al., 1992) and thus inhibit the release of histamine. Lanthanides work so efficiently as ATPase inhibitors due to their ionic radii, which are extremely similar to that of Ca^{2+}. In particular, Ce^{3+} is able to substitute for Ca^{2+} extremely well (Jakupec, Unfried, et al., 2005). This calcium-swapping feature is the foundation of cytophysiological effects of the lanthanides. It is postulated that the isomorphic capabilities of the lanthanide ions allow them to replace Ca(II) in the binding sites of nucleases, thus interrupting activation and preventing growth metabolism of bacteria (Balusamy, Kandhasamy, et al., 2012). In humans and animal cells, trivalent lanthanide ions block calcium channels and affect numerous enzymes very potently (Palasz and Czekaj, 2000).

The effects of Ce^{3+} specifically as a Ca^{2+} ATPase inhibitor have not been studied thoroughly; however, the strong ability of other lanthanides (with less ability to easily substitute for Ca^{2+} than Ce^{3+} has) leads to the conclusion that another important cytotoxic

pathway for Ce^{3+} could definitely be that of Ca^{2+} ATPase inhibition, as well as ATPase inhibition in general. Along with their Ce^{3+} impurities, CeO_2 NPs also tend to have large lanthanide impurities which could lend to further ATPase inhibition and cytotoxicity. Other trivalent lanthanides have been shown to block calineurin and regulate release and transport mechanisms for synaptic transmitters, as well as block membrane receptors like glutamate receptors and GABA (Palasz and Czekaj, 2000).

In conclusion, though the cytotoxic mechanism of CeO_2 NPs (or Ce^{3+}) has not been directly identified for denitrifying bacteria, a large amount of studies have been performed identifying the mechanisms in other bacterial organisms. A review of the literature on cytotoxic effects of CeO_2 NPs and ionic Ce^{3+} leads to two main conclusions as to the possible mechanism of CeO_2 NP toxicity in denitrifiers:

1) Exposure to the NPs results in enhanced ROS production via oxidative stress induced by NP adsorption to outer membrane of the bacterial cell; or
2) Cytotoxicity occurs as a result of ATPase (specifically, Ca^{2+} ATPase) inhibitor activity by Ce^{3+} and other lanthanide impurities in the NPs.

1.6 Research Hypotheses

A cerium compound of particular interest is nanoparticulate ceria, also known as cerium oxide (CeO_2). By far, cerium oxide nanoparticles (CeO_2 NPs) are the most widely commercially used cerium compound. It has been reported that global nanomaterial demands will increase by 20% per year and one estimate indicates that the global market for pure nanomaterials is expected to grow to $20.5 billion by 2015 (Palmberg and Tuomo, 2006). As the production of CeO_2 NP increases, so does the usage in the industry and consumer markets, posing questions about the fate of NPs in environment. A study by Limbach, et al. has shown that a significant fraction (~ 95%) of CeO_2 NPs accumulated in sewage sludge at wastewater treatment plants, and CeO_2 discharge into the aquatic environment was fairly limited as compared to accumulation levels in the soil (Limbach, Bereiter, et al., 2008). Thus, application of sludge to agricultural land serves as a significant environmental source of CeO_2 NP exposure to the terrestrial environment.

In the last decade, the scientific community has begun to uncover the effect of CeO_2 NPs on ecosystem health through toxicological studies of plants, bacteria, aquatic organisms, and mammals. However, the research findings are often difficult to extrapolate to natural aquatic and terrestrial systems since the majority of studies do not consider the effect of natural geochemical conditions on the CeO_2 NP reactivity (e.g., solubility and chemical speciation). In low-temperature geochemical environments, CeO_2 NPs are likely to react with ligands (e.g., protons, inorganic and organic acids) and/or partition into geomedia,

resulting in changes in chemical speciation. One should expect that these geochemical reactions could alter the toxicity of CeO_2 NPs as particulates or as dissolution products (e.g., $Ce(III)_{(aq)}$).

Based on the research questions above, the following two hypotheses are formulated:

- Hypothesis 1 (H1): Exposure to CeO_2 NPs can cause toxicity effects to soil denitrifying bacteria.
- Hypothesis 2 (H2): Effects of CeO_2 NP toxicity on the soil denitrification process are controlled by physicochemical factors and geochemical conditions (size, concentration, valence state ratio of Ce(III)/Ce(IV), pH, ligand concentration) which can alter the surface properties of CeO_2 NPs.

The soil denitrifying process was chosen because 1) the anaerobic system which facilitates the denitrification process is suited to study the toxicity of reduced Ce species (i.e., Ce(III)), 2) it is also ideal to study the response of soil microbial community since recent studies have indicated that land application of biosolids to agricultural soils may be a major exposure pathway (Limbach, Bereiter, et al., 2008), and 3) it serves an important role in water treatment systems and in the global N cycle in soil/water environments where CeO_2 NPs could have an impact. In addition to being one of the key players in the global nitrogen cycle, the denitrification process is also localized as an instrumental process for operations such as wetland remediations and wastewater treatment plants. Denitrifying bacteria are used to remove nitrogen from municipal

wastewater, sewage, and industrial wastes; they are also used in wetlands (Bachand and Horne, 2000) and riparian zones (Martin, Kaushik, et al., 1999) for removal of excess nitrate caused by the application of fertilizer to residential and agricultural land (Mulvaney, Khan, et al., 1997).

1.7 Research Objectives and Tasks

The objective of this study is to expand the scientific community's current knowledge of CeO_2 NP toxicity to heterogeneous systems by studying the impact of geochemical reactions on CeO_2 NP toxicity to the soil denitrification process. The following two major tasks are planned to test the hypotheses above: Task 1: Assessing the effect of geochemical conditions (pH, phosphate ligand) on the physicochemical properties of CeO_2 NPs, and Task 2: Investigating the effect of physicochemical properties (e.g., particle size, concentration, pH, ligand concentration) of CeO_2 NPs on the soil denitrifying process.

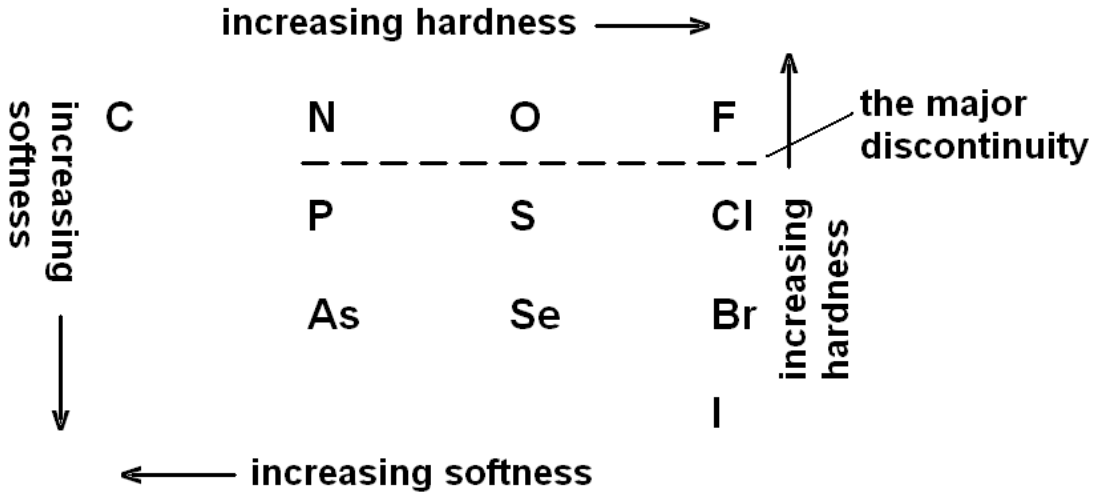

Figure 1.1. Distribution of hardness and softness for potential donor atoms for ligands in the periodic table. (Pearson, 1963)

Lanthanide	Reduction Potential (V)
Eu	-0.35
Yb	-1.15
Sm	-1.55
Tm	-2.30
Nd	-2.60
Dy	-2.60
Pr	-2.70
Ho	-2.90
La	-3.10
Er	-3.10
Ce	-3.20
Tb	-3.70
Gd	-3.90

Table 1.1. Lanthanide reduction potentials (Evans, 2000).

Species	$K_{sp}°$
CeO_2 bulk	0.00073338
CeO_2 NP	0.128205128
$Ce(OH)_3$	1.6E-20
$Ce(OH)_4$	2.00E-48
$CePO_4$	1.00E-23
Ce_2S_3	6.00E-11
$Ce_2(SO_4)_3 \cdot 2H_2O$	9.84 (L^3 mol^{-2})
$Ce(SO_4)_2$	9.84 (L^2 mol^{-2})
CeF_3	8.00E-16
$Ce(IO_3)_3$	3.20E-10
$Ce(IO_3)_4$	5.00E-17
$Ce_2(SeO_3)_3$	3.70E-25
$Ce(NO_3)_3$	234 (L^2 mol^{-2})

Table 1.2. Solubility constants (g per 100 g H_2O) for selected Ce compounds (Clever, Derrick, et al., 1992, Clever, Johnson, et al., 1985, Clever and Johnston, 1980, IUPAC, 1979-1992, Lide, 2005, Marcus, 1980).

Species	EN	Species	EN	Species	EN
Ar	0.4	Al	1.61	P	2.19
K	0.82	Zn	1.65	Pb	2.33
Na	0.93	Cd	1.69	C	2.55
Sr	0.95	Co	1.88	S	2.58
Ca	1	Si	1.9	N	3.04
Ce	1.12	Cu	1.9	Cl	3.16
Mg	1.31	Ni	1.91	O	3.44

Table 1.3. Electronegativity of cerium (Pauling scale) compared to other common species found in soils (Gordy and Thomas, 1956).

Mineral	Chemical Formula	Type Locality	System
Ancylite-(Ce)	$SrCe(CO_3)_2(OH) \cdot H_2O$	Greenland	Orthorhombic
Bastnäsite-(Ce)	$(Ce,La)(CO_3)F$	Sweden	Hexagonal
Burbankite	$(Na,Ca)_3(Sr,Ba,Ce)_3(CO_3)_5$	USA	Hexagonal
Calcioancylite	$(Ca,Sr)Ce(CO_3)_2(OH) \cdot H_2O$	Russia	Orthorhombic
Calkinsite	$(Ce,La)_2(CO_3)_3 \cdot 4H_2O$	USA	Orthorhombic
Carbocernaite	$(Ca,Na)(Sr,Ce,Ba)(CO_3)_2$	Russia	Orthorhombic
Cordylite-(Ce)	$NaBaCe_2(CO_3)_4F$	Greenland	Hexagonal
Huanghoite	$BaCe(CO_3)_2F$	China	Trigonal
Hydroxylbastnäsite-(Ce)	$(Ce,La)(CO_3)(OH,F)$	Russia	Hexagonal
Lanthanite-(Ce)	$(Ce,La,Nd)_2(CO_3)_3 \cdot 8H_2O$	Wales	Orthorhombic
Parisite-(Ce)	$Ca(Ce,La)_2(CO_3)_3F_2$	Colombia	Monoclinic
Rhabdophane	$(Ce,La)(PO_4) \cdot H_2O$	England	Hexagonal
Remondite-(Ce)	$Na_3(Ce,La,Ca,Na,Sr)_3(CO_3)_5$	Cameroon	Monoclinic
Rontgenite	$Ca_2(Ce,La)_3(CO_3)_5F_3$	Greenland	Trigonal
Sahamalite	$(Mg,Fe)(Ce,La,Nd)_2(CO_3)_4$	USA	Monoclinic
Synchysite-(Ce)	$Ca(Ce,La)(CO_3)_2F$	Greenland	Monoclinic
Thorbastnäsite	$Th(Ca,Ce)(CO_3)_2F_2 \cdot 3H_2O$	Russia	Hexagonal
Tundrite-(Ce)	$Na_2Ce_2Ti(SiO_4)(CO_3)_2O_2$	Russia	Triclinic

Table 1.4. Several members of the rare earth carbonates (Anthony).

Mineral	Chemical Formula	Type Locality	System
Agardite-(Ce)	$CeCu_6(AsO_4)_3(OH)_6 \cdot 3H_2O$	Germany	Hexagonal
Monazite-(Ce)	$(Ce,La,Nd,Th)(PO_4)$	Russia	Monoclinic

Table 1.5. Several members of the rare earth phosphates (Anthony).

Mineral	Chemical Formula	Type Locality	System
Allanite-(Ce)	$(CaCe)(Al_2Fe^{2+})(Si_2O_7)(SiO_4)O(OH)$	Greenland	Monoclinic
Cerite-(Ce)	$(Ce,Ca)_9(Fe,Mg)(SiO_4)_3(HSiO_4)_4(OH)_3$	Sweden	Trigonal
Gadolinite-(Ce)	$(Ce,La,Nd,Y)_2Fe^{2+}Be_2Si_2O_{10}$	Japan, Norway	Monoclinic
Joaquinite-(Ce)	$NaBa_2Ce_2FeTi_2[Si_4O_{12}]_2O_2(OH,F)\cdot H_2O$	USA	Monoclinic

Table 1.6. Several members of the rare earth silicates (Anthony).

Mineral	Chemical Formula	Type Locality	System
Aeschynite-(Ce)	$(Ce,Ca,Fe,Th)(Ti,Nb)_2(O,OH)_6$	Russia	Orthorhombic
Euxenite-(Y)	$(Y,Ca,Ce,U,Th)(Nb,Ti,Ta)_2O_6$	Norway	Orthorhombic
Perovskite	$CaTiO_3$ with Ce varieties	Russia	Orthorhombic

Table 1.7. Several members of the rare earth oxides and hydroxides (Anthony).

1.8 References

Abanades, S. and G. Flamant. 2006. Thermochemical hydrogen production from a two-step solar-driven water-splitting cycle based on cerium oxides. Sol. Energy 80: 1611-1623.

Abbasi, Z., M. Haghighi, E. Fatehifar and S. Saedy. 2011. Synthesis and Physicochemical Characterization of Nanostructured Pt/CeO(2) Catalyst Used for Total Oxidation of Toluene. International Journal of Chemical Reactor Engineering 9.

Abbasi, Z., M. Haghighi, E. Fatehifar and S. Saedy. 2011. Synthesis and physicochemical characterizations of nanostructured Pt/Al(2)O(3)-CeO(2) catalysts for total oxidation of VOCs. Journal of Hazardous Materials 186: 1445-1454.

Abreu, R.D. and C.A. Morais. 2010. Purification of rare earth elements from monazite sulphuric acid leach liquor and the production of high-purity ceric oxide. Minerals Engineering 23: 536-540.

Anthony, J.W., Bideaux, R.A., Bladh, K.W., and Nichols, M.C. 1995. Handbook of Mineralogy (Volume II- Elements, Silica, Silicates). Mineral Data Publishing, Tuscon, Arizona.

Anthony, J.W., Bideaux, R.A., Bladh, K.W., and Nichols, M.C. 1997. Handbook of Mineralogy (Volume III- Halides, Hydroxides, Oxides). Mineral Data Publishing, Tuscon, Arizon.

Anthony, J.W., Bideaux, R.A., Bladh, K.W., and Nichols, M.C. 2000. Handbook of Mineralogy (Volume IV- Arsenates, Phosphates, Vanadates). Mineral Data Publishing, Tuscon, Arizona.

Anthony, J.W., Bideaux, R.A., Bladh, K.W., and Nichols, M.C. 2003. Handbook of Mineralogy (Volume V- Borates, Carbonates, Sulfates). Mineral Data Publishing, Tuscon, Arizona.

Aston, F.W. 1925. CXIX. The mass-spectra of chemical elements.—Part VI. Accelerated anode rays continued. Philosophical Magazine Series 6 49: 1191-1201.

Babu, S., A. Velez, K. Wozniak, J. Szydlowska and S. Seal. 2007. Electron paramagnetic study on radical scavenging properties of ceria nanoparticles. Chem. Phys. Lett. 442: 405-408.

Bachand, P.A.M. and A.J. Horne. 2000. Denitrification in constructed free-water surface wetlands: II. Effects of vegetation and temperature. Ecological Engineering 14: 17-32.

Balusamy, B., Y.G. Kandhasamy, A. Senthamizhan, G. Chandrasekaran, M.S. Subramanian and S.K. Tirukalikundram. 2012. Characterization and bacterial toxicity of lanthanum oxide bulk and nanoparticles. Journal of Rare Earths 30: 1298-1302.

Birbaum, K., R. Brogioli, M. Schellenberg, E. Martinoia, W.J. Stark, D. Gunther, et al. 2010. No Evidence for Cerium Dioxide Nanoparticle Translocation in Maize Plants. Environmental Science & Technology 44: 8718-8723.

Chen, J., S. Patil, S. Seal and J.F. McGinnis. 2008. Nanoceria particles prevent ROI-induced blindness. In: R. E. Anderson, M. M. LaVail and J. G. Hollyfield, editors, Advances in Experimental Medicine and Biology. p. 53-59.

Chueh, W.C., C. Falter, M. Abbott, D. Scipio, P. Furler, S.M. Haile, et al. 2010. High-Flux Solar-Driven Thermochemical Dissociation of CO2 and H2O Using Nonstoichiometric Ceria. Science 330: 1797-1801.

Clever, H.L., M.E. Derrick and S.A. Johnson. 1992. The Solubility of Some Sparingly Soluble Salts of Zinc and Cadmium in Water and in Aqeuous-Electrolyte Solutions. Journal of Physical and Chemical Reference Data 21: 941-1004.

Clever, H.L., S.A. Johnson and M.E. Derrick. 1985. The Solubility of Mercury and Some Sparingly Soluble Mercury Salts in Water and Aqueous-Electrolyte Solutions. Journal of Physical and Chemical Reference Data 14: 631-681.

Clever, H.L. and F.J. Johnston. 1980. The Solubility of Some Sparingly Soluble Lead Salts- An Evaluation of the Solubility in Water and Aqueous-Electrolyte Solution. Journal of Physical and Chemical Reference Data 9: 751-784.

Cornelis, G., B. Ryan, M.J. McLaughlin, J.K. Kirby, D. Beak and D. Chittleborough. 2011. Solubility and Batch Retention of CeO2 Nanoparticles in Soils. Environmental Science & Technology 45: 2777-2782.

D'Angelo, B., S. Santucci, E. Benedetti, S. Di Loreto, R.A. Phani, S. Falone, et al. 2009. Cerium Oxide Nanoparticles Trigger Neuronal Survival in a Human Alzheimer Disease Model By Modulating BDNF Pathway. Curr. Nanosci. 5: 167-176.

Dimitrov, V., K. Kostova and M. Genov. 1996. Anhydrous cerium(III) chloride - Effect of the drying process on activity and efficiency. Tetrahedron Letters 37: 6787-6790.

Edelmann, F.T.P., P., Hermann, W.A. 1997. Synthetic Methods of Organometallic and Inorganic Chemistry. Georg Thieme Verlag, Stuttgart.

Estevez, A.Y., S. Pritchard, K. Harper, J.W. Aston, A. Lynch, J.J. Lucky, et al. 2011. Neuroprotective mechanisms of cerium oxide nanoparticles in a mouse hippocampal brain slice model of ischemia. Free Radic. Biol. Med. 51: 1155-1163.

Evans, W.J. 2000. Perspectives in reductive lanthanide chemistry. Coordination Chemistry Reviews 206: 263-283.

Garcia, A., L. Delgado, J.A. Tora, E. Casals, E. Gonzalez, V. Puntes, et al. 2012. Effect of cerium dioxide, titanium dioxide, silver, and gold nanoparticles on the activity of microbial communities intended in wastewater treatment. Journal of Hazardous Materials 199: 64-72.

Ginepro, J.Q., J. Snyder and M. Thoennessen. 2009. Discovery of the cerium isotopes. Atomic Data and Nuclear Data Tables 95: 805-814.

Gordy, W. and W.J. Thomas. 1956. Electronegativities of the Elements. J. Chem. Phys. 24: 439.

Gottschalk, F., T. Sonderer, R.W. Scholz and B. Nowack. 2009. Modeled Environmental Concentrations of Engineered Nanomaterials (TiO2, ZnO, Ag, CNT, Fullerenes) for Different Regions. Environmental Science & Technology 43: 9216-9222.

Gruner, S., I. Sehrt, G.M. Muller, A. Zwirner, D. Strunk and N. Sonnichsen. 1992. Inhibition of Histamine-Release from Human Granulocytes by Ions of the Rare-Earth Elements Lanthanum and Cerium. Agents and Actions 36: 207-211.

He, X., Y. Kuang, Y. Li, H. Zhang, Y. Ma, W. Bai, et al. 2012. Changing exposure media can reverse the cytotoxicity of ceria nanoparticles for Escherichia coli. Nanotoxicology 6: 233-240.

Heckert, E.G., A.S. Karakoti, S. Seal and W.T. Self. 2008. The role of cerium redox state in the SOD mimetic activity of nanoceria. Biomaterials 29: 2705-2709.

Hedrick, J.B. 2004. Rare Earths. Minerals Yearbook. Vol I. Metals and Minerals. US Geological Survey, US Department of the Interior, Reston, VA.

Hedrick, J.B. and S.P. Sinha. 1994. Cerium-Based Polishing Compounds- Discovery to Manufacture. Journal of Alloys and Compounds 207: 377-382.

Higgins, W.M., A. Churilov, E. van Loef, J. Glodo, M. Squillante and K. Shah. 2008. Crystal growth of large diameter LaBr3 : Ce and CeBr3. J. Cryst. Growth 310: 2085-2089.

Hoecke, K.V., J.T. Quik, J. Mankiewicz-Boczek, K. Schamphelaere, A. Elsaesser, P. Van der Meeren, et al. 2009. Fate and Effects of CeO2 Nanoparticles in Aquatic Ecotoxicity Tests. Environmental Science & Technology 43: 4537-4546.

Hoshino, A., K. Fujioka, T. Oku, M. Suga, Y.F. Sasaki, T. Ohta, et al. 2004. Physicochemical Properties and Cellular Toxicity of Nanocrystal Quantum Dots Depend on Their Surface Modification. Nano Letters 4: 2163-2169.

Institute, Health Effects. 2001. Evaluation of Human Health Risk from Cerium Added to Diesel Fuel. Health Effects Institute Communication 9.

IUPAC. 1979-1992. IUPAC Solubility Data Project: Solubility Data Series. Pergamon Press, Oxford.

Ivanov, V.K., A.B. Shcherbakov, I.G. Ryabokon, A.V. Usatenko, N.M. Zholobak and Y.D. Tretyakov. 2010. Inactivation of the nitroxyl radical by ceria nanoparticles. Dokl. Chem. 430: 43-46.

Ivanov, V.K., A.V. Usatenko and A.B. Shcherbakov. 2009. Antioxidant activity of nanocrystalline ceria to anthocyanins. Russ. J. Inorg. Chem. 54: 1522-1527.

Jakupec, M.A., P. Unfried and B.K. Keppler. 2005. Pharmacological properties of cerium compounds. In: S. G. Amara, E. Bamberg, R. Jahn, W. J. Lederer, A. Miyajima, H. Murer, S. Offermanns, G. Schultz and M. Schweiger, editors, Reviews of Physiology Biochemistry and Pharmacology. p. 101-111.

Jiang, W., H. Mashayekhi and B. Xing. 2009. Bacterial toxicity comparison between nano- and micro-scaled oxide particles. Environmental Pollution 157: 1619-1625.

Johnson, C.R. and B.D. Tait. 1987. A Cerium(III) Modification of the Peterson Reaction - Methylenation of Readily Enolizable Carbonyl Compounds. Journal of Organic Chemistry 52: 281-283.

Johnston, B.D., T.M. Scown, J. Moger, S.A. Cumberland, M. Baalousha, K. Linge, et al. 2010. Bioavailability of Nanoscale Metal Oxides TiO(2), CeO(2), and ZnO to Fish. Environmental Science & Technology 44: 1144-1151.

Karakoti, A., S. Singh, J.M. Dowding, S. Seal and W.T. Self. 2010. Redox-active radical scavenging nanomaterials. Chem. Soc. Rev. 39: 4422-4432.

Karakoti, A.S., N.A. Monteiro-Riviere, R. Aggarwal, J.P. Davis, R.J. Narayan, W.T. Self, et al. 2008. Nanoceria as antioxidant: Synthesis and biomedical applications. Jom 60: 33-37.

Kilbourn, B. 2003. Cerium and cerium compounds. Kirk-Othmer encyclopedia of chemical technology. John Wiley and Sons, Inc., New York, NY.

Kim, I.-S., M. Baek and S.-J. Choi. 2010. Comparative Cytotoxicity of Al2O3, CeO2, TiO2 and ZnO Nanoparticles to Human Lung Cells. J. Nanosci. Nanotechnol. 10: 3453-3458.

Kuang, Y.S., X. He, Z.Y. Zhang, Y.Y. Li, H.F. Zhang, Y.H. Ma, et al. 2011. Comparison Study on the Antibacterial Activity of Nano- or Bulk-Cerium Oxide. J. Nanosci. Nanotechnol. 11: 4103-4108.

Lanone, S., F. Rogerieux, J. Geys, A. Dupont, E. Maillot-Marechal, J. Boczkowski, et al. 2009. Comparative toxicity of 24 manufactured nanoparticles in human alveolar epithelial and macrophage cell lines. Part. Fibre Toxicol. 6.

Lead, J.R. and E. Smith. 2009. Environmental and Human Health Impacts of Nanotechnology. John Wiley and Sons, Ltd.

Lide, D.R. 2005. Handbook of chemistry and physics. CRC Press.

Limbach, L.K., R. Bereiter, E. Mueller, R. Krebs, R. Gaelli and W.J. Stark. 2008. Removal of oxide nanoparticles in a model wastewater treatment plant: Influence of agglomeration and surfactants on clearing efficiency. Environmental Science & Technology 42: 5828-5833.

Liu, J., D.A. Sonshine, S. Shervani and R.H. Hurt. 2010. Controlled Release of Biologically Active Silver from Nanosilver Surfaces. ACS Nano 4: 6903-6913.

Lopez-Moreno, M.L., G. de la Rosa, J.A. Hernandez-Viezcas, J.R. Peralta-Videa and J.L. Gardea-Torresdey. 2010. X-ray Absorption Spectroscopy (XAS) Corroboration of the Uptake and Storage of CeO(2) Nanoparticles and Assessment of Their Differential Toxicity in Four Edible Plant Species. Journal of Agricultural and Food Chemistry 58: 3689-3693.

Lu, K., Z.Y. Zhang, X.A. He, Y.H. Ma, K.B. Zhou, H.F. Zhang, et al. 2010. Bioavailability and Distribution and of Ceria Nanoparticles in Simulated Aquatic Ecosystems, Quantification with a Radiotracer Technique. J. Nanosci. Nanotechnol. 10: 8658-8662.

Lubick, N. 2008. Nanosilver toxicity: ions, nanoparticles-or both? Environmental Science & Technology 42: 8617-8617.

Ma, Y.H., L.L. Kuang, X. He, W. Bai, Y.Y. Ding, Z.Y. Zhang, et al. 2010. Effects of rare earth oxide nanoparticles on root elongation of plants. Chemosphere 78: 273-279.

Mahendra, S., H. Zhu, V.L. Colvin and P.J. Alvarez. 2008. Quantum Dot Weathering Results in Microbial Toxicity. Environmental Science & Technology 42: 9424-9430.

Marcus, Y. 1980. A Compilation and Evaluation of Solubility Data in the Mercury (U) Chloride-Water System. Journal of Physical and Chemical Reference Data 9: 1307-1329.

Martin, T.L., N.K. Kaushik, J.T. Trevors and H.R. Whiteley. 1999. Review: Denitrification in temperate climate riparian zones. Water Air and Soil Pollution 111: 171-186.

Moller, P., G. Morteani and P. Dulski. 2003. Anomalous gadolinium, cerium, and yttrium contents in the adige and isarco river waters and in the water of their tributaries (Provinces Trento and Bolzano/Bozen, NE Italy). Acta Hydrochimica Et Hydrobiologica 31: 225-239.

Monafo, W.W., S.N. Tandon, V.H. Ayvazian, J. Tuchschmidt, A.M. Skinner and F. Deitz. 1976. Cerium nitrate: a new topical antiseptic for extensive burns. Surgery 80: 465-473.

Moore, K.T., L. Belhadi, F. Decremps, D.L. Farber, J.A. Bradley, F. Occelli, et al. 2011. Watching a metal collapse: Examining cerium's gamma <-> alpha transformation using X-ray diffraction of compressed single and polycrystals. Acta Mater. 59: 6007-6016.

Mulvaney, R.L., S.A. Khan and C.S. Mulvaney. 1997. Nitrogen fertilizers promote denitrification. Biology and Fertility of Soils 24: 211-220.

Nalabotu, S.K., M.B. Kolli, W.E. Triest, J.Y. Ma, N. Manne, A. Katta, et al. 2011. Intratracheal instillation of cerium oxide nanoparticles induces hepatic toxicity in male Sprague-Dawley rats. Int. J. Nanomed. 6: 2327-2335.

Nesse, W.D. 2000. Introduction to MineralogyOxford University Press, Oxford, NY.

O'Neil, M. 2001. The Merck Index: an encyclopedia of chemicals, drugs, and biologicals. 13 ed. Merck and Co, Inc., Whitehouse Station, NJ.

Orge, C.A., J.J. Orfao, M.F. Pereira, A.M. de Farias, R.C. Neto and M.A. Fraga. 2011. Ozonation of model organic compounds catalysed by nanostructured cerium oxides. Appl. Catal. B-Environ. 103: 190-199.

Oxford, J.E. 2011. Nature's Building Blocks: An A-Z Guide to the Elements. 2 ed. Oxford University Press, Oxford, UK.

Palasz, A. and P. Czekaj. 2000. Toxicological and cytophysiological aspects of lanthanides action. Acta Biochimica Polonica 47: 1107-1114.

Palmberg, C. and N. Tuomo. 2006. Industrial renewal and growth through nanotechnology? An overview with focus on Finland. ETLA Discussion Papers, The Research Institute of the Finnish Economy.

Paquette, L.C., RM; Denmark, SE. 1999. Handbook of Reagents for Organic Syntsyhesis: Reagents, Auxiliaries and Catalysts for C-C Bond Formation. Wiley, New York, NY.

Park, E., J. Choi, Y. Park and K. Park. 2008. Oxidative stress induced by cerium oxide nanoparticles in cultured BEAS-2B cells. Toxicology 245: 90-100.

Patnaik, P. 2003. Handbook of inorganic chemicals. McGraw-Hill.

Pearson, R.G. 1963. J. Am. Chem. Soc.: 3533-3543.

Pelletier, D.A., A.K. Suresh, G.A. Holton, C.K. McKeown, W. Wang, B.H. Gu, et al. 2010. Effects of Engineered Cerium Oxide Nanoparticles on Bacterial Growth and Viability. Appl. Environ. Microbiol. 76: 7981-7989.

Pirmohamed, T., J.M. Dowding, S. Singh, B. Wasserman, E. Heckert, A.S. Karakoti, et al. 2010. Nanoceria exhibit redox state-dependent catalase mimetic activity. Chem. Commun. 46: 2736-2738.

Reinhardt, K. and H. Winkler. 2002. Cerium mischmetal, cerium alloys, and cerium compounds. Ullmann's encyclopedia of industrial chemistry. Wiley-VCH, Weinheim, Germany. p. 285-300.

Rodea-Palomares, I., K. Boltes, F. Fernandez-Pinas, F. Leganes, E. Garcia-Calvo, J. Santiago, et al. 2011. Physicochemical Characterization and Ecotoxicological Assessment of CeO(2) Nanoparticles Using Two Aquatic Microorganisms. Toxicol. Sci. 119: 135-145.

Rogers, N.J., N.M. Franklin, S.C. Apte, G.E. Batley, B.M. Angel, J.R. Lead, et al. 2010. Physico-chemical behaviour and algal toxicity of nanoparticulate CeO(2) in freshwater. Environmental Chemistry 7: 50-60.

Roh, J., Y. Park, K. Park and J. Choi. 2010. Ecotoxicological investigation of CeO(2) and TiO(2) nanoparticles on the soil nematode Caenorhabditis elegans using gene expression, growth, fertility, and survival as endpoints. Environmental Toxicology and Pharmacology 29: 167-172.

Rzigalinski, B.A., D. Bailey, L. Chow, S.C. Kuiry, S. Patil, S. Merchant, et al. 2003. Cerium oxide nanoparticles increase the lifespan of cultured brain cells and protect against free radical and mechanical trauma. Faseb Journal 17: A606-A606.

Schubert, D., R. Dargusch, J. Raitano and S.W. Chan. 2006. Cerium and yttrium oxide nanoparticles are neuroprotective. Biochem. Biophys. Res. Commun. 342: 86-91.

Sparks, D.L. 2003. Environmental Soil Chemistry. 2 ed. Academic Press, San Diego, CA 92101.

Stassis, C., T. Gould, O.D. McMasters, K.A. Gschneidner and R.M. Nicklow. 1979. Lattice and Spin Dynamics of Gamma-Ce. Physical Review B 19: 5746-5753.

Thill, A., O. Zeyons, O. Spalla, F. Chauvat, J. Rose, M. Auffan, et al. 2006. Cytotoxicity of CeO2 nanoparticles for Escherichia coli. Physico-chemical insight of the cytotoxicity mechanism. Environmental Science & Technology 40: 6151-6156.

Van Hoecke, K., K.A.C. De Schamphelaere, P. Van der Meeren, G. Smagghe and C.R. Janssen. 2011. Aggregation and ecotoxicity of CeO2 nanoparticles in synthetic and natural waters with variable pH, organic matter concentration and ionic strength. Environmental Pollution 159: 970-976.

van Loef, E.V.D., P. Dorenbos, C.W.E. van Eijk, K. Kramer and H.U. Gudel. 2001. High-energy-resolution scintillator: Ce(3+) activated LaBr(3). Appl. Phys. Lett. 79: 1573-1575.

Weeks, M.E. 1932. The discovery of the elements. XVI. The rare earth elements. Journal of Chemical Education 9: 1751.

Xia, T., M. Kovochich, M. Liong, L. Madler, B. Gilbert, H.B. Shi, et al. 2008. Comparison of the Mechanism of Toxicity of Zinc Oxide and Cerium Oxide Nanoparticles Based on Dissolution and Oxidative Stress Properties. ACS Nano 2: 2121-2134.

Yuan, Z.Y., V. Idakiev, A. Vantomme, T. Tabakova, T.Z. Ren and B.L. Su. 2008. Mesoporous and nanostructured CeO2 as supports of nano-sized gold catalysts for low-temperature water-gas shift reaction. Catalysis Today 131: 203-210.

Zhang, H., X. He, Z. Zhang, P. Zhang, Y. Li, Y. Ma, et al. 2011. Nano-CeO(2) Exhibits Adverse Effects at Environmental Relevant Concentrations. Environmental Science & Technology 45: 3725-3730.

Zhang, Z.Y., X. He, H.F. Zhang, Y.H. Ma, P. Zhang, Y.Y. Ding, et al. 2011. Uptake and distribution of ceria nanoparticles in cucumber plants. Metallomics 3: 816-822.

CHAPTER TWO

EFFECTS OF pH AND PHOSPHATE ON PHYSICOCHEMICAL PROPERTIES OF CeO_2 NANOPARTICLES

2.1 Abstract

Due to the rise of nanotechnology in industry, the concentrations of engineered metal oxide nanoparticles being released to the environment are increasing daily. To understand the chemical interactions of CeO_2 nanoparticles post-environmental release, the dissolution of small (10 – 30 nm) and large (50 – 105 nm) manufactured CeO_2 NPs was studied as a function of pH in the absence and presence of phosphate. It was found that Ce dissolution was negligible at pH > 7 and was only significant at pH < 5. When 100 μM phosphate was present, dissolution of CeO_2 NPs was significantly reduced. The rate constant in small NPs decreased by 15% at pH 1.65 and 75% at pH 4.5 and in large NPs decreased by 56% at pH 1.65 and 63% at pH 4.5. Phosphate-suppressed $Ce(IV)O_2$ dissolution was linked to the chemisorption of PO_4^{3-}. It was postulated that the Ce(III) impurity metal-centered complexation with PO_4^{3-} ligands could facilitate the formation of $Ce(III)PO_4$ surface precipitates at the $Ce(IV)O_2$-water interface. Phosphate ligands might play an important role in controlling the Ce release from CeO_2 NPs; this is an important consideration in determining the fate and transport of CeO_2 NPs in the aquatic and terrestrial environment.

2.2 Introduction

Cerium (Ce) is the most abundant of the rare-earth metals found in the earth's crust (Hedrick, 2004). Cerium comprises about 0.0046% of the earth's crust by weight, occurring at average concentrations of 50 mg kg^{-1}. Cerium minerals naturally occur with other lanthanide metals in an array of minerals in the environment including allanite ($(Ca,Ce)(Al_2Fe^{2+})(Si_2O_7)(SiO_4)O(OH)$), bastnäsite ($(Ce,La)(CO_3)F$), cerite ($(Ce,Ca)_9(Fe,Mg)(SiO_4)_3(HSiO_4)_4(OH)_3$), monazite ($(Ce,La,Nd,Th)(PO_4)$), and euxenite ($(Y,Ca,Ce,U,Th)(Nb,Ti,Ta)_2O_6$); however, of these minerals, only bastnäsite and monazite serve as important sources commercially. Acidification of these mixed lanthanide/metal followed by base titration improves purity of Ce, and a variety of Ce compounds have been synthesized for commercial and industrial applications(Abreu and Morais, 2010, Patnaik, 2003).

Popular applications of Ce compounds include pharmaceutical (antiemetic and antithrombic drugs) and industrial uses (mischmetal for metallurgical purposes, scintillation counters, abrasives) (Hedrick and Sinha, 1994, Jakupec, Unfried, et al., 2005, Kilbourn, 2003, van Loef, Dorenbos, et al., 2001). The most common applications are the uses of CeO_2 nanoparticles as catalysts, glass additives, and fuel additives. (Abbasi, Haghighi, et al., 2011, Reinhardt and Winkler, 2002). Because of the rapidly growing demand of Ce nanotechnology, the release of Ce is expected to increase in the environment. A majority (95%) of cerium is likely to be discharged from wastewater

treatment plants and/or accumulated in the sludge that is later used for soil amendments (Limbach, Bereiter, et al., 2008). Thus, industrial wastewaters serve as a significant environmental source of CeO_2 NPs. As in the case of many other metal NPs such as TiO_2, ZnO, and Ag NPs (Gottschalk, Sonderer, et al., 2009), it is believed that biosolids application to agricultural soils serves as one of the largest exposure routes for manufactured CeO_2 NPs (Cornelis, Ryan, et al., 2011). Thus, there is great interest in understanding the fate of CeO_2 nanoparticles in soils and sediments.

In low temperature geochemical environments, the most common oxidation states of Ce are trivalent and tetravalent. Cerium's coordination/ hydration number is generally six, which is a quite uncommon coordination number among other lanthanides. The Hard/Soft Acid/Base theory predicts the tendency of hard acidic Ce to strongly bond with hard base ligands such as hydroxyl ions and phosphates over species like sulfates and hydrides. In general, Ce(III) is more soluble than Ce(IV). Tetravalent Ce is known to undergo hydrolysis reactions to form insoluble $Ce(IV)(OH)_4$ (K_{sp}: 2×10^{-48}, whereas K_{sp} of $Ce(III)(OH)_3$ is 1.6×10^{-20}). However, Ce(III) could form the very insoluble phosphate compound, $Ce(III)PO_4$ as well (K_{sp}: 1×10^{-23}) (Bjerrum, 1958, Clever, Johnson, et al., 1985, Clever, Johnson, et al., 1992, Clever and Johnston, 1980, IUPAC, 1979-1992, Marcus, 1980). While other common O-donor organic acids (oxalate, tatrate) complex with Ce(III) to form solubility products ($Ce_2(C_2O_4)_3 \cdot 9H_2O$: K_{sp}: $3{,}2 \times 10^{-26}$), $Ce_2(tartrate)_3$ (K_{sp}: 1.0×10^{-19}), it seems that the role of hard basic ligands (hydroxyl and phosphate) in pore waters and soil solutions is undoubtedly important in predicting the

solubility of CeO_2 NPs in the aquatic-terrestrial environment. Unfortunately, due to the relativeness newness of CeO_2 nanotechnology, the reactivity of CeO_2 NP in low temperature geochemical environments has not been extensively investigated, leaving uncertainties in predicting the fate of CeO_2 NPs.

The objective of this study is to understand the sorption dissolution of manufactured CeO_2 NPs as a function of pH and phosphate concentration. Batch phosphate sorption on CeO_2 NPs and CeO_2 dissolution experiments were carried out using two uncapped CeO_2 NPs (33 and 78 nm) as a function of pH (3 – 8). Phosphate was chosen as an inorganic ligand since it is largely environmentally relevant, found widely in soils (especially agricultural soils) as well as in agricultural drainage and lake surface waters at 0.05 – 1 and 0.01 – 0.04 mg L^{-1}, respectively (Snoeyink and Jenkins, 1980). Cerium oxide NPs are characterized for physicochemical properties (valence state and particle size, zeta potential, exchangeable Ce) to better interpret the results of batch sorption and dissolution experiments. Results from this work should help in predicting the chemical fate of CeO_2 NPs under environmentally relevant geochemical conditions.

2.3 Materials

Cerium oxide NPs (powder) of two different particle sizes were obtained from US Research Nanomaterials (Houston, TX) and Nanostructured and Amorphous Materials, Inc. (Houston, TX). Brunauer-Emmett-Teller (BET) surface area, density and chemical

impurity data were provided by the manufacturers. To improve understanding of the reactivity of the CeO_2 NPs, exchangeable Ce was measured. A 0.3 g portion of CeO_2 NPs was suspended in 10 mL of 0.5 M $Ca(NO_3)_2$ solution and sonified. The NP suspensions were agitated on an end-over shaker for 18 h at 12 rpm. Nanomaterials were spun down using a high speed centrifugation method, and acid digested aliquots were analyzed for total Ce using inductively coupled plasma atomic emission spectroscopy (ICP-AES) and for dissolved Ce(III) using the fluorimetric method and dissolved Ce(IV) using the spectrophotometric method detailed in the dissolution section.

Zeta Potential and Particle Size Characterization

Cerium NP solutions were analyzed for zeta potential and particle size (via dynamic light scattering, DLS) using a Brookhaven Instruments particle separation system (Brookhaven Instruments, Holtsville, New York). Cerium nanoparticle suspensions (0.15 g L^{-1}) were prepared by hydrating the NPs for several days at pH ~ 4 in 0.01 M $NaNO_3$.

2.4 Methods

Phosphate Sorption Envelope on CeO_2 Nanoparticles

Phosphate adsorption was studied as a function of pH (3.5 – 8.5), $[PO_4^{3-}]$ = 0.48 and 2.39 mM, and particle size of the CeO_2 nanoparticles. All experiments were conducted at 21 ± 1.2 ^oC, at ionic strength I = 0.017 M $NaNO_3$, and under $pCO_2 = 10^{-3.45}$ atm unless otherwise mentioned in the text. Cerium oxide nanoparticle stock suspensions were

freshly prepared in the same background electrolyte solution prior to the experiment. Hydration of adsorbent was carried out in two steps. In the first step, 20 mL of sonified CeO_2 stock suspensions were transferred into 30 mL high speed Oakridge centrifuge tubes. Next, the pH of the suspensions was adjusted to values ranging between 3 and 9 using either 1 M HNO_3 or 1 M NaOH, and equilibrated for 24h. The appropriate amount of sodium bicarbonate was also added to achieve desired bicarbonate concentrations at targeted pH values that were estimated using the chemical speciation program VisualMinteq ver. 3.0 (Gustaffson, 2007).After hydration, an appropriate amount of 23.87 mM phosphate monobasic monohydrate stock solution was added to achieve an initial PO_4^{3-} concentration of 0.48 or 2.39 mM and the final suspension density of CeO_2 = 1g L^{-1}. The samples were reacted for 48 h on an end-over shaker at 12 rpm. The reaction time of 48 h was chosen through preliminary experiments showing that there is a minimum kinetic effect on total PO_4^{3-} uptake after 48 h (i.e., reaching near steady-state after 2 days). After 48 h of shaking, the final pH was measured in the suspension. Prior to the filtration of aliquots, the following nanoparticle separation method was developed using modified Stokes' law. The large NPs were centrifuged at 10,000 rpm for 13 min and the small NPs were centrifuged at 17,000 rpm for 60 min. After centrifugation, 5 mL of supernatant were filtered through 0.20 µm Whatman (polyvinylidene difluoride) PVDF filters. The molybdenum blue method (He, Baligar, et al., 1998, Murphy and Riley, 1986) was used to analyze for soluble phosphate.

Phosphate Sorption Isotherm on CeO_2 Nanoparticles

All experiments were conducted in duplicate under ambient conditions (22 ± 1.2 ^{o}C and $pCO_2 = 10^{-3.45}$ atm). Prior to the sorption experiments, cerium oxide nanoparticle (NP) stock suspensions (large nanoparticles, 50 – 105 nm, and small nanoparticles, 10 – 30 nm) were freshly prepared in a 0.017 M $NaNO_3$ background electrolyte solution. First, 10 mL of sonified CeO_2 stock suspensions were transferred into 30 mL Nalgene high speed centrifuge tubes. Next, the pH of the suspensions was adjusted to 4.5 and 7.5 using 10 mL of 30 mM sodium acetate and 3-morpholino-2-hydroxypropanesulfonic acid sodium salt, 3-(N-morpholinyl)-2- hydroxypropanesulfonic acid (MOPSO) buffer solutions, respectively. The pH values were readjusted using either 1 M HNO_3 or 1 M NaOH and the solutions were allowed to equilibrate for 24 h. After the equilibration, an appropriate amount of sodium phosphate monobasic monohydrate stock solution and $NaNO_3$ background electrolyte solution was added to achieve $[P]_{total}$ =0.10 – 1.30 mM, the final suspension density of CeO_2 = 1 g L^{-1}, and I = 0.017 M $NaNO_3$. The samples were then placed on an end-over shaker for 48 h. In order to separate the NPs from solution, the following centrifugation method was developed from the modified Stokes' law. After 48 h of shaking, the large NP samples were centrifuged at 10,000 rpm for 13 min and the small NP samples were centrifuged at 17,000 rpm for 60 min. After centrifugation, 5 mL aliquots of the supernatant were filtered through 0.20 µm Whatman (polyvinylidene fluoride) PVDF filters. The molybdenum blue method (He, Baligar, et al., 1998 and Murphy, J. and Riley, J.P., 1962) was then used to analyze the filtrate for total phosphate.

Phosphate Desorption

Phosphate sorbed CeO_2 NP samples (0.48 and 2.39 mM PO_4^{3-} in 0.017 M $NaNO_3$ at pH = 4.5 and 7.5) were prepared using the sorption isotherm method described above. Suspensions were centrifuged using the method described in the previous section. The remaining supernatant was decanted completely. The entire 30 mL of supernatant was filtered through 0.20 µm Whatman (polyvinylidene fluoride) PVDF filters. Then, 30 mL of fresh PO_4^{3-}-free background electrolyte solutions (0.017 M $NaNO_3$ adjusted to pH 4.5 or 7.5 with 30 mM sodium acetate or 3-morpholino-2-hydroxypropanesulfonic acid, respectively) were introduced to respective pH systems. The equilibrium shift in [PO_4^{3-}] drove the desorption of PO_4^{3-}. After addition of PO_4^{3-} free background electrolyte solutions, the tubes were placed on an end-over shaker for 24 h at 12 rpm. The replenishment process was repeated at time periods of 1, 2, 3, 5, 10, 15, and 30 days. The filtrates were acidified in 1% HNO_3 and analyzed for to total PO_4^{3-} and Ce using ICP-AES.

Aqueous Speciation Calculation

Cerium(III) aqueous speciation and solubility products were estimated using the chemical speciation program VisualMinteq ver. 3.0 (Gustaffson, 2007).

Dissolution Experiments

To assess the solubility of CeO_2 NPs, dissolution experiments were conducted as a function of particle size, pH, phosphate concentration (0 and 0.1 mM). All experiments

were performed at $[Ce]_{total}$ 500 mg L^{-1}. Ionic strength was maintained with 0.005 M $NaNO_3$.

Four pH values, which were controlled by 0.1 M HNO_3 for pH = 1.65 ± 0.05, 0.02 M sodium acetate for pH 4.5 ± 0.05, 0.02 M 3-morpholino-2-hydroxypropanesulfonic acid sodium salt (MOPSO) buffer for pH 7.5 ± 0.05 and 0.1 M NaOH for pH = 12.40 ± 0.05, were used in the experiments. Solutions were kept in 50 mL Oak Ridge Nalgene polycarbonate high speed centrifuge tubes for the systems at pH < 5 and Nalgene polypropylene high speed centrifuge tubes for the systems at pH > 8. Tubes were shaken on a reciprocal shaker at 15 rpm up to 6 days. At each sampling period (24, 48, 72, 96, 120, and 144 h), CeO_2 NPs were separated from the bulk solution using the high-speed centrifugation method described above. Concentrations of $[Ce]_{Total}$ were measured using the ICP-AES and [Ce(III)] using the fluorimetric method described below. Using the linear portion of the dissolution data, the rate was modeled using a linear empirical rate law under the assumption of zero order kinetics for solid phase. The rate (k) can be described in the following equation, $C = C_o + kt$.

Ce(III) Fluorimetric Analysis

Subsamples of filtrates from the denitrification experiments were used for Ce(III) fluorimetric analysis (Rakicioglu and Akseli, 1998). In 96-well microplates, samples were prepared for analysis in triplicate. The filtrates were combined with 0.033 g L^{-1} sodium pyrophosphate and degassed DI water, then 200 µL portions were immediately

evaluated for total [Ce(III)] using a Synergy Mx Biotek (Biotek U.S. Winooski, VT) using an excitation wavelength of 300 nm and an emission wavelength of 350 nm.

Ce(IV) Spectrophotometric Analysis

Similarly, 1 mL of filtrates from the denitrification experiments were analyzed for [$Ce(IV)_{(aq)}$] using a spectrophotometric method described by Agrawal, Sekhar, and Pandey (Agrawal, Sekhar, et al., 1994). A 1 mL aliquot of the filtrates was combined with 2 mL of 1 M H_2SO_4, and 5 mL of 0.1 % o-phenylenediamine (OPD) reagent. In 96-well microplates, 200 µL portions of these solutions were added in triplicate for immediate analysis with a Synergy Mx Biotek at an absorbance wavelength of 470 nm.

2.5 Results and Discussion

Nanoparticle characterization

Table 2.1 describes the physicochemical properties of the cerium oxide nanoparticles (CeO_2 NPs) used in this study. The species CeO_2_S denotes the small CeO_2 NP while CeO_2_L denotes the large nanoparticle. The density of the two species is identical but they differ greatly in BET surface area and zeta potential values. The BET surface area of small and large NP is 40 $m^2\ g^{-1}$ and 11.5 $m^2\ g^{-1}$, respectively. The manufacturers reported that the smaller NP is more X-ray amorphous than the larger NP (Nanostructured & Amorphous Materials, Inc., Houston, TX and US Research Nanomaterials, Houston, TX). The zeta potential value is positive for both NPs at pH ~ 4. This agrees with

literature values (Berg, Romoser, et al., 2009). Lastly, perhaps the most important characterization in Table 2.1 is that of exchangeable Ce(III) in the NPs. While the larger NPs contain 1.56 mM kg^{-1} of exchangeable Ce(III), the small NPs feature only 0.3 mM kg^{-1}. To assess the exchangeable Ce(III), first the total Ce was determined using ICP-AES, and then the Ce(IV) analysis was conducted using the Ce(IV) UV-VIS method (Agrawal, Sekhar, et al., 1994). The Ce(IV) concentration was below detection limits (0.1 mg L^{-1}), suggesting that > 99% of exchangeable $[Ce]_{total}$ was Ce(III). The Ce(III) fluorimetric method (Rakicioglu and Akseli, 1998) was also attempted to quantify [Ce(III)]. However, it did not yield in any useful informative due to the interference from ions in background electrolyte (sulfates, nitrates, and most especially phosphates). In summary, total Ce concentration was interpreted as predominantly $Ce(III)_{(aq)}$.

Tables 2.2 and 2.3 list the catalogued impurities in the small and large NPs, respectively (Nanostructured & Amorphous Materials, Inc., Houston, TX and US Research Nanomaterials, Houston, TX). As reviewed in Ch 1, Ce bearing minerals (e.g., monazite and bastnäsite) contain many lanthanide elements. It is likely that these lanthanide elements (e.g., La, Pr, Y, Nd, Sm, Eu) are sources of impurities in synthetic CeO_2 NPs. Iron, Ce, and Si are also notable impurities (as high as 99 mg kg^{-1} in large NPs and 63 mg kg^{-1} in small NPs). While Ca is considered as an isomorphic element for Ce(III) in the CeO_2 structure, SiO_2 and Fe_2O_3 might originate from the manufacturing process of these NPs.

Phosphate adsorption envelope

Figure 2.1 features the phosphate sorption envelope onto the surface of small and large CeO_2 NPs (1 g L^{-1}), both sizes either spiked with a low (0.48 mM L^{-1}) or a high (2.39 mM L^{-1}) phosphate concentration. The data were collected over a pH range of ~ 3.5 – 10.5. As expected, the samples spiked with higher [PO_4^{3-}] exhibited higher levels of sorption than the samples spiked with lower [PO_4^{3-}]. The fact that the small NPs have much greater surface area than the larger NPs likely accounts for the different affinity for phosphate.

The pH dependent sorption behavior of the phosphate anion is demonstrated most clearly for the small NPs with high added PO_4^{3-}. The sorption trend is similar to that of aluminum oxides (De, 1961, Hsu and Rennie, 1962, Muljadi, Posner, et al., 1966, Torrent, Barron, et al., 1990) that have a high PZC (~ 9) like CeO_2. The sorption decreases strongly with increasing pH when CeO_2_S is reacted with either low or high PO_4^{3-} concentrations; a more dramatic decrease is observed at the high PO_4^{3-} concentration. As the $pH_{solution}$ approaches PZC of CeO_2 (~ 9) (Kosmulski, 2001), the surface of CeO_2 becomes more negative and repels anionic HPO_4^{2-} and or PO_4^{3-} species, resulting in a small amount of sorption. On the contrary, large NPs feature far less pH-dependent sorption behavior. Regardless of the different $[PO_4^{3-}]_{initial}$, pH does not affect the uptake of phosphate as greatly as it does for the small NPs. These seemingly pH-independent sorption mechanisms might be attributed to the surface precipitation of Ce(III)PO_4. Since large CeO_2 NPs contain more exchangeable Ce(III) than the small NPs,

it is possible that exchangeable Ce(III) facilitated the precipitation of Ce(III)PO_4 at the CeO_2-water interface. The solubility constant (K_{sp}: 1.00E-23) indicates that Ce(III)PO_4 is an extremely insoluble compound (Table 1.2). Under the reaction conditions, the system is supersaturated with respect to Ce(III)PO_4 (low PO_4^{3-}: saturation index value for Ce(III)$PO_{4(s)}$ at pH 3.5 = 7.179, at pH 10.5 = 11.254; high PO_4^{3-} at pH 3.5 = 7.845, at pH 10.5 = 11.951).

Phosphate adsorption isotherm

Figures 2.2 and 2.3 show the phosphate sorption isotherm in small and large CeO_2 NPs, respectively. At pH 4.5 and 7.5, phosphate sorption generally increases with increasing $[PO_4^3]_{initial}$. A typical L(Langmuir)-shape isotherm curve (Sposito, 1984) is observed in Figures 2.2 and 2.3. A decreasing slope is observed as concentration increases since vacant sites decreases as the sorption sites are filled. Such sorption suggests very high affinity of phosphate for CeO_2 NPs. Similar experimental evidence has been reported by other studies (Ogata, Tominaga, et al., 2011, Recillas, Garcia, et al., 2012). The sorption values (for the same PO_4^{3-} concentration) differed very little in both pH values (Figures 2.2 and 2.3), suggesting pH independent sorption behavior as a function of $[PO_4^{3-}]_{initial}$ at pH 4.5 – 7 5. Comparing the total phosphate sorption between two NPs, the small NPs exhibited a greater sorption than the large NPs did at all C_{eq} values. The high surface area of the small CeO_2 NPs is likely resulting in more surface sites for dissolved phosphate.

Phosphate desorption isotherm

To assess the reversibility of sorbed phosphate, phosphate desorption experiments were conducted in samples from the phosphate sorption isotherm experiments (Figure 2.4). A large amount of desorption was observed over the course of 30 days. Under each reaction condition, predominant phosphate aqueous species are predicted to be $H_2PO_4^-$ at pH 4.5 (log activity: -3.39 for the small NP system, -3.71 for the large NP system) and HPO_4^{2-} at pH 7.5 (log activity: -3.03 for both systems). In the case of the small NPs at pH 4.5, nearly 80% of sorbed phosphate was released after 30 days. The most irreversible effect was observed in the large NP at pH 7.5. Only ~ 45% of sorbed phosphate was released at pH 4.5. Overall, the release of phosphate kinetics was biphasic. The initial fast desorption was followed by a slow continuum release up to 30 days. The release was also pH dependent in both NPs. The total PO_4^{3-} desorption decreases with increasing pH from 4.5 to 7.5. This suggests that release of phosphate was not occurring via ligand (hydroxyl) exchange mechanisms. One can postulate the following mechanism for dissolution of $CePO_4$ bulk/surface precipitates. First, the saturation index of $Ce(III)PO_4$ was calculated using VisualMinteq ver 3.0 (Gustaffson, 2007). For the calculation, the concentration of exchangeable Ce(III) was first used as total labile Ce(III). The addition of phosphate was known to result in the formation of $Ce(III)PO_4$ in both NPs. Saturation index values of $Ce(III)PO_4$ for the large NP system are 5.95 - 6.59 at pH 4.5 and 8.76 at pH 7.5, and for the small NP system are 5.26 - 5.87 at pH 4.5 and 8.05 at pH 7.5. Greater saturation index values at higher pH values suggest that the formation of $Ce(III)PO_{4(s)}$ is enhanced with increasing pH form 4.5 to 7.5. If there is any structural Ce(III) impurity in $Ce(IV)O_2$

NPs, the surface precipitation of $Ce(III)PO_4$ cannot be excluded during the phosphate sorption. Considering the insoluble nature of $Ce(III)PO_{4(s)}$ at pH > 7, this could explain enhanced phosphate release at acidic pH.

Effects of pH and phosphate on CeO_2 NP dissolution kinetics

Figures 2.5 and 2.6 show the effect of pH and phosphate on the dissolution of CeO_2 NPs. Four different pH values (1.65, 4.45, 7.45, and 12.40) were used in the presence and absence of 100 µM PO_4^{3-} (indicated in these figures as P). The experiments at pH 7.45 and 12.40 did not yield in the dissolution of Ce (i.e., dissolution was below the detection limit of ICP-AES, 0.01 mg L^{-1}). For this reason, only the data at pH 1.65 and 4.45 are presented.

To facilitate the discussion of the dissolution data, the rate constants for Ce dissolution data were estimated using the time period 24 – 120 h as shown in Figure 2.5. The highest dissolution was found at pH 1.65 without PO_4^{3-}. It reached ~ 10 mM Ce kg^{-1} of CeO_2. The addition of PO_4^{3-} suppressed the Ce dissolution. The rate constant decreased from 0.449 to 0.038 (mM Ce kg CeO_2^{-1} h^{-1}) with the addition of PO_4^{3-} at pH 1.65 (Table 2.4). At pH 4.45, the release of Ce decreased more than 50% comparing to that in the respective systems at pH 1.65. The rate constant changes from (0.0249 to 0.0060 mM Ce kg CeO_2^{-1} h^{-1}) after with PO_4^{3-}, suggesting that PO_4^{3-} suppressed the dissolution of CeO_2. When the concentration of dissolved PO_4^{3-} was monitored during the dissolution (Figure 2.7), the release of PO_4^{3-} was near negligible at pH 1.65 and 4.45, suggesting near 100%

sorption of PO_4^{3-} on the CeO_2 surfaces. Several conclusions can be yielded from this experiment: 1) dissolution is a pH-dependent process, 2) CeO_2 NPs are insoluble at pH > 7 and 3) addition of phosphate to CeO_2 NPs inhibits the dissolution of Ce species from the NPs. Dissolution mechanisms can be postulated as follows. Proton promoted dissolution of metal oxides has been extensively studied (Schwertmann, 1991, Stumm, 1997). It is known that the surface coordination properties of H^+ form an array of surface complexes whose reactivities determine the mechanisms of many surface-controlled processes. Dissolution is generally enhanced when the activity of proton is increased. Interestingly, ligand attachment on the mineral surfaces is known to inhibit non-reductive dissolution of various metal (hydr)oxides. Pronounced effects are commonly observed when ligands (e.g., phosphate, arsenate) form inner-sphere binuclear surface complexes (Biber, Afonso, et al., 1994, Rubasinghege, 2012). The effects observed with CeO_2 NPs are similar to those expected to occur with other oxide and aluminosilicate minerals.

Figure 2.6 describes the dissolution of large CeO_2 NPs as a function of pH with and without 100 µM phosphate. The steady release of Ce is observed in all systems after 24 h and the same trend as in the small NPs is observed in the large NPs. Proton promoted dissolution is more pronounced at pH 1.65, and the total dissolution at pH 4.45 is approximately 50% of total Ce release at pH 1.65. The effects of PO_4^{3-} on CeO_2 dissolution can be clearly seen in Figure 2.6. The rate constant also supports the evidence. The addition of PO_4^{3-} suppressed the Ce dissolution. The rate constant decreased from 0.061 to 0.0268 (mM Ce kg CeO_2^{-1} h^{-1}) with the addition of PO_4^{3-} at pH

1.65 (Table 2.4). At pH 4.45, the release of Ce decreased ~ 50% comparing to that in the respective systems at pH 1.65. The rate constant changes from 0.0219 to 0.008 (mM Ce kg CeO_2^{-1} h^{-1}) after addition of PO_4^{3-}, suggesting that PO_4^{3-} suppressed the dissolution of CeO_2. The rapid reduction of [PO_4^{3-}] in the system at pH 1.65 and 4.45 can be observed in Figure 2.8, indicating that the surface coverage of PO_4^{3-} was quickly achieved less than 5 h.

When the total Ce dissolution was compared between two NPs, total Ce release was more than twice in the large NPs. At pH 1.65, the small NP features [Ce] of around 10 mM Ce kg^{-1} CeO_2 for both added PO_4^{3-} and no added PO_4^{3-}; the large NP features [Ce] close to 30 mM kg^{-1} CeO_2 for no PO_4^{3-} added and close to 25 mM Ce kg^{-1} CeO_2 when PO_4^{3-} was added. For pH 4.45, the small NP values were around 3 mM Ce kg^{-1} CeO_2 for no PO_4^{3-} added and around 2 mM Ce kg^{-1} CeO_2 for added PO_4^{3-} while the large NP values were around 15 mM Ce kg^{-1} CeO_2 (no PO_4^{3-}) and 10 mM Ce kg^{-1} CeO_2 (added PO_4^{3-}). In general, greater surface area of solids enhances the dissolution. Therefore, greater dissolution would normally be expected in smaller NPs. However, this is not the case. The larger release of Ce by the large NPs is probably attributed to the different exchangeable Ce(III) in each solid. As discussed earlier (Table 2.1), exchangeable Ce(III) in the large NPs was around three times greater than that in the small NPs.

2.6 Summary

The dissolution of manufactured CeO_2 NPs was studied as a function of pH in the absence and present of phosphate. Small and large uncapped CeO_2 NPs (average particle size: 33 nm and 78 nm) had positive zeta potentials (25 and 33 mV, respectively), and large surface areas (40 m^2 g^{-1} and 11 m^2 g^{-1}, respectively). The pH dependent phosphate sorption was more pronounced in small NPs than in larger NPs. Adsorption isotherms showed that both NPs exhibited the L-type shape isotherm curve, revealing a high affinity for phosphate. Interestingly, the reversibility of sorbed PO_4^{3-} increased with decreasing pH. The dissolution of Ce(III)PO_4 surface precipitate might be controlling the dissolved PO_4^{3-} concentration. The dissolution of CeO_2 was most effective in both NPs at pH 1.65, and there was near negligible dissolution at pH > 7.5. Phosphate ligands effectively reduced the release of Ce in both NPs at pH 1.65 and 4.45.

The dissolution properties of CeO_2 NPs affected by pH and phosphate may be considered in assessing the fate of CeO_2 NPs in the aquatic and terrestrial environment. Phosphate is one of most common oxyanions present in surface and subsurface waters. The interaction between PO_4^{3-} and Ce(III) impurities in manufactured CeO_2 NPs might be critical since it greatly affects the surface charge properties and structure. Especially, the formation of Ce(III) solubility products/surface precipitates involving the binding of a metal center (like Ce(III) or Ce(IV)) to a ligand (PO_4^{3-}) to form a coordination complex could potentially control the solubility of Ce in environment.

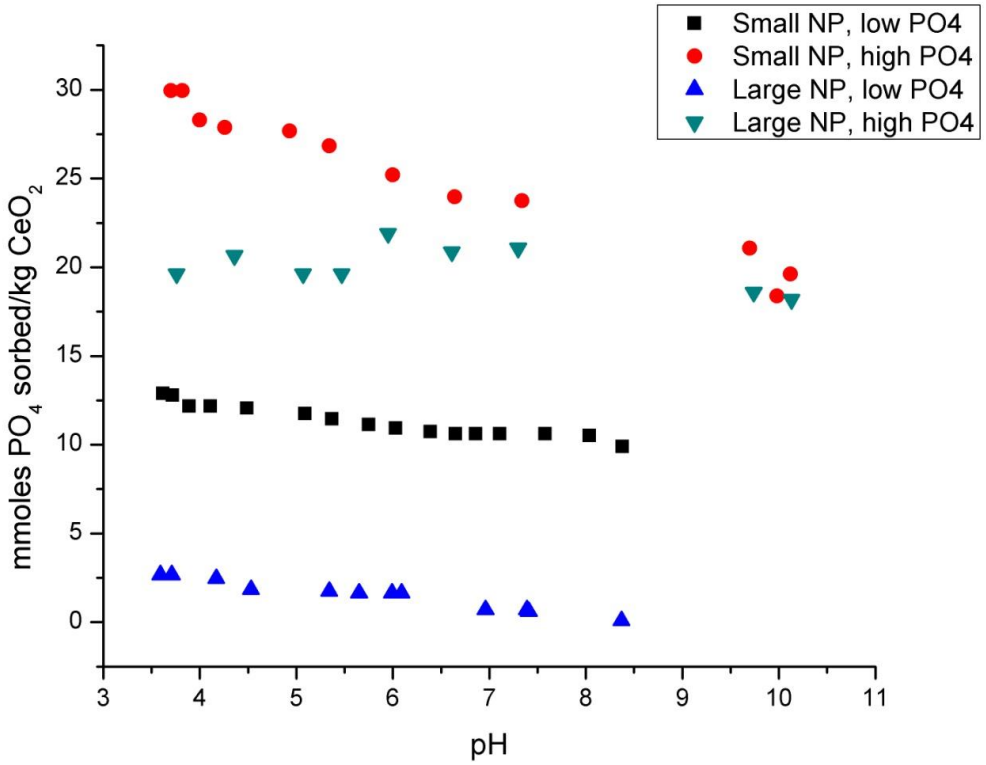

Figure 2.1. Phosphate sorption envelope onto both small (10-30 nm) and large (50-105 nm) CeO_2 nanoparticle surfaces for two different concentrations of PO_4^{3-} (standard deviation < 0.103 mmoles PO_4^{3-} sorbed kg^{-1} CeO_2).

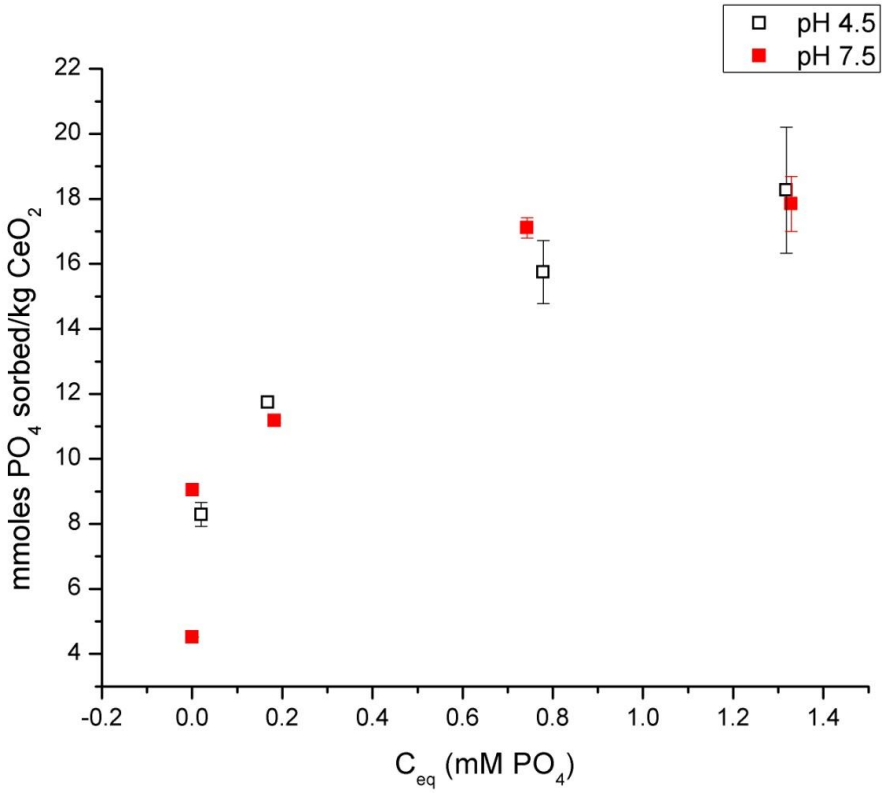

Figure 2.2. Phosphate sorption isotherm for small CeO_2 NP at pH 4.5 and 7.5.(Error bars included for all data points; some error bars are hidden within data symbols.)

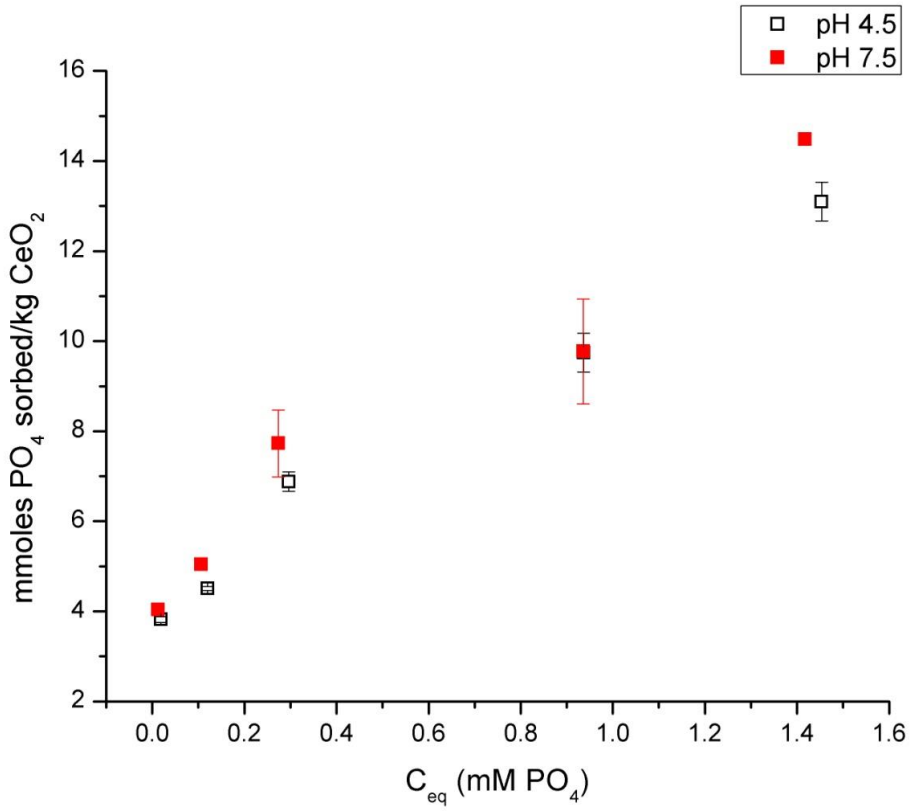

Figure 2.3. Phosphate sorption isotherm for large CeO_2 NP at pH 4.5 and 7.5. (Error bars included for all data points; some error bars are hidden within data symbols.)

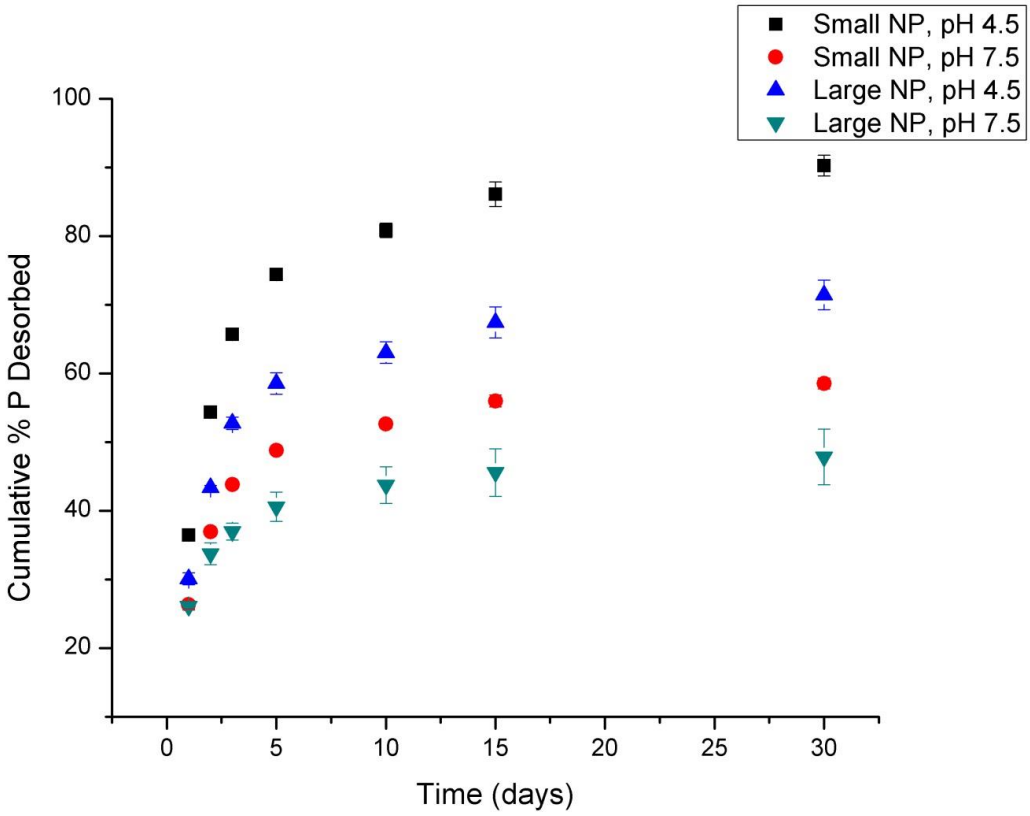

Figure 2.4. Desorption of phosphate from small and large CeO_2 NP surface at pH 4.5 and 7.5. (Error bars included for all data points; some error bars are hidden within data symbols.)

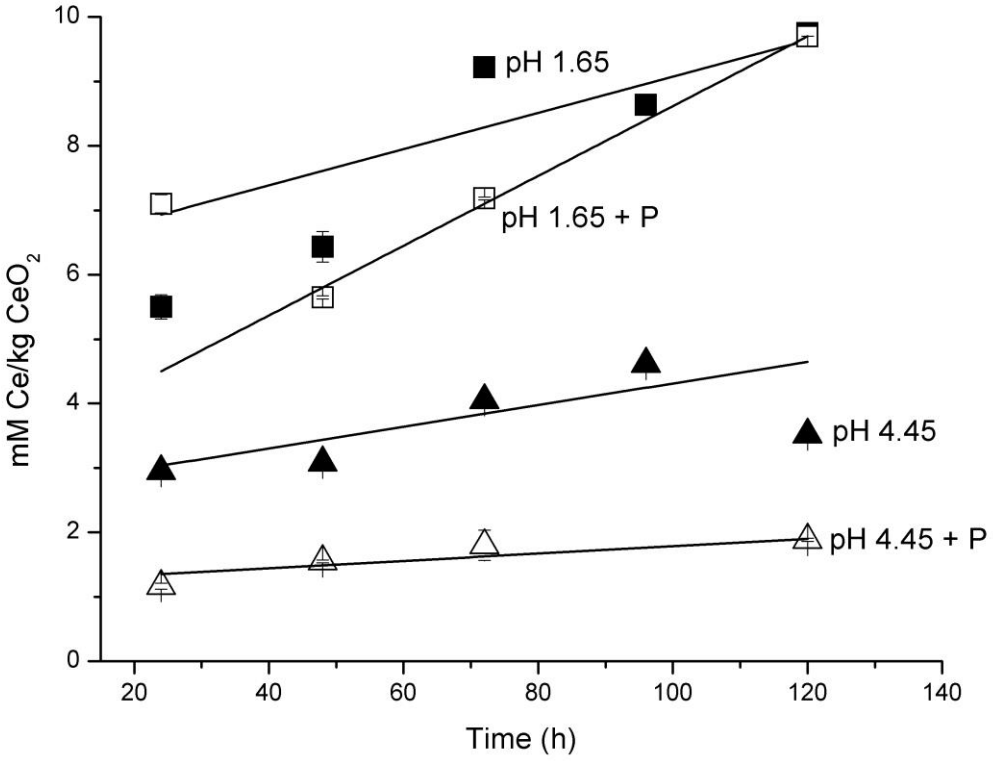

Figure 2.5. Dissolution of cerium from surface of small CeO_2 NP over five days at two different pH values in the absence and presence of 100 µM PO_4^{3-} (indicated by "P"). Lines indicate the portion of the dissolution data from which rate constants were calculated.

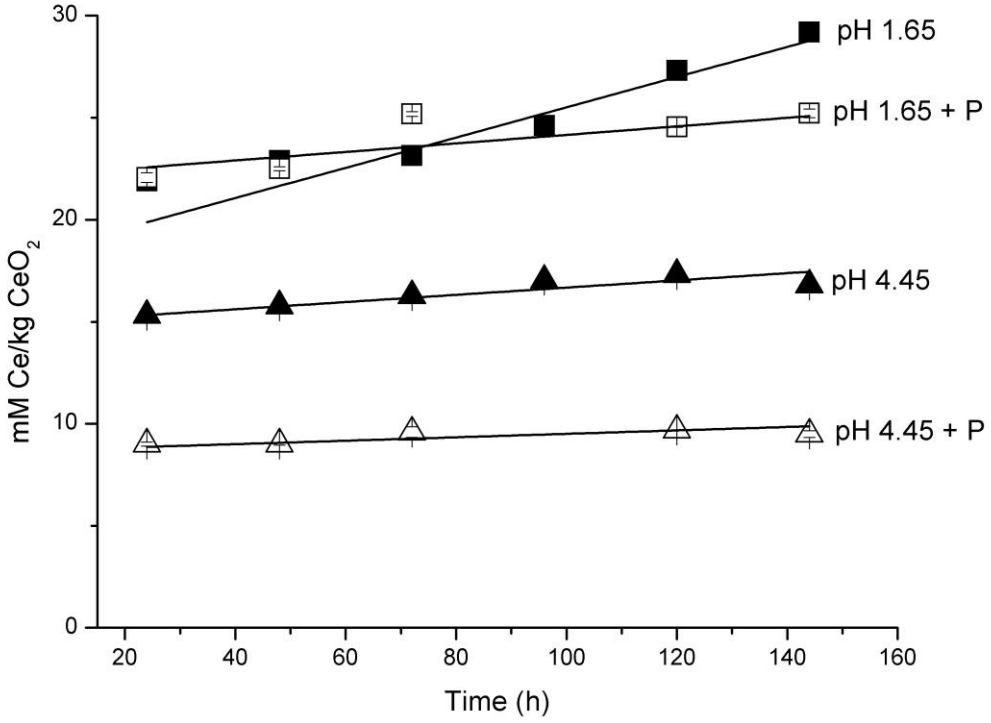

Figure 2.6. Dissolution of cerium from surface of large CeO_2 NP over six days at two different pH values in the absence and presence of 100 µM PO_4^{3-} (indicated by "P"). Lines indicate the portion of the dissolution data from which rate constants were calculated.

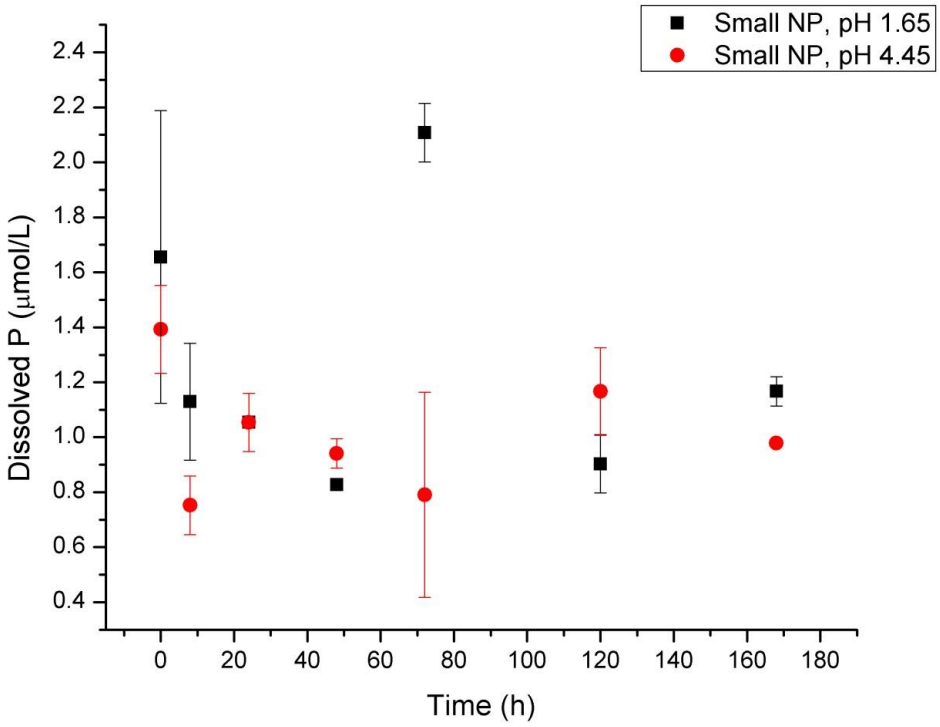

Figure 2.7. Dissolved phosphorus concentration during small cerium oxide NP dissolution experiments at two different pH values over seven days.

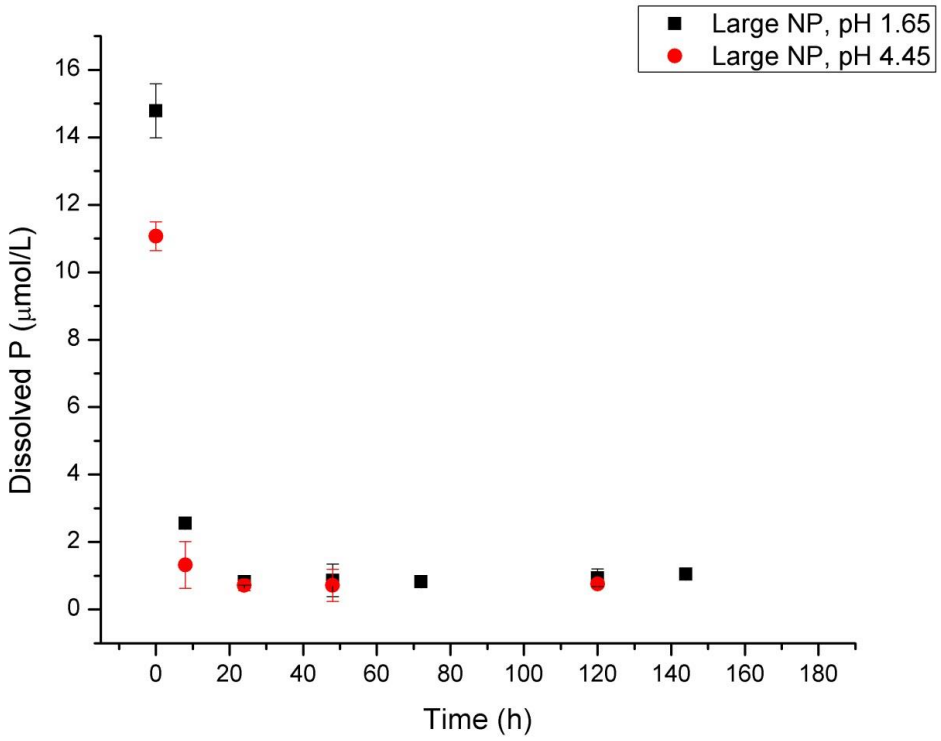

Figure 2.8. Dissolved phosphorus concentration during large cerium oxide NP dissolution experiments at two different pH values over seven days.

Nanoparticle identification	Cerium purity	Particle size (nm)	Density (g cm^{-3})	BET surface area (m^2 g^{-1})	Zeta potential (mV)	Exchange-able Ce(III) (mmoles kg^{-1})
CeO_2_S	99.9%	32.5 (± 17.5)	7.13	40 (± 10)	25.98 (± 1.92)	0.30 (± 0.001)
CeO_2_L	99.97%	77.5 (± 27.5)	7.13	11.5 (± 3.5)	33.11 (± 2.14)	1.56 (± 0.004)

Table 2.1. Characterization of physicochemical properties of manufactured cerium oxide nanoparticles. Based on the average particle size reported by Nanostructured & Amorphous Materials, Inc. (Houston, TX) and US Research Nanomaterials (Houston, TX), the following abbreviations were given: CeO_2_S for 32.5nm and CeO_2_L for 77.5nm. *The values are from dynamic light scattering analysis in this study. In the zeta potential measurement (suspension density 0.16 g L^{-1} in milli-Q water), pH of large and small NPs are is 4.05 and 4.18, respectively.

Impurity	Classification	Concentration ($mg\ kg^{-1}$)
La_2O_3	Rare earth oxide	< 86
Pr_6O_{11}	Rare earth oxide	< 36
Nd_2O_3	Rare earth oxide	< 22
Sm_2O_3	Rare earth oxide	< 10
Eu_2O_3	Rare earth oxide	< 10
Gd_2O_3	Rare earth oxide	< 10
Tb_4O_7	Rare earth oxide	< 10
Dy_2O_3	Rare earth oxide	< 10
Ho_2O_3	Rare earth oxide	< 10
Er_2O_3	Rare earth oxide	< 10
Tm_2O_3	Rare earth oxide	< 10
Yb_2O_3	Rare earth oxide	< 10
Lu_2O_3	Rare earth oxide	< 10
MgO	Alkaline earth oxide	< 12
CaO	Alkaline earth oxide	< 65
TiO_2	Transition metal oxide	< 5
Cr_2O_3	Transition metal oxide	< 5
MnO_2	Transition metal oxide	< 5
Fe_2O_3	Transition metal oxide	< 24
Co_2O_3	Transition metal oxide	< 5
NiO	Transition metal oxide	< 5
CuO	Transition metal oxide	< 5
ZnO	Transition metal oxide	< 5
Y_2O_3	Transition metal oxide	< 10
ZrO_2	Transition metal oxide	< 5
Al_2O_3	Metal oxide	13
SiO_2	Metalloid oxide	< 56
PbO	Heavy metal oxide	< 5

Table 2.2. Impurities of manufactured cerium oxide nanoparticles, CeO_2_S (10-30 nm, supplied by US Research Nanomaterials, Inc.).

Impurity	Classification	Concentration (mg kg^{-1})
La_2O_3	Rare earth oxide	< 100
Pr_6O_{11}	Rare earth oxide	< 50
Nd_2O_3	Rare earth oxide	< 100
Sm_2O_3	Rare earth oxide	< 50
Yb_2O_3	Rare earth oxide	< 0.01
CaO	Alkaline earth oxide	< 100
Fe_2O_3	Transition metal oxide	< 100
NiO	Transition metal oxide	< 0.001
CuO	Transition metal oxide	< 0.001
SiO_2	Metalloid oxide	< 100
PbO	Heavy metal oxide	< 0.001

Table 2.3. Impurities of manufactured cerium oxide nanoparticles, CeO_2_L (50-105 nm, supplied by Nanostructured & Amorphous Materials, Inc.).

	Small NP (10-30 nm)	Large NP (50-105 nm)
pH 1.65, PO_4^{3-} added	0.0380	0.0268
pH 1.65, no PO_4^{3-} added	0.0449	0.0610
pH 4.45, PO_4^{3-} added	0.0060	0.0080
pH 4.45, no PO_4^{3-} added	0.0249	0.0219

Table 2.4. Rates (mM Ce kg CeO_2^{-1} h^{-1}) for dissolution of Ce species from CeO_2 nanoparticulate surface comparing size effect, pH effect, and ligand effect.

2.7 References

Abbasi, Z., M. Haghighi, E. Fatehifar and S. Saedy. 2011. Synthesis and Physicochemical Characterization of Nanostructured Pt/CeO(2) Catalyst Used for Total Oxidation of Toluene. International Journal of Chemical Reactor Engineering 9.

Abreu, R.D. and C.A. Morais. 2010. Purification of rare earth elements from monazite sulphuric acid leach liquor and the production of high-purity ceric oxide. Minerals Engineering 23: 536-540.

Agrawal, A., K.C. Sekhar and L.P. Pandey. 1994. Spectrophotometric Determination of Ce(IV) Using O-Phenylenediamine in Steels. Bulletin of Materials Science 17: 1467-1471.

Berg, J.M., A. Romoser, N. Banerjee, R. Zebda and C.M. Sayes. 2009. The relationship between pH and zeta potential of similar to 30 nm metal oxide nanoparticle suspensions relevant to in vitro toxicological evaluations. Nanotoxicology 3: 276-283.

Biber, M.V., M.D. Afonso and W. Stumm. 1994. The Coordination Chemistry of Weathering .4. Inhibition of the Dissolution of Oxide Minerals. Geochimica Et Cosmochimica Acta 58: 1999-2010.

Bjerrum, S., and Sillen. 1958. Stability Constants of Metal Complexes, part II, London.

Clever, H.L., S.A. Johnson and M.E. Derrick. 1985. Ibid. 14.

Clever, H.L., S.A. Johnson and M.E. Derrick. 1992. Ibid. 21.

Clever, H.L. and F.J. Johnston. 1980. J. Phys. Chem. Ref. Data 9.

Cornelis, G., B. Ryan, M.J. McLaughlin, J.K. Kirby, D. Beak and D. Chittleborough. 2011. Solubility and Batch Retention of CeO2 Nanoparticles in Soils. Environmental Science & Technology 45: 2777-2782.

De, S.K. 1961. Adsorption of phosphate ion by hydrous ferric, chromic, and aluminium oxides. Part I. With inorganic materials added. Kolloid-Zeitschrift 179: 134-140.

Gottschalk, F., T. Sonderer, R.W. Scholz and B. Nowack. 2009. Modeled Environmental Concentrations of Engineered Nanomaterials (TiO2, ZnO, Ag, CNT, Fullerenes) for Different Regions. Environmental Science & Technology 43: 9216-9222.

Gustaffson, J.P. 2007. VisualMinteq. Division of Land and Water Resources, Royal Institute of Technology. Stockholm, SWE.

He, Z.L., V.C. Baligar, D.C. Martens and K.D. Ritchey. 1998. Determination of soluble phosphorus in the presence of organic ligands or fluoride. Soil Sci. Soc. Am. J. 62: 1538-1541.

Hedrick, J.B. 2004. Rare Earths. Minerals Yearbook. Vol I. Metals and MineralsUS Geological Survey, US Department of the Interior, Reston, VA.

Hedrick, J.B. and S.P. Sinha. 1994. Cerium-Based Polishing Compounds- Discovery to Manufacture. Journal of Alloys and Compounds 207: 377-382.

Hsu, P.H. and D.A. Rennie. 1962. Reactions of phosphate in aluminium systems. Part I. Adsorption of phosphate by X-ray amorphous aluminium hydroxide. Canadian Journal of Soil Science 42: 197-209.

IUPAC. 1979-1992. Solubility Data Series. Permagon Press, Oxford.

Jakupec, M.A., P. Unfried and B.K. Keppler. 2005. Pharmacological properties of cerium compounds. In: S. G. Amara, E. Bamberg, R. Jahn, W. J. Lederer, A. Miyajima, H. Murer, S. Offermanns, G. Schultz and M. Schweiger, editors, Reviews of Physiology Biochemistry and Pharmacology. p. 101-111.

Kilbourn, B. 2003. Cerium and cerium compounds. Kirk-Othmer encyclopedia of chemical technology. John Wiley and Sons, Inc., New York, NY.

Kosmulski, M. 2001. Chemical Properties of Material Surfaces. CRC Press, New York.

Limbach, L.K., R. Bereiter, E. Mueller, R. Krebs, R. Gaelli and W.J. Stark. 2008. Removal of oxide nanoparticles in a model wastewater treatment plant: Influence of agglomeration and surfactants on clearing efficiency. Environmental Science & Technology 42: 5828-5833.

Marcus, Y. 1980. Ibid. 9.

Muljadi, D., A.M. Posner and J.P. Quirk. 1966. The Mechanism of Phosphate Adsorption by Kaolinite, Gibbsite, and Pseudoboehmite. Journal of Soil Science 17.

Murphy, J. and J.P. Riley. 1986. A Modified Single Solution Method for the Determination of Phosphate in Natural-Waters. Current Contents/Agriculture Biology & Environmental Sciences: 16-16.

Ogata, F., H. Tominaga, H. Yabutani and N. Kawasaki. 2011. Phosphate Adsorption Ability of Granular Gibbsite and Cerium Hydroxide. Journal of Oleo Science 60: 133-138.

Patnaik, P. 2003. Handbook of inorganic chemicals. McGraw-Hill.

Rakicioglu, Y. and A. Akseli. 1998. New fluorimetric reagents, sodium pyrophosphate, sodium trimetaphosphate, and sodium tetrametaphosphate, for the determination of cerium(III). Journal of Fluorescence 8: 45-52.

Recillas, S., A. Garcia, E. Gonzalez, E. Casals, V. Puntes, A. Sanchez, et al. 2012. Preliminary study of phosphate adsorption onto cerium oxide nanoparticles for use in water purification; nanoparticles synthesis and characterization. Water Science and Technology 66: 503-509.

Reinhardt, K. and H. Winkler. 2002. Cerium mischmetal, cerium alloys, and cerium compounds. Ullmann's encyclopedia of industrial chemistry. Wiley-VCH, Weinheim, Germany. p. 285-300.

Rubasinghege, G.K., PK; Scherer, MM; Grassian, VH. 2012. Proton-promoted dissolution of α-FeOOH nanorods and microrods: size dependence, anion effects (carbonate and phosphate), aggregation and surface adsorption. J Colloid Interface Sci. 385: 15-23.

Schwertmann, U. 1991. Solubility and Dissolution of Iron-Oxides. Plant and Soil 130: 1-25.

Snoeyink, V.L. and D. Jenkins. 1980. Precipitation and Dissolution. Water Chemistry. John Wiley & Sons, Inc., New York. p. 243-315.

Sposito, G. 1984. Surface Chemistry of Soils. Oxford University Press, New York.

Stumm, W. 1997. Reactivity at the mineral-water interface: Dissolution and inhibition. Colloids and Surfaces a-Physicochemical and Engineering Aspects 120: 143-166.

Torrent, J., V. Barron and U. Schwertmann. 1990. Phosphate Adsorption and Desorption by Goethites Differing in Crystal Morphology. Soil Sci. Soc. Am. J. 54: 1007-1012.

van Loef, E.V.D., P. Dorenbos, C.W.E. van Eijk, K. Kramer and H.U. Gudel. 2001. High-energy-resolution scintillator: Ce(3+) activated LaBr(3). Appl. Phys. Lett. 79: 1573-1575.

CHAPTER THREE

EFFECTS OF PHYSICOCHEMICAL PROPERTIES OF CeO_2 NANOPARTICLES ON SOIL DENITRIFYING PROCESSES

3.1 Abstract

Cerium-based compounds such as nanoparticulate ceria (NP CeO_2) have received much attention in the last several years due to their popular applications in industrial and commercial uses. To understand the impact of NP CeO_2 on microbially mediated nutrient cycles, a subchronic toxicity study of CeO_2 NPs on soil denitrification process was conducted as a function of particle size (33 and 78 nm), total Ce concentration (50-500 mg L^{-1}), and speciation (Ce(IV) vs. Ce(III)). Statistical analyses on the antimicrobial effect on soil denitrifiers were conducted using both steady-state evaluation and zero-order kinetic models in order to compare the toxicity effects. It was found that soluble Ce(III) was far more toxic than Ce(IV)O_2 NPs when an equal total concentration of Ce was evaluated. Particle-size dependent toxicity, species-dependent toxicity, and concentration-dependent toxicity were all observed in this study for both the steady-state and the kinetic evaluations. It was found that all Ce species exhibited particularly strong sorption properties with soil, and there are some chemical speciation changes in small NPs. The mechanism of CeO_2 NP toxicity to soil denitrifiers can be explained in terms of Ce chemical speciation and reactivity of CeO_2 in soils.

3.2 Introduction

In the last few decades, there has been rapid growth in the number of nanotechnology application for industrial uses and consumer products. Along with nanosilver and TiO_2, cerium oxide nanoparticles (CeO_2 NPs) are one of the most widely used manufactured NPs in the global market (Hendren, Mesnard, et al., 2011). It has been reported that global nanomaterial demands will increase by 20 % per year and one estimate indicates that the global market for pure nanomaterials is expected to grow to $20.5 billion by 2015 (Palmberg and Tuomo, 2006), posing questions about the fate and toxicological impact of NPs in environment.

The environmental fate of CeO_2 NPs is highly dependent on its applications and uses. Cerium oxide nanoparticles are best known for their use as catalysts, fuel cells, glass pigmentators and polishers, and fuel additives (EPA, 2009). Although the popular usage of NP CeO_2 as a diesel fuel additive (Institute, 2001) could potentially escape in the emissions, a recent transport modeling study predicted that a major source of CeO_2 NPs to environment is likely to be from industrial processing plants (e.g., ceramic manufactures). It is likely to accumulate in sewage sludge at wastewater treatment plants, and CeO_2 discharge into the aquatic environment can be fairly limited (Limbach, Bereiter, et al., 2008). Thus, amendments of sludge to agricultural land become a major pathway of CeO_2 NP to the terrestrial environment (Cornelis, Ryan, et al., 2011). The EPA governs the allowed concentrations in biosolids of many metals with demonstrated

toxic effects; however, cerium is not one of these metals, meaning levels are unmonitored and unregulated (EPA, 2007). Unfortunately, due to the relativeness newness of discovery of CeO_2 NP environmental chemistry as a field, the impact of CeO_2 NPs on ecosystem health (e.g., toxicological effects on aquatic-terrestrial organisms) has not been well understood.

In general, there are two major considerations for NP toxicity: physical (e.g., size effects) and chemical effects (e.g., dissolution of ionic species). Nanoparticle toxicity characteristically exhibits size-dependent effects. For a large variety of NPs including species such as nano-silver, -silicon dioxide, and -titanium dioxide it has been demonstrated that smaller sizes (and thus larger reactivities) lead to heightened toxicity effects across biological systems. Nanoparticles tend to exhibit much higher toxicities than their bulk counterparts; this tendency is especially exaggerated in bacteria due to the NP's higher affinity for attachment to bacterial cell walls (Jiang, Mashayekhi, et al., 2009) that could potentially perturb the electron transfer reaction and respiration. Capping agents (or lack thereof) also play a large part in NP toxicity. Capping agents stabilize NPs by covering a large portion of their surface area and preventing aggregation as well as introducing multiple functionalities such as enhanced solubility effects. Polymers are popular capping agents along with other organic materials (Lead and Smith, 2009).

Chemical toxicity has also been reported for a variety of NPs (carbon nanotube, fullerenes and TiO_2): cellular damage by reactive oxygen species (ROS) and dissolution of toxic ions/species. A primary mechanism of NP toxicity is the ability to generate ROS such as free radicals (Lead and Smith, 2009). Reactive oxygen species contain unpaired valence electrons which yield extremely high chemical reactivity and the ability to induce severe damage to cells, including DNA and RNA damage, oxidations of lipids and proteins, and enzyme (cytochrome P) deactivation. The release of metal ions from quantum dots (e.g., CdSe) and nanosilver can be highly toxic to bacterial cells (Liu, Sonshine, et al., 2010, Lubick, 2008) as well as organic coatings of NPs (Hoshino, Fujioka, et al., 2004, Mahendra, Zhu, et al., 2008).

In the case of CeO_2 NPs, both physically- and chemically-driven effects have been shown in recent investigations. Particle size-dependent toxicity was reported in a soil nematode, *Caenorhabditis elegans* (Roh, Park, et al., 2010), and in the bacteria *E. coli* (Pelletier, Suresh, et al., 2010) and *B. subtilis* (Pelletier, Suresh, et al., 2010). Several studies also showed concentration dependent toxicity to bacteria such as *E. coli* (Pelletier, Suresh, et al., 2010, Thill, Zeyons, et al., 2006) and *B. subtilis* (Pelletier, Suresh, et al., 2010), the aquatic cyanobacteria *Anabaena* CPB4337 (Rodea-Palomares, Boltes, et al., 2011) and the green alga *P. subcapitata* (Rodea-Palomares, Boltes, et al., 2011, Rogers, Franklin, et al., 2010). Interestingly, there are several reports showing no acute toxicity of CeO_2 NPs on two crustaceans *Daphnia magna* and *Thamnocephalus platyurus* (up to 5,000 mg L^{-1})

(Hoecke, Quik, et al., 2009) and no growth inhibitory effect on *S. oneidensis* (Pelletier, Suresh, et al., 2010).

While these studies provided fundamental knowledge on CeO_2 NP toxicity, causes of toxicological response to these organisms still remain unclear since most studies have failed to document the role of Ce chemical speciation with respect to its toxicity. Cerium oxide nanoparticles are most often noted for their catalytic and antioxidant properties, which are largely affected by redox state of Ce. The nanoparticles are often largely composed of Ce(III) (up to 55 % in some cases) as well as Ce(IV); the more Ce(IV) in the nanoparticles, the stronger the catalase mimetic activity (Babu, Velez, et al., 2007, Heckert, Karakoti, et al., 2008, Ivanov, Shcherbakov, et al., 2010, Karakoti, Monteiro-Riviere, et al., 2008, Nalabotu, Kolli, et al., 2011, Pirmohamed, Dowding, et al., 2010, Rzigalinski, Bailey, et al., 2003). Furthermore, Ce(III) is a more soluble form than Ce(IV) at environmentally relevant pH values (e.g., 4.5-7.5).

To gain a comprehensive understanding of CeO_2 NP toxicity, it seems critical to elucidate the speciation of Ce (i.e., trivalent or tetravalent). To address the relative importance of reduced soluble $Ce(III)_{(aq)}$, subchronic toxicity studies were performed with Ce(III) and CeO_2 NPs on soil denitrifying bacterial communities in reduced soils. The response of the soil microbial community is important since recent studies have indicated that land application of biosolids to agricultural soils may be a major environmental exposure pathway (Limbach, Bereiter, et al., 2008) for CeO_2 NPs. In soils, denitrification processes

readily take place and are an extremely important part of the global nitrogen cycle. Denitrifying bacteria such as *Pseudomonas*, *Bacillus*, and *Alcaligenes* serve to metabolize N-containing compounds via nitrate reductase and other important enzymes to turn oxides back into nitrogen gas or nitrogen oxides for energy generation. The denitrification process also has the benefits of ameliorating eutrophication and removing excess nitrate from drinking water; however, it is also capable of limiting primary productivity and contributing to global warming via nitrous oxide formation. Thus, characterization of toxicological effects of CeO_2 NPs to soil denitrifiers is strongly necessary as the scientific community moves forward in its understanding of the effect of NPs on soil bacteria as a whole.

In this study, batch denitrification experiments were conducted as a function of reaction conditions (e.g., particle sizes, concentration, and Ce speciation (Ce(III) vs. NP CeO_2)). The effects on denitrification process are discussed using the results of NP characterization (particle size, ratio of Ce(III)/Ce(IV), zeta potential) and solid state Ce speciation data using X-ray absorption near edge structure spectroscopy (XANES) analysis.

3.3 Materials

Soil Characterization

Surface soils (top 10 – 30 cm) of Toccoa sandy loam (coarse-loamy, thermic typic Udifluvents) were collected from the Clemson University organic farm (SC, USA) from an unfarmed side plot (in order to avoid composition change in bacteria from farming, nitrogen fixation disruption, etc.). The soils were collected in May and September of 2012. Characterization of soils was reported in the work by VandeVoort, et al. (VandeVoort and Arai, 2012). Cation exchange capacity (CEC), % organic matter (OM), and pH are 7.4 $cmol_c\ kg^{-1}$, 1.5% and 5.2 ± 0.2, respectively. The clay mineralogy is quartz, kaolinite, hydroxyl interlayer vermiculite, gibbsite, hematite, and goethite.

Reagents

All reagents were prepared in degassed distilled deionized Milli-Q water (18.2 MΩ) unless otherwise mentioned in the text. The following ACS grade salts were used: cerium(III) sulfate octahydrate (Alfa Aesar, Ward Hill, MA), dextrose (D-glucose) anhydrous, sodium nitrate (Fisher Scientific, Pittsburgh, PA) and sodium sulfate (JT Baker, Phillipsburg, NJ).

Cerium Nanoparticle Characterization

Cerium oxide nanoparticles of two different sizes (small, 10 – 30 nm and large, 50 – 105 nm) were obtained from commercial companies (US Research Nanomaterials, Inc.

Houston, TX and Nanostructured & Amorphous Materials, Inc. Houston, TX). Physicochemical properties of NPs are summarized in Table 2.1. Lanthanide impurities in the small and large NPs were also assessed to ensure that no cytotoxic effects could result from concentrated impurities (Tables 3.5 and 3.6)

3.4 Methods

Ce(III) and CeO_2 NP Sorption Isotherm in Soils

All experiments were conducted in duplicate under ambient conditions (22 ± 1.2 ^{o}C and $pCO_2 = 10^{-3.45}$ atm) unless otherwise mentioned in the text. A 6.2 (± 0.02) g portion of air dry soil was transferred to each 50 mL Nalgene tube. A 15 mL portion of 0.017 M Na_2SO_4 was added to each tube and the tubes were sealed and placed on a turn-over shaker overnight. After 24 h of shaking, 15 mL of Ce(III) sulfate solution or CeO_2 NPs was added to each tube in order to constitute samples at 50, 100, 250, and 500 mg L^{-1} $[Ce]_T$. The pH of each sample was adjusted to 5.5 with 0.1 M NaOH, and the tubes were sealed and shaken for an additional 24 h. After shaking, Ce(III) samples were centrifuged at 17000 rpm for 10 min, then a 5 mL aliquot was drawn out with a syringe and filtered through 0.2 µm Millex® polyvinylidene fluoride (PVDF) syringe filters. The NPs were centrifuged at 17000 rpm for 50 min and aliquots were filtered through 0.2 µm PVDF filters. The centrifugation method was calculated using modified Stokes' law. Filtrates were immediately acidified and analyzed for $[Ce]_T$ using ICP-AES. Cerium sorption in soils was analyzed in order to develop a context for the sorption properties of cerium

species after they were added to the denitrification batch experiments and to determine if a large portion of the cerium species were likely sorbing to colloidal surfaces or remaining in solution. The soils were determined to have a high sorption capacity for Ce(III) (100% sorption of Ce at concentrations up to 200 mg L^{-1}).

Phosphate Sorption Isotherm in Soils

To simulate the reaction condition of denitrification experiments, the following reagents were chosen (0.017 M Na_2SO_4 as a background electrolyte and 30 mM of sodium acetate buffer at pH 4.5). Portions of 6.2 $\pm$ 0.02 g of oven dry soils were weighed, and transferred into 50 mL Nalgene high speed centrifuge tubes. Soil suspensions were hydrated in 20 mL of 0.017 M Na_2SO_4 solutions for 24 h, and then an appropriate amount of 400 mM sodium acetate buffer solution at pH 4.5 was added to assure the final volume of 30 mL, $[P]_{total}$= 0.10–1.30 mM and sodium acetate buffer = 30 mM. The pH was readjusted to 4.5 (± 0.1) using 1 M HNO_3. The tubes were then shaken on an end-over shaker at 12 rpm for 48 h. After 48 h, the samples were centrifuged at 10,000 rpm for 13 min. Then, 5 mL of each supernatant solution were filtered through 0.20 µm Whatman polyvinylidene difluoride (PVDF) filters. Samples were acidified with 10 % HNO_3 and then analyzed for phosphate using ICP-AES.

Batch Denitrification Experiments

Batch denitrification experiments were conducted in duplicate to evaluate the effect of CeO_2 NPs on the denitrification process. The following physical and chemical conditions

were varied: particle size (33 and 78 nm), $[Ce]_T$ = 0, 50, 100, 250 mg L^{-1}, Ce speciation (Ce(III) VS. Ce(IV)O_2 NPs). Cerium nanoparticle stock solutions (12.29 g L^{-1}) were freshly prepared in 0.017 M sodium sulfate that was used in the denitrification experiment. The use of high Ce concentrations was to meet the detection limit of X-ray absorption spectroscopic analysis in this study

Fifty ($\pm$ 0.03) g of fresh moist soil (at field capacity) was transferred into a 200 mL of background solution (1 % glucose, 50 mg L^{-1} NO_3^- as sodium nitrate, and 0.017 M sodium sulfate). Each 250 mL Nalgene bottles, which were wrapped with aluminum foil, were placed inside an anaerobic chamber for 24 h preceding sample constitution. After the 200 mL of solution was constituted for each soil sample, the bottles were kept in the glove bag. Caps were loosened to allow gaseous nitrogen species to escape during the incubation study. At each sampling period (every 3 h up to 70 h), the bottles were shaken and redox potential and pH values were immediately measured. Soil solution aliquots of 5 mL were taken and then filtered through PVDF 0.45 µm filters. Nitrate concentration was measured using a nitrate ion selective electrode (Analytical Sensors & Instruments Ltd., Sugar Land, TX). The use of the ISE is advantageous in these experiments because the sample is immediately analyzed without matrix modification. The ISE limits of detection of nitrate (0.4 to 70 mg L^{-1}) as well as pH and temperature demands of the instrument (pH range 2.5 to 11, 0 to 21 $\pm$ 20 ^oC) are well-suited for experimental conditions. A standard curve (0.1-5 mg L^{-1} NO_3^-) was generated using the same background matrices of soil solutions in the denitrification experiments. Known

interferences (ClO_4^-, I^-, ClO_3^-, F^-) for this ISE were found to be negligible. The nitrate analysis was repeated every 3 – 6 h until the denitrification process was complete (the nitrate levels in the samples dropped to below 1 mg L^{-1}). The assessment of toxicity was conducted using the steady-state approach for both 50% nitrate depletion and 90% nitrate depletion as well as with zero-order kinetic models to analyze the denitrification rate. The application of zero order kinetic models for the soil denitrification process has been demonstrated by several other researchers in the past (Boaventura and Rodrigues, 1997, Dawson and Murphy, 1972, van Haandel, Ekama, et al., 1981). In order to understand the statistical significance of each data set, T-tests were conducted using JMP®10 statistical software (Cary, NC).

Synchrotron based X-ray Microprobe Analysis

Synchrotron based micro(μ)-XRF mapping (50-10,000 μm^2) was conducted on denitrification samples (as thin sections) at beam line X27A at National Synchrotron Light Source, Upton, NY.

This beam line is suited for Ce L_3 absorption energy (5,723 eV), and can conduct microfocused X-ray absorption near edge structure analysis to understand micron-scale valence state and or phase determination of Ce in soils. Cerium nanoparticle-reacted soils samples were used to prepare a thin section (30 μm) according to the method described by Arai et al., 2007 (Arai et al., 2007). Spent denitrification batches were first filtered through Whatman-2 filters, and air-dried in the anaerobic glove bag for 2 weeks. This

drying process was necessary for the Epotek 301 resin (Epoxy Technology, Inc. Billerica, Massachusetts, US) to cure at room temperature. To eliminate the background metal(loid) impurities, quartz slides and super glue were used for this process, as these materials have proven to be near metal(loid) free, which is necessary for backing materials during the μ-XRF analysis. The μ-XRF compositional maps of Ce were conducted at above the Ce K absorption edge using a Canberra SL30165 Si(Li) detector. Eleven spots were sampled for each map and of these, the three to four most representative spots with the cleanest spectra were featured in the reported data.

3.5 Results and Discussion

Sorption isotherm

Sorption of Ce(III) as well as small and large Ce(IV)O_2 NPs was evaluated in Toccoa sandy loam (soil properties are summarized in Table 3.1) at $[Ce]_{total}$ = 25, 50, 100, 200, and 500 mg L^{-1}. The Ce(III) sorption isotherm is shown in Figure 3.1. A typical L-shape isotherm curve (Sposito, 1984) shows that slope decreases as concentration increases since unreacted sites decreases as the sorption sites are filled. Such sorption suggests high affinity of Ce(III) in the soils. The Freundlich model (Figure 3.1b) shows a K_d value of 1198 L kg^{-1}. While sorption mechanisms cannot be elucidated without spectroscopic evidence, the retention could be indirectly described by a combination of adsorption on variable-charged mineral surfaces and the formation of bulk precipitates. When the dissolved PO_4^{3-} concentration was monitored during the Ce(III) sorption, it decreases

with increasing [$Ce(III)_{(aq)}$ from 50 mg L^{-1} to 500 mg L^{-1} (Figure 3.2), indirectly suggesting the complexation of $Ce(III)_{(aq)}$ with dissolved PO_4^{3-} soil solution. In fact, the saturation index was supersaturated with respect to bulk $Ce(III)PO_4$ when the initial [Ce(III)] and Mehlich 1 extractable PO_4^{3-} (35 mg kg^{-1}) were used in the chemical speciation calculation using VisualMinteq ver. 3.0 (Gustaffson, 2007).

Due to the strong retention (> 98%) of CeO_2 NPs in soils at all initial Ce concentrations, the equilibrium concentration of Ce in soil solutions was near zero. For this reason, sorption isotherm plots for CeO_2 NPs are not shown. Instead, the distribution coefficient, K_d = (added [Ce as CeO_2] - [Ce] in filtrate)/([Ce] in filtrate), was estimated. The distribution coefficient for small and large NPs ranged from 5,101 to 102,039 L kg^{-1}, and from 5,356 to 71,427 L kg^{-1}, respectively. These values cover the K_d value previously reported by Cornelis et al. (Cornelis, Ryan, et al., 2011) in work reporting the sorption of bulk CeO_2 salts in 16 different Australian soils with varying physical and chemical properties. When soils were reacted with 11.7 mmol kg^{-1} bulk CeO_2, the resultant K_d value was 136,355 L kg^{-1}. Unlike in the Ce(III) sorption isotherm, the changes in dissolved PO_4^{3-} concentration are not clearly correlated with Ce addition as CeO_2 NPs. Instead, low concentrations remain (~ 0.01 – 0 04 mg L^{-1}) (Figure 3.2). This might be attributed to the strong PO_4^{3-} retention in CeO_2 NPs (covered in the discussion section in Chapter 2). While the sorption isotherm provides important information about Ce affinity in soils, the chemical state of Ce in Ce(III) and CeO_2 NPs reacted soils remains

unknown. The following section discusses synchrotron based X-ray microprobe analysis of Ce(III) and CeO_2 NP-reacted soils samples.

Synchrotron based X-ray microprobe analysis

X-ray fluorescence maps of Ce are shown in Figure 3.3a. Cerium hot spots with high concentrations appear as in yellowish green in each map. When soils were reacted with $Ce(III)_{(aq)}$, the expected results were diffused large areas assuming that Ce(III) would adsorb on soil inorganic and organic components. Instead, Ce occurrences appear as hot spots (Figure 3.3a). Similarly, several hot spots in CeO_2 NPs reacted soils (Figures 3.3b and 3.3c). To better understand the chemical speciation of Ce in these soils, microfocused XANES data are discussed below.

Figure 3.4 summarizes the Ce speciation of hot spots in Figure 3.3a. Spectra were compared with known Ce(IV) sulfate and Ce(III) phosphate reference compounds. The Ce(III) shows a single whiteline peak at ~ 5723 eV, while Ce(IV) species have two whitelines (~ 5723eV and ~ 5732 eV). In the soil sample, all XANES spectra contain a single whiteline peak, indicating the presence of Ce (III). When the pre- and post-edge features are compared, the spectra at three hot spots resemble that of $Ce(III)PO_4$. It is likely that some of Ce(III) was precipitated out with soluble phosphate in soils. Overall, the XANES analysis suggests that $Ce(III)PO_4$ species will not readily undergo oxidative transformation to Ce(IV) in the suboxic soils.

Figure 3.5 summarizes the micro-XANES spectra of NP reacted soils with several Ce reference compounds ($Ce(III)PO_4$ and $Ce(III)_2S_3$) including small and large CeO_2 NPs. The doublet feature in CeO_2 NPs indicate that CeO_2 NPs are at the predominantly Ce(IV) state. Interestingly, small $Ce(IV)O_2$ NPs seemed to undergo reduction in soils while large CeO_2 NPs remain as Ce(IV). In Chapter 2, the sorption capacity of PO_4^{3-} in two NPs was discussed. While both NPs strongly retain PO_4^{3-}, the reversibility of PO_4^{3-} was less in the large NPs. This might indirectly suggest the formation of $Ce(III)PO_4$ surface precipitates that were formed with exchangeable Ce(III) in large NPs. Since $Ce(III)PO_4$ is extremely insoluble, such mineral coatings potentially inhibit the electron transfer reaction in large NPs, resulting in lack of reduction in soils.

Batch denitrification experiments

Values for denitrification rates and depletion end-points are summarized in Table 3.2. The results of zero order kinetic modeling are shown in Figures 3.8, 3.9, and 3.10; from the equation of the line, the 90% and 50% depletions time were calculated by solving for the time at which only 5 mg L^{-1} and 25 mg L^{-1} NO_3-N remained in each sample. Rate data and depletion time data are interpreted separately; first, depletion time data will be discussed. Figures 3.11, 3.12, and 3.13 summarize pH and Eh values that were monitored during the denitrification process for Ce(III), small CeO_2 NPs, and large CeO_2 NPs, respectively. As denitrification progressed, pH values fluctuated between 5 and 5.7. Eh values became more and more negative, indicating the reaction condition was becoming more reduced over time. To better understand the effect of chemical speciation and

particle size, t-test statistical analysis was conducted on 1) steady-state endpoint data and 2) zero order kinetic rate as a function of chemical species and particle size. Below, the results of the steady-state endpoint analysis and the kinetic rate analysis are discussed separately, and then summarized.

Steady-state endpoint analysis

Figure 3.6 shows a histogram of the 90% nitrate depletion times for all species and concentrations. It can be seen in Table 3.2 that the 90% depletion times for all species across all concentrations differed significantly from the control vessel; thus, it can be concluded that all species suppressed the soil denitrification process. When the 50% depletion times were calculated, almost all of the 50% depletion time also differed from the control vessel, with the exception of 50 mg L^{-1} small NP and 250 mg L^{-1} large NP. The 90% depletion time for the control vessel (0 mg L^{-1} Ce) was a short 32.1 hours. Each species (ionic Ce(III), Ce(IV) as small Ce(IV)O_2 NP, and Ce(IV) as large Ce(IV)O_2 NP) was evaluated for toxicity at 50, 250, and 500 mg L^{-1}. Again, the use of high Ce concentrations was to meet the detection limit of X-ray absorption spectroscopic analysis in this study. It can clearly be seen that for each species, the 90% depletion time increases with increasing concentration of Ce. The 50% depletion time is also shown to increase with increasing concentrations of Ce.

Steady state: effects of concentration

By far, ionic Ce(III) exhibited the highest toxicity of the three Ce species. At 50 mg L^{-1} Ce(III), the 90% depletion time was increased to 37.6 h. Increasing the concentration to 250 mg L^{-1} caused a drastic rise in 90% depletion time to 42.8 h; further increasing the concentration to 500 mg L^{-1} raised the 90% depletion time to 60 h. Statistical tests revealed that the 90% depletion times for all three concentrations differed significantly from each other (Table 3.3); thus, ionic Ce(III) exhibits concentration-dependent toxicity effects on nitrate depletion time in soil denitrification processes. The increase in depletion time with increasing concentration does not appear to follow a linear fashion; a 5x increase from 50 mg L^{-1} to 250 mg L^{-1} only raised the 90% depletion time by 5.2 h, whereas an additional 2x increase from 250 mg L^{-1} to 500 mg L^{-1} raised the 90% depletion time by a drastic 17.2 h. The observed dose-response relationship is consistent with normal toxicological expectations. For the 50% depletion times, only the Ce(III) species exhibited concentration-dependent toxicity.

The mechanism of Ce(III) toxicity to soil denitrifiers is not well-defined; however, based on the available literature, a likely mechanism can be postulated. Many of the lanthanides have been identified as ATPase inhibitors (Gruner, Sehrt, et al., 1992, Palasz and Czekaj, 2000). Lanthanides function so efficiently as ATPase inhibitors due to their ionic radii, which are extremely similar to that of Ca(II). In particular, Ce(III), is able to substitute for Ca(II) extremely well (Jakupec, Unfried, et al., 2005). This calcium-swapping feature allows for suppression of the activities of Ca(II) ions and it is the foundation of

cytophysiological effects of the lanthanides. It is postulated that the isomorphic capabilities of the ions allow them to replace Ca(II) in the binding sites of nucleases, thus interrupting activation and preventing growth metabolism of bacteria (Balusamy, Kandhasamy, et al., 2012). The effects of Ce(III) specifically as a Ca(II) ATPase inhibitor have not been studied thoroughly; however, the strong ability of other lanthanides (with less ability to easily substitute for Ca(II) than Ce(III) has) leads to the conclusion that an important cytotoxic pathway for Ce(III) could definitely be that of Ca(II) ATPase inhibition, as well as ATPase inhibition in general.

Normally, a trend is seen in toxicological literature revealing markedly more toxic effects for smaller nanoparticles than for larger nanoparticles (of the same species) (Carlson, Hussain, et al., 2008, Choi and Hu, 2008, Karlsson, Gustafsson, et al., 2009, Napierska, Thomassen, et al., 2009, Pan, Neuss, et al., 2007, Pelletier, Suresh, et al., 2010, Roh, Park, et al., 2010). However, the opposite effect was seen for CeO_2 nanoparticles in this study (small NP at 10-30 nm and large NP at 50-105 nm). Though this observation is counterintuitive, it can be explained by the relative Ce(III) impurities in the nanoparticles. The large CeO_2 NPs had much greater exchangeable Ce(III) impurity (1.56mM kg^{-1}) than the small CeO_2 NPs (0.3 mM kg^{-1}); since toxicity is controlled largely by Ce(III) species and not Ce(IV)(Ce(IV) is insoluble at pH > 3), it is likely that the nanoparticulate species able to yield more Ce(III) release would also cause more toxicity.

Like Ce(III), an unfortunately small amount of literature exists detailing possible toxicity mechanisms of CeO_2 NPs to denitrifying bacteria. However, the mechanism of CeO_2 NP toxicity is well-defined for other bacteria, especially *E. coli*; thus, it can be hypothesized that the mechanism is likely similar in denitrifiers. Multiple studies support the phenomena of CeO_2 NP adsorption to the outer membrane of bacterial cells without penetration (He, Kuang, et al., 2012, Kuang, He, et al., 2011, Pelletier, Suresh, et al., 2010, Thill, Zeyons, et al., 2006). Once adsorbed, the ratio of Ce(IV):Ce(III) has been shown to decrease sharply, indicating reduction of the Ce species taking place at the cell surface. Significant cytotoxicity has been associated with this adsorption and concurrent reduction, revealing that the surface adsorption of the NPs is associated with oxidative stress in the bacterial cells (Thill, Zeyons, et al., 2006). It has been confirmed that direct contact of the NPs with the surface of bacterial cells results in an increase in intracellular ROS levels, thus inducing cytotoxicity (Kuang, He, et al., 2011). In conclusion, the mechanism of toxicity for CeO_2 NPs to denitrifiers can likely be described as follows: the NPs adsorb to the surface of bacterial cells, but do not penetrate the cells. The direct contact between the cell and the NP results in reduction of Ce species, thus inducing oxidative stress in the bacterial cells. This oxidative stress leads to increased ROS production and, thus, cytotoxic effects.

Earlier, possible mechanisms of Ce(III) toxicity to soil denitrifiers were discussed. It is important to note that a discussion of ceria cytotoxicity would be incomplete without also considering the large amount of Ce(III) impurity that is inherent in the NPs (some

manufacturers have reported up to 55% Ce(III) impurity). Again, in the denitrification study, though all species showed significant toxicity, the NP-treated soils exhibited much less inhibition of denitrification (and thus, denitrifier toxicity) than the ionic Ce(III)-treated soils. Along with their Ce(III) impurities, CeO_2 NPs also tend to have a large amount of lanthanide impurities which could lend to further ATPase inhibition and cytotoxicity at high enough concentrations. At experimental conditions and concentrations, it is unlikely that the lanthanide impurities could be playing a role in observed cytotoxic effects (Tables 3.5 and 3.6), but the Ce(III) impurity is significant enough to possibly contribute (Table 2.1). For each lanthanide impurity, the literature was reviewed in order to assess the lowest known concentration for which toxicity effects are observed in bacteria. Since the literature on lanthanide oxides is very sparse, not all impurities have been studied for bacteria. For the impurities with no published bacterial toxicity studies, references were accumulated for other organisms. Several species featured no studies showing toxicity to any organism, but rather featuring beneficial effects. The results of this literature review are summarized for both the small and large NP impurities in Tables 3.5 and 3.6, which indicate that the lanthanide impurities in the NPs are not present in high enough concentrations to contribute to the observed toxic effects. It should also be noted that lanthanides have been demonstrated to feature the same strong affinity for phosphate as Ce (Aime, Botta, et al., 1998, Atkinson, Murray, et al., 2006, Majdan and Zdenek, 1993, Sherry, 1997) and thus, similar to Ce species, may become bound in natural systems and thus unavailable to lend to cytotoxic effects. In

conclusion, the lanthanide impurities in the NPs are not causing any toxicity effects due to a combination of low concentrations and little bioavailability.

For both nanoparticulate species, it should be made clear that concentration values denote the concentration of total Ce, not the concentration of CeO_2. Thus, the concentration 50 mg L^{-1} denotes 50 mg L^{-1} of Ce added in the form of CeO_2 NP. For the small NP, the addition of 50 mg L^{-1} Ce to the denitrification vessel slowed the 90% depletion time to 36.6 h. This value is comparable to the 90% depletion times for Ce(III) at 50 mg L^{-1} (37.6 h) and the large NP at 50 mg L^{-1} (37.7 h). In fact, at 50 mg L^{-1}, none of the 90% depletion times are significantly different from each other (Table 3.3). For the small NP at 250 mg L^{-1} the 90% depletion time was 38.1 h and at 500 mg L^{-1} the time was slowed to 38.8 h. Though mathematically the 90% depletion times did increase with increasing concentration, statistical tests revealed no significant difference between any of the concentrations for the small NP (Table 3.3). This suggests that the 90% nitrate depletion time for the small CeO_2 NP is not concentration-dependent.

The large NP featured similar 90% depletion times; however, statistics did reveal concentration-dependent toxicity for the large NP (Table 3.3, $Ce(IV)_l50$ vs 500). The 90% depletion time at 50 mg L^{-1} was 37.7 h; at 250 mg L^{-1}, the time increased barely to 38.3 h; and lastly, at 500 mg L^{-1}, the 90% depletion time slowed further to 41.6 h. Thus far, concentration-dependent toxicity has been discussed. Size-dependent toxicity and species-dependent toxicity are also important considerations.

Steady state: effects of particle size

Size-dependent toxicity for the nanoparticles can be determined by comparing two different sized nanoparticles at the same concentration. As seen in Table 3.3, the 90% depletion times for the NPs at both 50 mg L^{-1} and 250 mg L^{-1} were not statistically different. However, at 500 mg L^{-1} the small and large NP exhibit significant differences in 90% depletion times. Thus, it can be concluded that size-dependent toxicity effects on 90% depletion time do exist for the NPs (though these effects may only be detectable for "high" concentrations). The same statistical trends exist for the 50% depletion time data.

Steady state: effects of Ce chemical species

Like size-dependent toxicity, species-dependent toxicity was also only featured at the 500 mg L^{-1} concentrations across species. As seen in Table 3.3, the comparisons at 50 mg L^{-1} and 250 mg L^{-1} were not significant when the small and large NPs were compared to Ce(III); however, Ce(III) at 500 mg L^{-1} showed significant difference from both the small NP at 500 mg L^{-1} and the large NP at 500 mg L^{-1} in terms of 90% depletion time. This should be attribute to the difference in exchangeable Ce(III) impurity in these NPs (see Ch2). Thus, species-dependent toxicity effects on 90% depletion time also exist for Ce compounds. The same statistical trends exist for the 50% depletion time data.

Kinetic analysis

Rate data is also important to consider for any toxicological assessment. Figure 3.7 indicates the denitrification rate data for all species and concentrations. An interesting

visual trend can be observed in this figure: denitrification rates for Ce(III) and the large CeO_2 NP decrease with increasing Ce concentration, but the denitrification rates for the small CeO_2 NP actually increase with increasing concentration. This trend disagreement is the reason it is important to perform steady state (nitrate depletion time) analysis as well as kinetic (rate) analysis.

Kinetic: effects of concentration

Denitrification rates are reported in terms of mg L^{-1} of NO_3-N depleted per hour (mg L^{-1} h^{-1}). The denitrification rate in the control vessel was 2.33 mg L^{-1} h^{-1} (Table 3.2). It can be seen in Table 3.2 that the kinetic rates for almost all vessels differed significantly from the control vessel; however, there were a few exceptions. The rate for the small NP at 500 mg L^{-1} did not differ significantly from the control; the rates for the large NP at both 50 mg L^{-1} and 250 mg L^{-1} also did not differ significantly. The Ce(III) species rates differed from the control at all three concentrations while the small NP differed at two concentrations and the large NP differed at only one concentration. The lack of differences for the NPs is not largely meaningful in terms of the results of this study; if anything, this lack of differences reinforces the much stronger denitrification inhibitory effects of ionic Ce(III) species vs. CeO_2 NPs as demonstrated in the steady state analysis. It should also be noted that all Ce species kinetic rates were mathematically lower than the control vessel, though all rates did not statistically differ significantly.

The smallest kinetic rate indicates the slowest progression of denitrification and thus the most inhibitory, or toxic, effect. For Ce(III), kinetic rates slowed as the Ce concentration was increased. This type of behavior is expected typically in toxicological studies. At 50 mg L^{-1}, the kinetic rate was 1.91 mg L^{-1} h^{-1}; at 250 mg L^{-1}, the rate was slowed to 1.74 mg L^{-1} h^{-1}; and finally at 500 mg L^{-1} the rate was again decreased to 1.93 mg L^{-1} h^{-1}. Statistical analysis revealed that the rate at 500 mg L^{-1} differed significantly from the rate at both 50 mg L^{-1} and 250 mg L^{-1}, indicating concentration-dependent rate toxicity effects for Ce(III).

For the small NP, the addition of 50 mg L^{-1} Ce to the denitrification vessel slowed the kinetic rate to 1.52 mg L^{-1} h^{-1}. Surprisingly, the addition of more Ce did not slow the denitrification rate, but instead quickened it. At 250 mg L^{-1}, the denitrification rate increased to 1.77 mg L^{-1} h^{-1} and at 500 mg L^{-1} the rate jumped again to 1.93 mg L^{-1} h^{-1} (which did not differ significantly from the control).Though mathematically the kinetic rates did decrease with increasing concentration, statistical tests revealed no significant difference between any of the concentrations for the small NP (Table 3.4). This means that the denitrification kinetic rate for the small CeO_2 NPs is not concentration-dependent.

The large NP featured much faster kinetic rates than the small NP. Generally, smaller NPs are expected to yield in greater toxicity to bacterial processes (Choi and Hu, 2008, Napierska, Thomassen, et al., 2009, Pan, Neuss, et al., 2007). In the previous X-ray

microprobe analysis, Ce chemical speciation was not altered during the 30 d of incubation. It was nearly all Ce(IV), supporting the lack of Ce toxicity (i.e., fast kinetic rate). At 50 mg L^{-1} the kinetic rate for the large NP was 2.23 mg L^{-1} h^{-1}. This value, as well as the value for 250 mg L^{-1} (2.17 mg L^{-1} h^{-1}) did not differ significantly from the control. The kinetic rate at 500 mg L^{-1} (1.90 mg L^{-1} h^{-1}) did differ significantly from the control, but not from the kinetic rate of small NP at the same concentration. Given the increasing rate trend of the small NP and the decreasing rate trend of the large NP, it is likely a safe assumption that the expected behavior (slower rates for large NP) would have been observed had the concentration range been extended to include higher values. However, for the concentration range studied, Ce(III) and the large NP became more inhibitory with increasing concentration and the small NP became less inhibitory with increasing concentration. Statistical analysis revealed concentration-dependent toxicity effects on denitrification rate for the large NPs (Table 3.4, Ce(IV)l 250 vs 500).

Kinetic: effects of particle size

Size-dependent toxicity effects are the only area where the steady-state analysis and the kinetic rate analysis strongly disagree. As seen in Table 3.4, the denitrification rates for the NPs at both 250 mg L^{-1} and 500 mg L^{-1} were not statistically different. At these concentration, the strong sorption NPs (K_d: 5,101 to 102,039 L kg^{-1} for small NPs, and from 5,356 to 71,427 L kg^{-1} for large NPs) reduce the availability of NPs in soil solutions, resulting in the diminished particle size dependent toxicity. However, at 50 mg L^{-1} the small and large NP exhibit significant differences in depletion times. Thus, it can

be concluded that size-dependent toxicity effects on depletion time do exist for the NPs (though these effects may only be detectable for "low" concentrations).

Kinetic: effects of Ce chemical species

When all three species are compared at identical concentrations, statistical tests reveal significant differences between Ce(III) and small NP at 500 mg L^{-1} (1.35 mg L^{-1} h^{-1} and 1.93 mg L^{-1} h^{-1}, respectively) as well as significant differences between Ce(III) and the large NP at both 250 mg L^{-1} (1.35 mg L^{-1} h^{-1} and 2.17 mg L^{-1} h^{-1}, respectively) and 500 mg L^{-1} (1.35 mg L^{-1} h^{-1} and 1.90 mg L^{-1} h^{-1}, respectively) (Table 3.4). Thus, species-dependent toxicity effects exist on denitrification rate and Ce(III) is more toxic than the nanoparticulate Ce species at the same concentration. Another interesting result of species comparisons is that the kinetic rate for the small NP at 500 mg L^{-1} (1.93 mg L^{-1} h^{-1}) and for the large NP at 500 mg L^{-1} (1.90 mg L^{-1} h^{-1}) are extremely similar to the kinetic rate for Ce(III) at the much lower concentration of 50 mg L^{-1} (1.91 mg L^{-1} h^{-1}). At tenfold the concentration of ionic Ce(III) species, the NP species have the same effect on kinetic rate. This supports the conclusion that ionic Ce(III) species much more strongly suppress the denitrification processes than do CeO_2 NP species.

3.6 Summary

The results of the steady state and kinetic analysis agreed strongly for almost all considerations. Conclusions supported by both the steady state and the kinetic analysis are as follows.

The first major conclusion of the statistical analyses is that the Ce species used in this study do exhibit depletion time and denitrification rate toxicity effects to soil denitrifying bacteria. For the steady state analysis, the 90% depletion times of all species at all concentrations differed significantly from the control vessel. For the kinetic rate analysis, the kinetic rates of all species differed from the control vessel for at least concentration.

The second major conclusion is that the ionic Ce(III) and the large CeO_2 NP exhibit concentration-dependent toxicity effects on both depletion time and kinetic rate. However, for both analyses, the small CeO_2 NP was not shown to exhibit any concentration-dependent effects.

The third major conclusion is where the results of the statistical analyses differ. In terms of steady state toxicity, the large NP was found to be significantly *more* toxic than the small NP when both were at the same concentration (500 mg L^{-1}). Thus, size-dependent toxicity effects are observed in the NPs and the large NP was found to suppress denitrification more strongly than the small NP in terms of depletion time. However, in

the kinetic rate analyses, it was found that the large NP was significantly *less* toxic than the small NP at the same concentration (50 mg L^{-1}). Thus, size-dependent toxicity effects again were observed, but this time the small NP was found to suppress denitrification more strongly than the large NP in terms of kinetic rate. The strong NP retention in soils might be providing greater opportunities for microbes to be exposed.

The fourth major conclusion is that ionic Ce(III) is significantly more toxic than the small CeO_2 NP or the large CeO_2 NP when all three are at the same total Ce concentration (500 mg L^{-1}). Thus, species-dependent toxicity was clearly observed and ionic Ce(III) exhibited significantly more toxic effects on depletion time and denitrification rate than either NP. X-ray microprobe analysis of Ce(III) spiked soils showed that trivalent state Ce(III) was retained in soils.

It can be seen by comparing these four major conclusions that the results from the steady state and kinetic analyses only disagree in one way: whether the small or large NP is less toxic. The steady-state analysis finds that size-dependent toxicity is only detectable at high concentrations while the kinetic rate analysis only predicts size-dependent toxicity at low concentrations. As previously stated, it is likely that the results of the kinetic rate analysis would possibly agree with the steady state findings that the large NP is more toxic if the concentration range had been expanded to include higher levels of Ce. However, it must be taken into account that 1) changes occur in the microbial community in soils, and 2) changes in NP physical properties occur as well. The bacterial community

could have shifted as the NPs underwent phase transformation which would likely impact denitrification kinetics. Furthermore, if NPs gradually disperse/aggregate, this would also likely affect denitrification kinetics. The strong sorption affinity for Ce(III) to soils was demonstrated in Figure 3.1, confirming the clear likelihood of physicochemical transformation of the Ce species via sorption mechanisms. Cerium species are already fairly insoluble and are even more insoluble when PO_4^{3-} ligand is present, as demonstrated in Chapter 2. This conclusion, coupled with the results from Chapter 3, support the possibility that Ce species have a large potential to build up in sediments over time; thus, toxicological studies such as these detailing the environmental fate and reactivity of CeO_2 NPs are largely necessary.

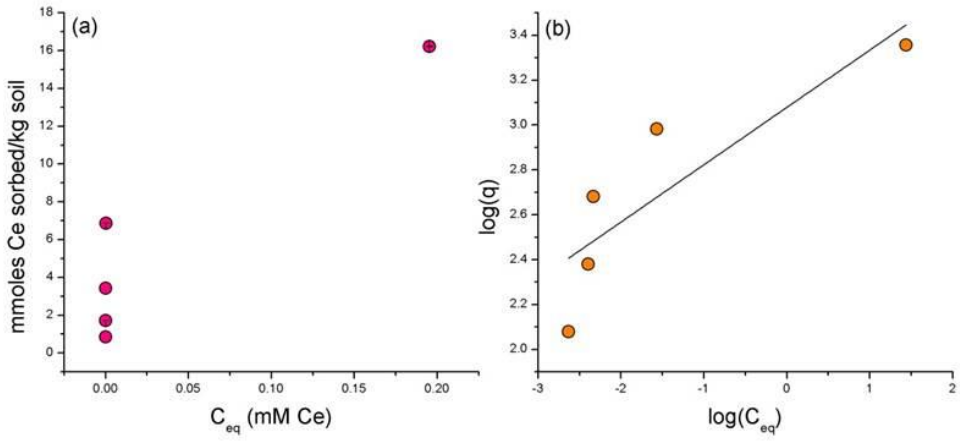

Figure 3.1. Sorption data in Toccoa sandy loam soil for Ce(III) as $Ce(III)(NO_3)_3$. Data is shown as a) sorption isotherm plot for Ce(III) and b) Freundlich model for the Ce(III) isotherm. Error bars indicate one standard deviation above and below value.

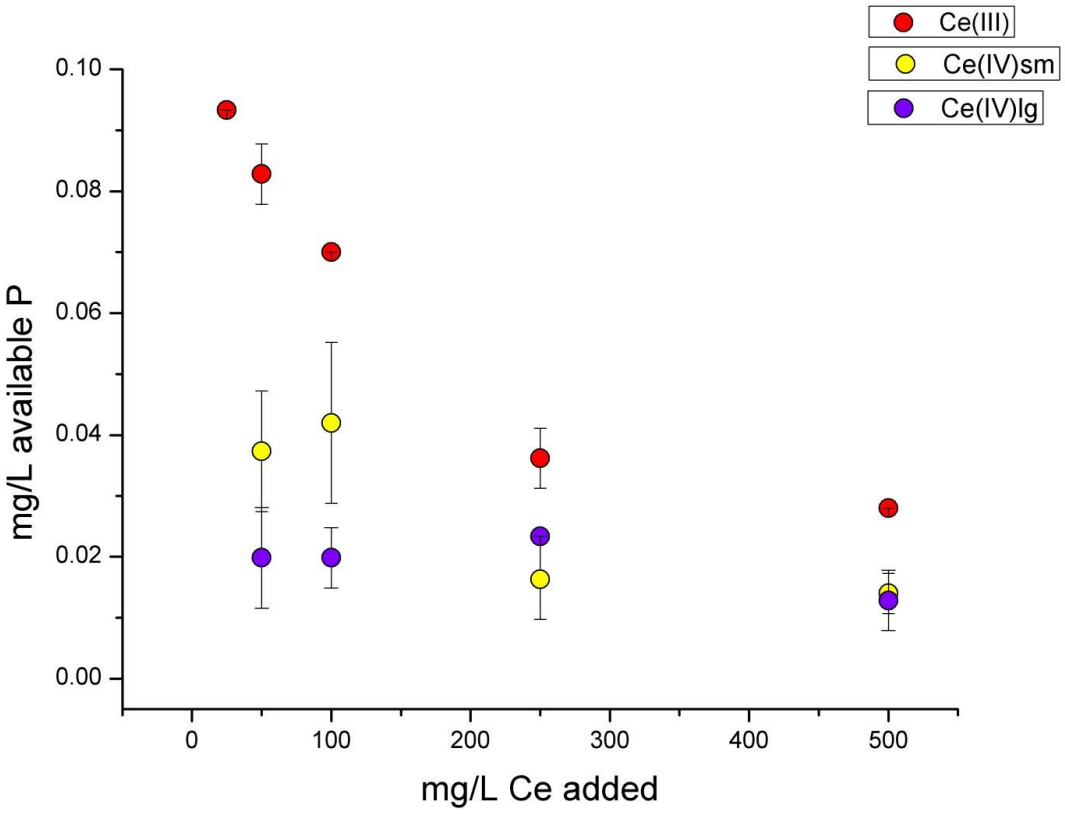

Figure 3.2. Dissolved phosphate concentration during Ce(III)or CeO_2 NPs sorption in Toccoa sandy loam shown in Figure 3.1. a) [PO_4^{3-}] during Ce(III) sorption, b) [PO_4^{3-}] during CeO_2small NP sorption, and c) [PO_4^{3-}] during CeO_2 large NP sorption. Error bars indicate one standard deviation above and below value.

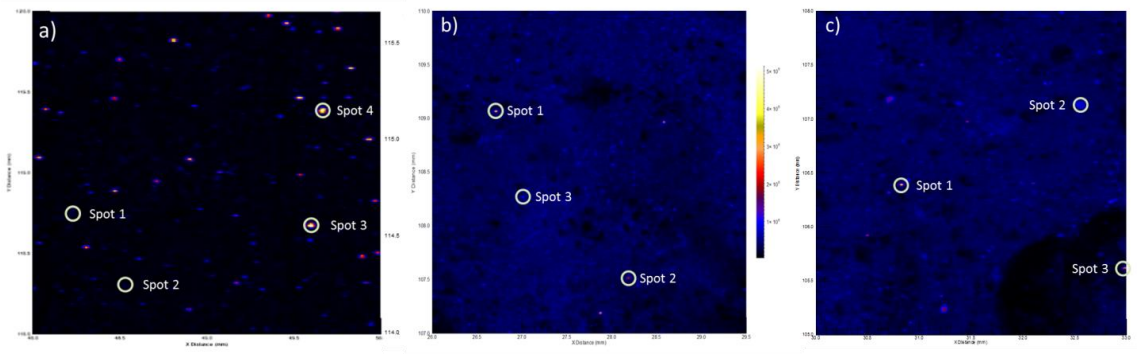

Figure 3.3. Microfocused(μ)-XRF maps of Ce $L_{\beta 1}$ fluorescence line in Toccoa entisol soil samples amended with a) Ce(III)(H: 2 mm X V: 2 mm), b) small CeO_2 NP (H: 3 mm X V: 3.5 mm), and c) large CeO_2 NP (H: 3 mm X V: 3 mm). The intensity of each color pixel is proportional to the relative concentration of the corresponding element. Spots (open white circles) indicate areas where μ-XANES spectra were taken (displayed in Figures 3.4 and 3.5).

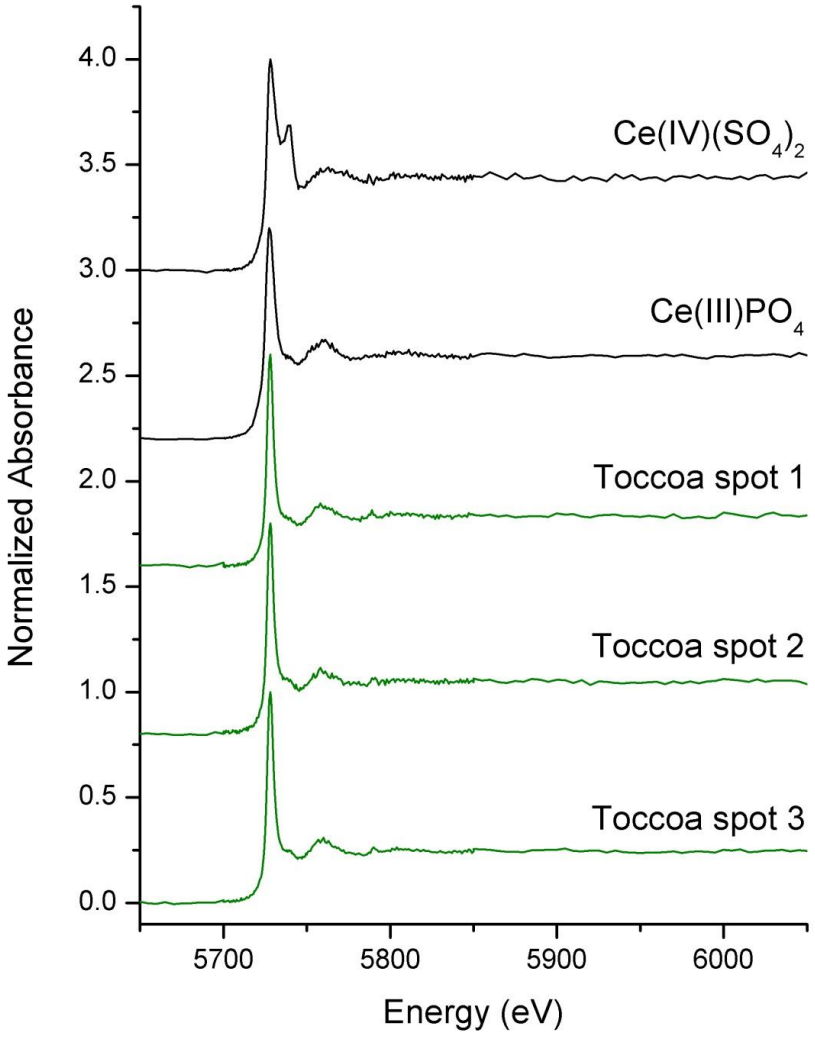

Figure 3.4. Normalized microfocused(μ) Ce L_3-edge XANES spectra of Ce reference compounds ($Ce(IV)(SO_4)_2$, $Ce(III)PO_4$), and selected spots from μ-XRF maps of Ce(III)-treated soils shown in Figure-3.3a.

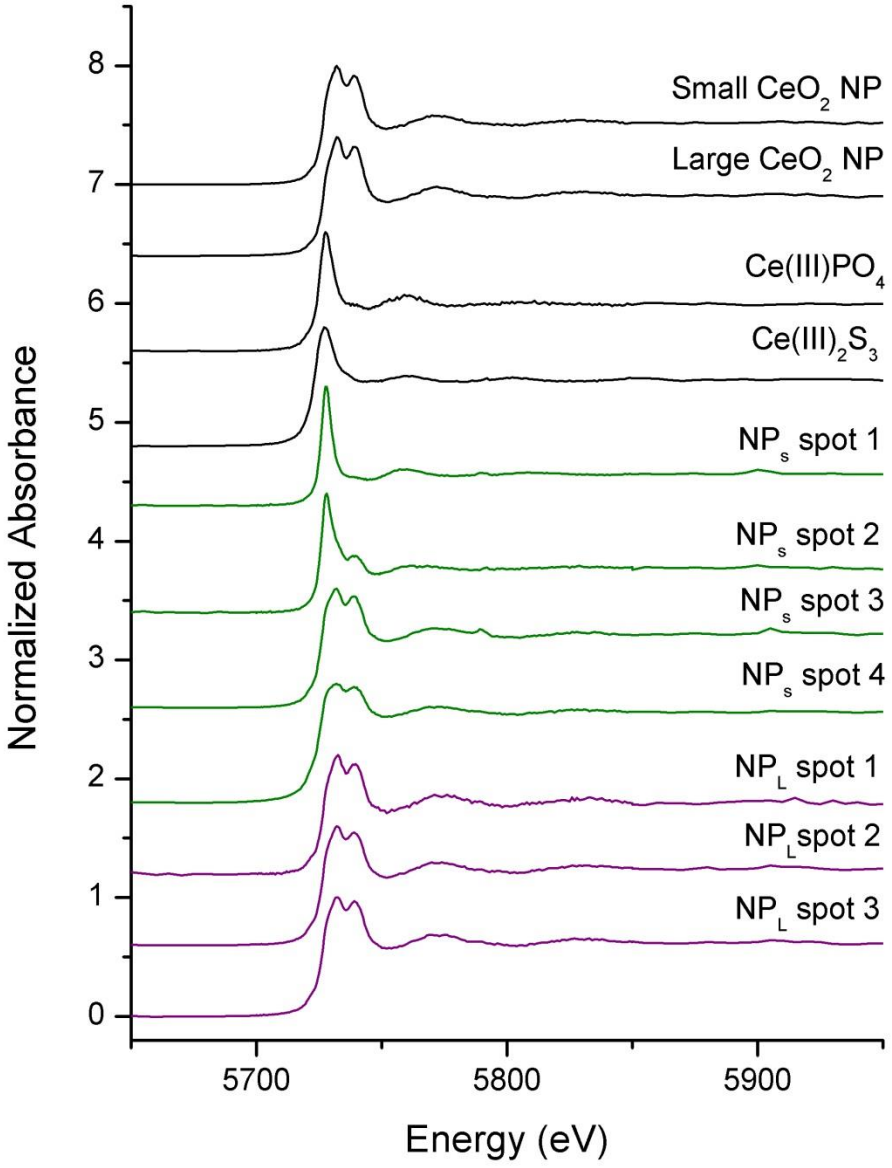

Figure 3.5. Normalized microfocused(μ) Ce L_3-edge XANES spectra of Ce reference compounds (small Ce(IV)O_2 NP, large Ce(IV)O_2 NP, Ce(III)PO_4, Ce(III)$_2S_3$), and selected spots from μ-XRF maps of NP-treated soils shown in Figures 3.3b and 3.3c.

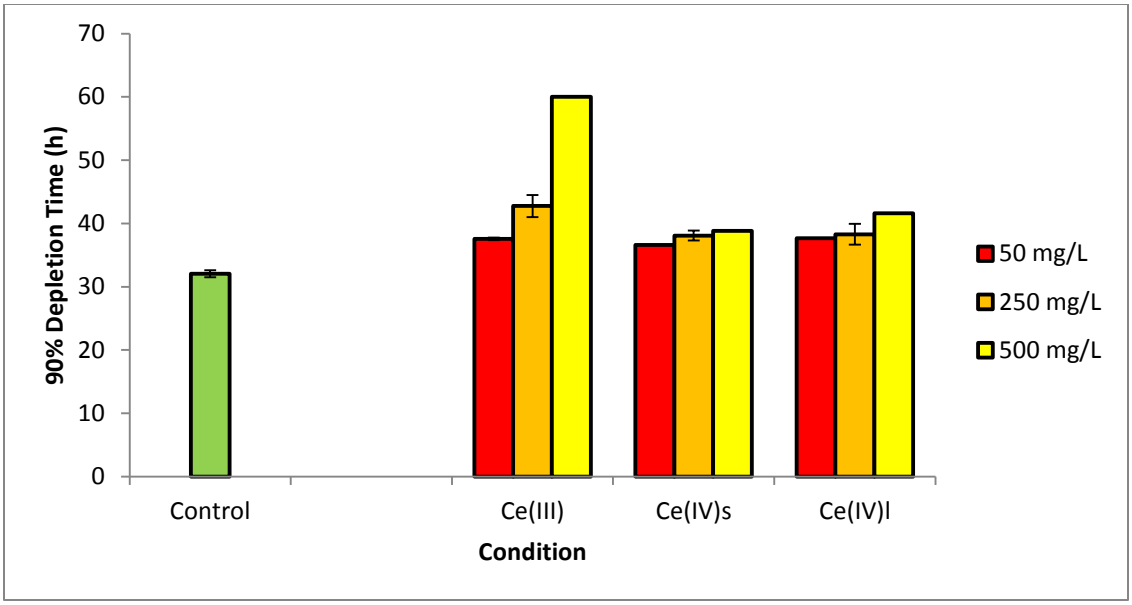

Figure 3.6. Histogram of denitrification activity in Toccoa sandy loam as indicated by 90% nitrate depletion time. Time is measured from the point of maximum [nitrate] until [nitrate] decreases to < 5 mg L^{-1}. For each of the three sets Ce(III), small NP (Ce(IV)s), and large NP (Ce(IV)l), the first bar corresponds to a concentration of 50 mg L^{-1} added Ce; the second bar, 250 mg L^{-1}; the third bar, 500 mg L^{-1}. The control bar corresponds to a concentration of 0 mg L^{-1} added Ce.

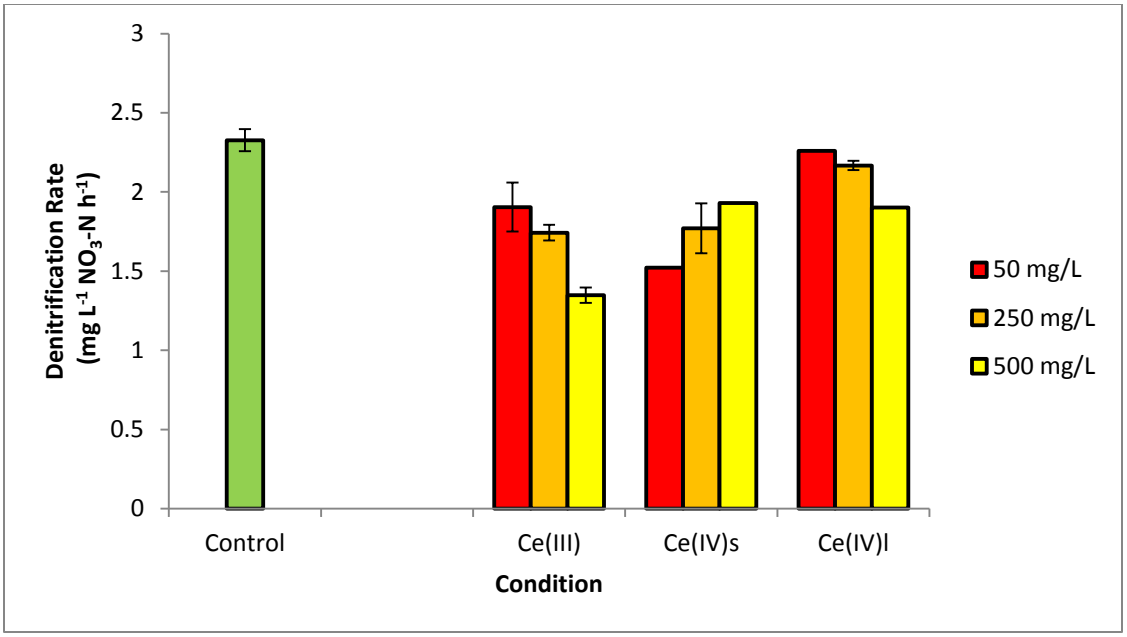

Figure 3.7. Histogram of denitrification zero-order kinetic rates in Toccoa sandy loam. Kinetic fits for the rates shown in this figure are displayed in Figures 3.8, 3.9, and 3.10 below. For each of the three sets (Ce(III), small NP (Ce(IV)s), and large NP (Ce(IV)l)), the first bar corresponds to a concentration of 50 mg L^{-1} added Ce; the second bar, 250 mg L^{-1}; and the third bar, 500 mg L^{-1}. The control bar corresponds to a concentration of 0 mg L^{-1} added Ce.

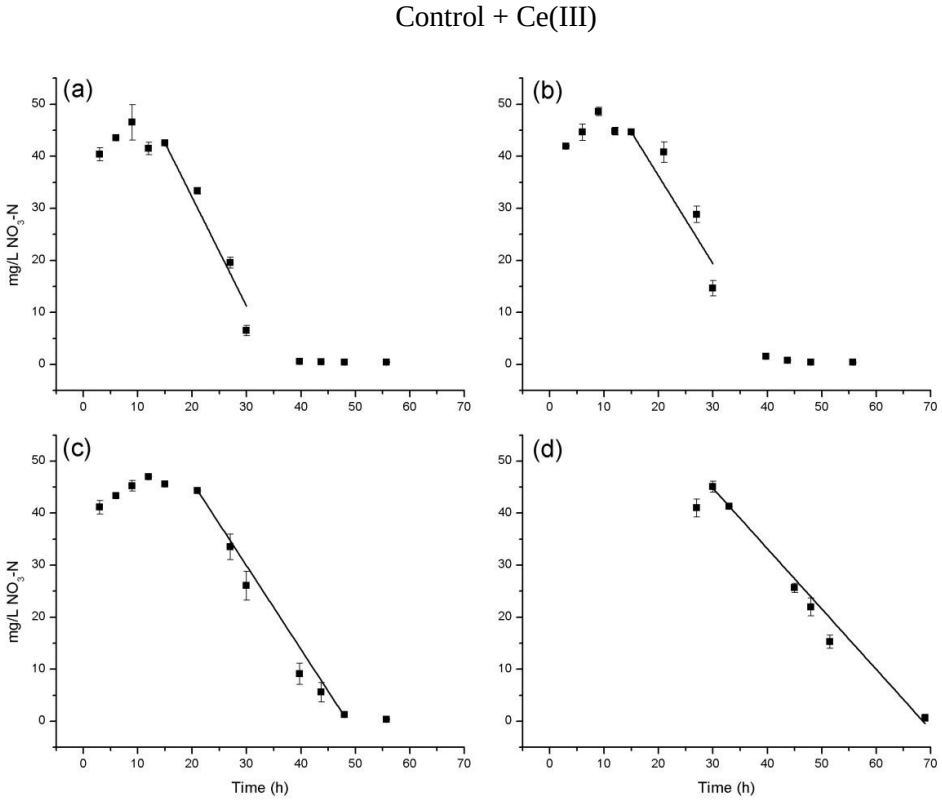

Figure 3.8. Denitrification kinetic data of native soil bacteria in a reducing environment. Each graph displays nitrate depletion over time for one batch per treatment condition. The line represents zero-order kinetic modeling, and corresponds to values listed in Table 3.2. Each graph represents a different reaction condition: a) control; b) Ce(III) at 50 mg L^{-1}; c) Ce(III) at 250 mg L^{-1}; d) Ce(III) at 500 mg L^{-1}. All Ce(III) was added in the form of cerium(III) sulfate octahydrate.

Control + Small NP

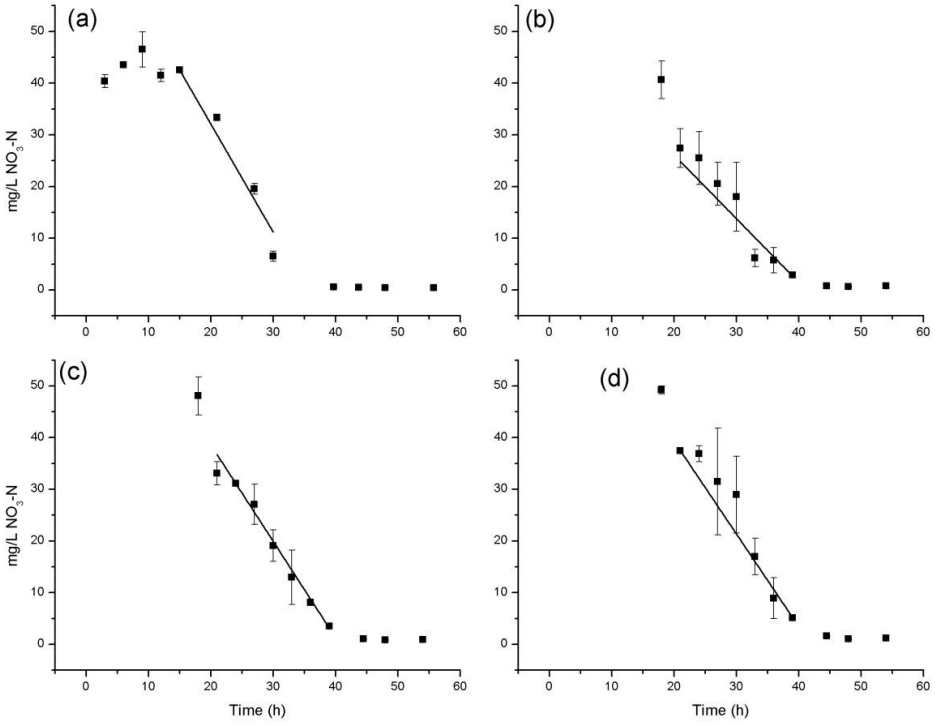

Figure 3.9. Denitrification kinetic data of native soil bacteria in a reducing environment. Each graph displays nitrate depletion over time for one batch per treatment condition. The line represents zero-order kinetic modeling, and corresponds to values listed in Table 3.2. Each graph represents a different reaction condition: a) control; b) Ce(IV) at 50 mg L^{-1}; c) Ce(IV) at 250 mg L^{-1}; d) Ce(IV) at 500 mg L^{-1}. All Ce(IV) was added in the form of small (10-30 nm) cerium oxide nanoparticle.

Control + Large NP

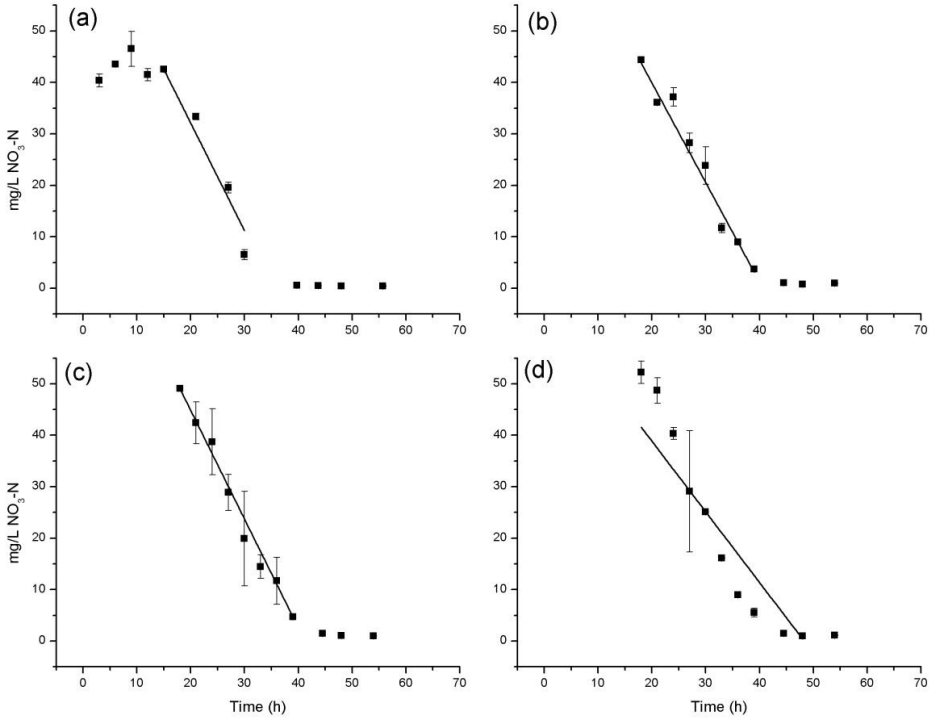

Figure 3.10. Denitrification kinetic data of native soil bacteria in a reducing environment. Each graph displays nitrate depletion over time for one batch per treatment condition. The line represents zero-order kinetic modeling, and corresponds to values listed in Table 3.2. Each graph represents a different reaction condition: a) control; b) Ce(IV) at 50 mg L^{-1}; c) Ce(IV) at 250 mg L^{-1}; d) Ce(IV) at 500 mg L^{-1}. All Ce(IV) was added in the form of large (50-105 nm) cerium oxide nanoparticle.

Control + Ce(III)

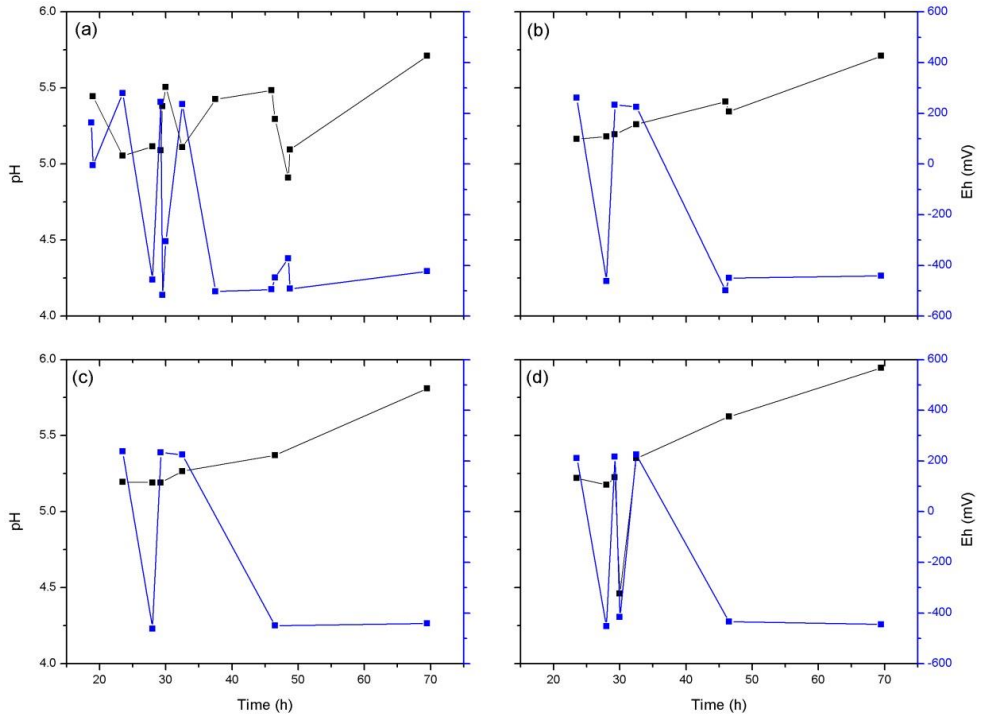

Figure 3.11. Measurements of pH (black lines) and Eh values (mV) (blue lines) during denitrification batch experiments for a) control; b) Ce(III) at 50 mg L^{-1}, c) Ce(III) at 250 mg L^{-1}, and d) Ce(III) at 500 mg L^{-1}.

Control + Small NP

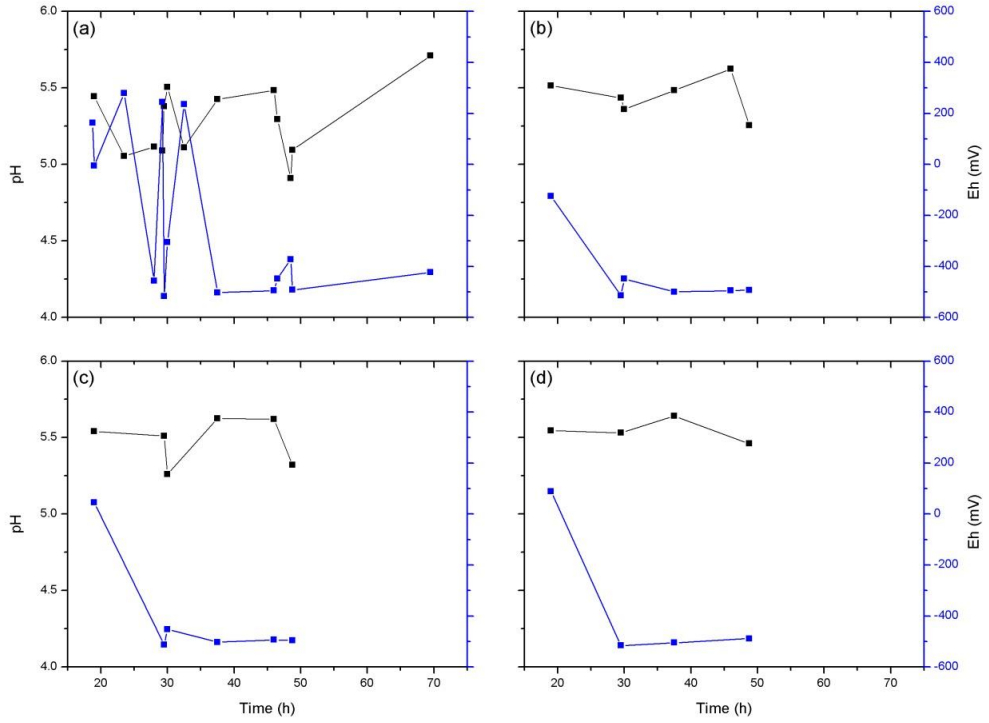

Figure 3.12. Measurements of pH (black lines) and Eh values (mV) (blue lines) during denitrification batch experiments for a) control; b) Ce(IV)s at 50 mg L^{-1}, c) Ce(IV)s at 250 mg L^{-1}, and d) Ce(IV)s at 500 mg L^{-1}.

Control + Large NP

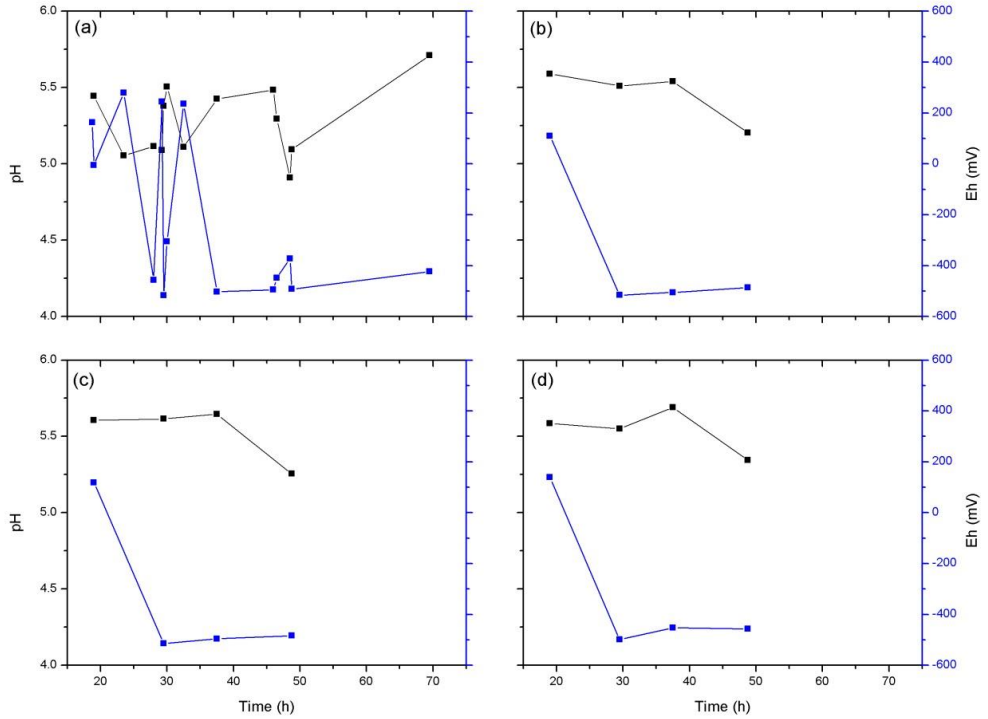

Figure 3.13. Measurements of pH (black lines) and Eh values (mV) (blue lines) during denitrification batch experiments for a) control; b) Ce(IV)l at 50 mg L^{-1}, c) Ce(IV)l at 250 mg L^{-1}, and d) Ce(IV)l at 500 mg L^{-1}.

pH	Clay	% OM	CEC	Acidity	Exchangeable Cations		
					K^+	Ca^{2+}	Mg^{2+}
5.2	K, HIV, H, G	1.53	7.4	5.2	0.22	1.62	0.37

Table 3.1. Texture, physicochemical properties, organic matter, and clay mineralogy of Toccoa sandy loam surface soil. The values for CEC, acidity, and exchangeable cations are in $cmol_c\ kg^{-1}$. K= kaolinite, HIV = hydroxyl interlayer vermiculite, G= goethite, H= hematite (VandeVoort and Arai, 2012).

Condition	Total [Ce] (mg L^{-1})	Rate, *k* (mg L^{-1} NO_3-N depleted h^{-1}) ± 1 standard deviation	R^2	90% Depletion Time, *t* (h) ± 1 standard deviation	50% Depletion Time, *t* (h) ± 1 standard deviation
Control	0	2.33 ± 0.069	1	32.1 ± 0.552	23.5 ± 0.295
Ionic Ce(III)	50	1.91 ± 0.096*	0.915	37.6 ± 1.36*	27.1 ± 0.830*
	250	1.74 ± 0.049*	0.999	42.8 ± 1.75*	31.3 ± 1.42*
	500	1.35 ± 0.107*	0.994	60.0 ± 1.88*	45.1 ± 0.670*
Small $Ce(IV)O_2$ NP	50	1.52 ± 0.215*	0.895	36.6 ± 1.34*	23.3 ± 3.21
	250	1.77 ± 0.158*	0.999	38.1 ± 0.799*	26.8 ± 0.209*
	500	1.93 ± 0.152	0.996	38.8 ± 0.284*	28.4 ± 0.537*
Large $Ce(IV)O_2$ NP	50	2.23 ± 0.155	0.996	37.7 ± 0.195*	28.8 ± 0.804*
	250	2.17 ± 0.030	1	38.3 ± 1.64*	29.1 ± 1.77
	500	1.90 ± 0.049*	0.981	41.6 ± 0.050*	31.1 ± 0.321*

Table 3.2. Denitrification kinetic rates and 90% and 50% depletion times for denitrification batch reaction vessels. Kinetic rate (*k*) was calculated from linear fits of zero-order kinetic models using the data presented in Figures 3.8, 3.9, and 3.10. R^2 values correspond to goodness of fit for these models. Each item under the Condition column describes the type of cerium (e.g. Ce(III) or small/large CeO_2 NP) followed by the cerium concentration in mg L^{-1}. The notation * indicates statistically significant difference from the control vessel at $p = 0.05$.

Comparison	90% Depletion Time T-test Value	50% Depletion Time T-test Value
Concentration dependency		
Ce(III) 50 vs 250?	0.0433*	0.0465*
Ce(III) 50 vs 500?	0.0038*	0.0010*
Ce(III) 250 vs 500?	0.0056*	0.0094*
Ce(IV)s 50 vs 250?	0.165	0.1852
Ce(IV)s 50 vs 500?	0.121	0.1289
Ce(IV)s 250 vs 500?	0.199	0.0529
Ce(IV)l 50 vs 250?	0.342	0.4347
Ce(IV)l 50 vs 500?	0.0076*	0.0580
Ce(IV)l 250 vs 500?	0.106	0.1701
Species dependency		
Ce(III) 50 vs Ce(IV)s 50?	0.272	0.1674
Ce(III) 250 vs Ce(IV)s 250?	0.0605	0.0662
Ce(III) 500 vs Ce(IV)s 500?	0.0180*	0.0010*
Ce(III) 50 vs Ce(IV)l 50?	0.473	0.0847
Ce(III) 250 vs Ce(IV)l 250?	0.0593	0.1517
Ce(III) 500 vs Ce(IV)l 500?	0.0230*	0.0038*
Size dependency		
Ce(IV)s 50 vs Ce(IV)l 50?	0.231	0.1174
Ce(IV)s 250 vs Ce(IV)l 250?	0.452	0.1573
Ce(IV)s 500 vs Ce(IV)l 500?	0.0201*	0.0208*

Table 3.3. T-test results for 90% and 50% depletion times. The notation * indicates statistically significant difference at $p = 0.05$.

Comparison	T-test value
Concentration dependency	
Ce(III) 50 vs 250?	0.105
Ce(III) 50 vs 500?	0.0163*
Ce(III) 250 vs 500?	0.0394*
Ce(IV)s 50 vs 250?	0.163
Ce(IV)s 50 vs 500?	0.0865
Ce(IV)s 250 vs 500?	0.206
Ce(IV)l 50 vs 250?	0.276
Ce(IV)l 50 vs 500?	0.0821
Ce(IV)l 250 vs 500?	0.0181*
Species dependency	
Ce(III) 50 vs Ce(IV)s 50?	0.101
Ce(III) 250 vs Ce(IV)s 250?	0.423
Ce(III) 500 vs Ce(IV)s 500?	0.0289*
Ce(III) 50 vs Ce(IV)l 50?	0.0671
Ce(III) 250 vs Ce(IV)l 250?	0.0087*
Ce(III) 500 vs Ce(IV)l 500?	0.0250*
Size dependency	
Ce(IV)s 50 vs Ce(IV)l 50?	0.0342*
Ce(IV)s 250 vs Ce(IV)l 250?	0.0820
Ce(IV)s 500 vs Ce(IV)l 500?	0.421

Table 3.4. T-test results for denitrification rates. The notation * indicates statistically significant difference at $p = 0.05$.

Impurity	Maximum impurity in 500 mg L^{-1} Ce bottle (mg L^{-1})	Do demonstrated toxicity effects for bacteria or other organisms exist at this impurity concentration?	Reference
La_2O_3	0.053	No	(Balusamy, Kandhasamy, et al., 2012)
Pr_6O_{11}	0.022	No	MSDS
Nd_2O_3	0.014		No literature available
Sm_2O_3	0.006	No	(Aleksakhina, Miriasova, et al., 2002)
Eu_2O_3	0.006	No	MSDS
Gd_2O_3	0.006	No	(Jha, Prasad, et al., 2010)
Tb_4O_7	0.006		No literature available
Dy_2O_3	0.006	No	(Aleksakhina, Miriasova, et al., 2002)
Ho_2O_3	0.006	No	(Brown and Mathiasen, 2011)
Er_2O_3	0.006	No	(Blaise, Gagne, et al., 2008)
Tm_2O_3	0.006		No literature available
Yb_2O_3	0.006	No	(Zhang, Ma, et al., 2012)
Lu_2O_3	0.006	No	(Aleksakhina, Miriasova, et al., 2002)

Table 3.5. Calculated lanthanide impurities in denitrification vessels with small NPs. Impurity concentrations in the small NP can be found in Table 2.2.

Impurity	Maximum impurity in 500 mg L^{-1} Ce bottle (mg L^{-1})	Do demonstrated toxicity effects for bacteria or other organisms exist at this impurity concentration?	Reference
La_2O_3	0.061	No	(Balusamy, Kandhasamy, et al., 2012)
Pr_6O_{11}	0.031	No	MSDS
Nd_2O_3	0.061	No	MSDS
Sm_2O_3	0.031	No	(Aleksakhina, Miriasova, et al., 2002)
Yb_2O_3	6.14×10^{-6}	No	(Zhang, Ma, et al., 2012)

Table 3.6. Calculated lanthanide impurities in denitrification vessels with large NPs. Impurity concentrations in the large NP can be found in Table 2.3.

3.7 References

Abanades, S. and G. Flamant. 2006. Thermochemical hydrogen production from a two-step solar-driven water-splitting cycle based on cerium oxides. Sol. Energy 80: 1611-1623.

Abbasi, Z., M. Haghighi, E. Fatehifar and S. Saedy. 2011. Synthesis and Physicochemical Characterization of Nanostructured Pt/CeO(2) Catalyst Used for Total Oxidation of Toluene. International Journal of Chemical Reactor Engineering 9.

Abbasi, Z., M. Haghighi, E. Fatehifar and S. Saedy. 2011. Synthesis and physicochemical characterizations of nanostructured Pt/Al(2)O(3)-CeO(2) catalysts for total oxidation of VOCs. Journal of Hazardous Materials 186: 1445-1454.

Abreu, R.D. and C.A. Morais. 2010. Purification of rare earth elements from monazite sulphuric acid leach liquor and the production of high-purity ceric oxide. Minerals Engineering 23: 536-540.

Agrawal, A., K.C. Sekhar and L.P. Pandey. 1994. Spectrophotometric Determination of Ce(IV) Using O-Phenylenediamine in Steels. Bulletin of Materials Science 17: 1467-1471.

Aime, S., M. Botta, M. Fasano and E. Terreno. 1998. Lanthanide(III) chelates for NMR biomedical applications. Chem. Soc. Rev. 27: 19-29.

Aleksakhina, N.N., L.V. Miriasova and I.A. Basnak'ian. 2002. Effect of metal oxides on the growth, hemolytic and serologic properties of Klebsiella pneumoniae. Zh Mikrobiol Epidemiol Immunobiol. 6: 8-13.

Anthony, J.W., Bideaux, R.A., Bladh, K.W., and Nichols, M.C. 1995. Handbook of Mineralogy (Volume II- Elements, Silica, Silicates). Mineral Data Publishing, Tuscon, Arizona.

Anthony, J.W., Bideaux, R.A., Bladh, K.W., and Nichols, M.C. 1997. Handbook of Mineralogy (Volume III- Halides, Hydroxides, Oxides). Mineral Data Publishing, Tuscon, Arizon.

Anthony, J.W., Bideaux, R.A., Bladh, K.W., and Nichols, M.C. 2000. Handbook of Mineralogy (Volume IV- Arsenates, Phosphates, Vanadates). Mineral Data Publishing, Tuscon, Arizona.

Anthony, J.W., Bideaux, R.A., Bladh, K.W., and Nichols, M.C. 2003. Handbook of Mineralogy (Volume V- Borates, Carbonates, Sulfates). Mineral Data Publishing, Tuscon, Arizona.

Aston, F.W. 1925. CXIX. The mass-spectra of chemical elements.—Part VI. Accelerated anode rays continued. Philosophical Magazine Series 6 49: 1191-1201.

Atkinson, P., B.S. Murray and D. Parker. 2006. A cationic lanthanide complex binds selectively to phosphorylated tyrosine sites, aiding NMR analysis of the phosphorylated insulin receptor peptide fragment. Organic & Biomolecular Chemistry 4: 3166-3171.

Babu, S., A. Velez, K. Wozniak, J. Szydlowska and S. Seal. 2007. Electron paramagnetic study on radical scavenging properties of ceria nanoparticles. Chem. Phys. Lett. 442: 405-408.

Bachand, P.A.M. and A.J. Horne. 2000. Denitrification in constructed free-water surface wetlands: II. Effects of vegetation and temperature. Ecological Engineering 14: 17-32.

Balusamy, B., Y.G. Kandhasamy, A. Senthamizhan, G. Chandrasekaran, M.S. Subramanian and S.K. Tirukalikundram. 2012. Characterization and bacterial toxicity of lanthanum oxide bulk and nanoparticles. Journal of Rare Earths 30: 1298-1302.

Berg, J.M., A. Romoser, N. Banerjee, R. Zebda and C.M. Sayes. 2009. The relationship between pH and zeta potential of similar to 30 nm metal oxide nanoparticle suspensions relevant to in vitro toxicological evaluations. Nanotoxicology 3: 276-283.

Biber, M.V., M.D. Afonso and W. Stumm. 1994. The Coordination Chemistry of Weathering .4. Inhibition of the Dissolution of Oxide Minerals. Geochimica Et Cosmochimica Acta 58: 1999-2010.

Birbaum, K., R. Brogioli, M. Schellenberg, E. Martinoia, W.J. Stark, D. Gunther, et al. 2010. No Evidence for Cerium Dioxide Nanoparticle Translocation in Maize Plants. Environmental Science & Technology 44: 8718-8723.

Bjerrum, S., and Sillen. 1958. Stability Constants of Metal Complexes, part II, London.

Blaise, C., F. Gagne, J.F. Ferard and P. Eullaffroy. 2008. Ecotoxicity of selected nano-materials to aquatic organisms. Environmental Toxicology 23: 591-598.

Boaventura, R.A.R. and A.E. Rodrigues. 1997. Denitrification kinetics in a rotating disk biofilm reactor. Chemical Engineering Journal 65: 227-235.

Brown, S. and S. Mathiasen. 2011. Particle-Dissociating Peptides. Advanced Materials 23.

Carlson, C., S.M. Hussain, A.M. Schrand, L.K. Braydich-Stolle, K.L. Hess, R.L. Jones, et al. 2008. Unique Cellular Interaction of Silver Nanoparticles: Size-Dependent Generation of Reactive Oxygen Species. Journal of Physical Chemistry B 112: 13608-13619.

Chen, J., S. Patil, S. Seal and J.F. McGinnis. 2008. Nanoceria particles prevent ROI-induced blindness. In: R. E. Anderson, M. M. LaVail and J. G. Hollyfield, editors, Advances in Experimental Medicine and Biology. p. 53-59.

Choi, O. and Z. Hu. 2008. Size dependent and reactive oxygen species related nanosilver toxicity to nitrifying bacteria. Environmental Science & Technology 42: 4583-4588.

Chueh, W.C., C. Falter, M. Abbott, D. Scipio, P. Furler, S.M. Haile, et al. 2010. High-Flux Solar-Driven Thermochemical Dissociation of CO2 and H2O Using Nonstoichiometric Ceria. Science 330: 1797-1801.

Clever, H.L., M.E. Derrick and S.A. Johnson. 1992. The Solubility of Some Sparingly Soluble Salts of Zinc and Cadmium in Water and in Aqueous-Electrolyte Solutions. Journal of Physical and Chemical Reference Data 21: 941-1004.

Clever, H.L., S.A. Johnson and M.E. Derrick. 1985. Ibid. 14.

Clever, H.L., S.A. Johnson and M.E. Derrick. 1985. The Solubility of Mercury and Some Sparingly Soluble Mercury Salts in Water and Aqueous-Electrolyte Solutions. Journal of Physical and Chemical Reference Data 14: 631-681.

Clever, H.L., S.A. Johnson and M.E. Derrick. 1992. Ibid. 21.

Clever, H.L. and F.J. Johnston. 1980. J. Phys. Chem. Ref. Data 9.

Clever, H.L. and F.J. Johnston. 1980. The Solubility of Some Sparingly Soluble Lead Salts- An Evaluation of the Solubility in Water and Aqueous-Electrolyte Solution. Journal of Physical and Chemical Reference Data 9: 751-784.

Cornelis, G., B. Ryan, M.J. McLaughlin, J.K. Kirby, D. Beak and D. Chittleborough. 2011. Solubility and Batch Retention of CeO2 Nanoparticles in Soils. Environmental Science & Technology 45: 2777-2782.

D'Angelo, B., S. Santucci, E. Benedetti, S. Di Loreto, R.A. Phani, S. Falone, et al. 2009. Cerium Oxide Nanoparticles Trigger Neuronal Survival in a Human Alzheimer Disease Model By Modulating BDNF Pathway. Curr. Nanosci. 5: 167-176.

Dawson, R.N. and K.L. Murphy. 1972. The temperature dependency of biological denitrification. Water Res. 6: 71-83.

De, S.K. 1961. Adsorption of phosphate ion by hydrous ferric, chromic, and aluminium oxides. Part I. With inorganic materials added. Kolloid-Zeitschrift 179: 134-140.

Dimitrov, V., K. Kostova and M. Genov. 1996. Anhydrous cerium(III) chloride - Effect of the drying process on activity and efficiency. Tetrahedron Letters 37: 6787-6790.

Edelmann, F.T.P., P., Hermann, W.A. 1997. Synthetic Methods of Organometallic and Inorganic Chemistry. Georg Thieme Verlag, Stuttgart.

EPA, U.S. 2007. Protection of Environment: Standards for the Use or Disposal of Sewage Sludge- Land Application: Pollutant Limits. 40. p. 9-11.

EPA, U.S. 2009. Toxicological Review of Cerium Oxide and Cerium Compounds. Washington, DC.

Estevez, A.Y., S. Pritchard, K. Harper, J.W. Aston, A. Lynch, J.J. Lucky, et al. 2011. Neuroprotective mechanisms of cerium oxide nanoparticles in a mouse hippocampal brain slice model of ischemia. Free Radic. Biol. Med. 51: 1155-1163.

Evans, W.J. 2000. Perspectives in reductive lanthanide chemistry. Coordination Chemistry Reviews 206: 263-283.

Garcia, A., L. Delgado, J.A. Tora, E. Casals, E. Gonzalez, V. Puntes, et al. 2012. Effect of cerium dioxide, titanium dioxide, silver, and gold nanoparticles on the activity of microbial communities intended in wastewater treatment. Journal of Hazardous Materials 199: 64-72.

Ginepro, J.Q., J. Snyder and M. Thoennessen. 2009. Discovery of the cerium isotopes. Atomic Data and Nuclear Data Tables 95: 805-814.

Gordy, W. and W.J. Thomas. 1956. Electronegativities of the Elements. J. Chem. Phys. 24: 439.

Gottschalk, F., T. Sonderer, R.W. Scholz and B. Nowack. 2009. Modeled Environmental Concentrations of Engineered Nanomaterials (TiO2, ZnO, Ag, CNT, Fullerenes) for Different Regions. Environmental Science & Technology 43: 9216-9222.

Gruner, S., I. Sehrt, G.M. Muller, A. Zwirner, D. Strunk and N. Sonnichsen. 1992. Inhibition of Histamine-Release from Human Granulocytes by Ions of the Rare-Earth Elements Lanthanum and Cerium. Agents and Actions 36: 207-211.

Gustaffson, J.P. 2007. VisualMinteq. Division of Land and Water Resources, Royal Institute of Technology. Stockholm, SWE.

He, X., Y. Kuang, Y. Li, H. Zhang, Y. Ma, W. Bai, et al. 2012. Changing exposure media can reverse the cytotoxicity of ceria nanoparticles for Escherichia coli. Nanotoxicology 6: 233-240.

He, Z.L., V.C. Baligar, D.C. Martens and K.D. Ritchey. 1998. Determination of soluble phosphorus in the presence of organic ligands or fluoride. Soil Sci. Soc. Am. J. 62: 1538-1541.

Heckert, E.G., A.S. Karakoti, S. Seal and W.T. Self. 2008. The role of cerium redox state in the SOD mimetic activity of nanoceria. Biomaterials 29: 2705-2709.

Hedrick, J.B. 2004. Rare Earths. Minerals Yearbook. Vol I. Metals and Minerals. US Geological Survey, US Department of the Interior, Reston, VA.

Hedrick, J.B. and S.P. Sinha. 1994. Cerium-Based Polishing Compounds- Discovery to Manufacture. Journal of Alloys and Compounds 207: 377-382.

Hendren, C.O., X. Mesnard, J. Droge and M.R. Wiesner. 2011. Estimating Production Data for Five Engineered Nanomaterials As a Basis for Exposure Assessment. Environmental Science & Technology 45: 2562-2569.

Higgins, W.M., A. Churilov, E. van Loef, J. Glodo, M. Squillante and K. Shah. 2008. Crystal growth of large diameter LaBr3 : Ce and CeBr3. J. Cryst. Growth 310: 2085-2089.

Hoecke, K.V., J.T. Quik, J. Mankiewicz-Boczek, K. Schamphelaere, A. Elsaesser, P. Van der Meeren, et al. 2009. Fate and Effects of CeO2 Nanoparticles in Aquatic Ecotoxicity Tests. Environmental Science & Technology 43: 4537-4546.

Hoshino, A., K. Fujioka, T. Oku, M. Suga, Y.F. Sasaki, T. Ohta, et al. 2004. Physicochemical Properties and Cellular Toxicity of Nanocrystal Quantum Dots Depend on Their Surface Modification. Nano Letters 4: 2163-2169.

Hsu, P.H. and D.A. Rennie. 1962. Reactions of phosphate in aluminium systems. Part I. Adsorption of phosphate by X-ray amorphous aluminium hydroxide. Canadian Journal of Soil Science 42: 197-209.

Institute, Health Effects 2001. Evaluation of Human Health Risk from Cerium Added to Diesel Fuel. Health Effects Institute Communication 9.

IUPAC. 1979-1992. IUPAC Solubility Data Project: Solubility Data Series. Pergamon Press, Oxford.

Ivanov, V.K., A.B. Shcherbakov, I.G. Ryabokon, A.V. Usatenko, N.M. Zholobak and Y.D. Tretyakov. 2010. Inactivation of the nitroxyl radical by ceria nanoparticles. Dokl. Chem. 430: 43-46.

Ivanov, V.K., A.V. Usatenko and A.B. Shcherbakov. 2009. Antioxidant activity of nanocrystalline ceria to anthocyanins. Russ. J. Inorg. Chem. 54: 1522-1527.

Jakupec, M.A., P. Unfried and B.K. Keppler. 2005. Pharmacological properties of cerium compounds. In: S. G. Amara, E. Bamberg, R. Jahn, W. J. Lederer, A. Miyajima, H. Murer, S. Offermanns, G. Schultz and M. Schweiger, editors, Reviews of Physiology Biochemistry and Pharmacology. p. 101-111.

Jha, A.K., K. Prasad and A.R. Kulkarni. 2010. Synthesis of Gd2O3 Nanoparticles Using Lactobacillussp: A Novel Green Approach. International Journal of Green Nanotechnology: Physics and Chemistry 2.

Jiang, W., H. Mashayekhi and B. Xing. 2009. Bacterial toxicity comparison between nano- and micro-scaled oxide particles. Environmental Pollution 157: 1619-1625.

Johnson, C.R. and B.D. Tait. 1987. A Cerium(III) Modification of the Peterson Reaction - Methylenation of Readily Enolizable Carbonyl Compounds. Journal of Organic Chemistry 52: 281-283.

Johnston, B.D., T.M. Scown, J. Moger, S.A. Cumberland, M. Baalousha, K. Linge, et al. 2010. Bioavailability of Nanoscale Metal Oxides TiO(2), CeO(2), and ZnO to Fish. Environmental Science & Technology 44: 1144-1151.

Karakoti, A., S. Singh, J.M. Dowding, S. Seal and W.T. Self. 2010. Redox-active radical scavenging nanomaterials. Chem. Soc. Rev. 39: 4422-4432.

Karakoti, A.S., N.A. Monteiro-Riviere, R. Aggarwal, J.P. Davis, R.J. Narayan, W.T. Self, et al. 2008. Nanoceria as antioxidant: Synthesis and biomedical applications. Jom 60: 33-37.

Karlsson, H.L., J. Gustafsson, P. Cronholm and L. Moller. 2009. Size-dependent toxicity of metal oxide particles-A comparison between nano- and micrometer size. Toxicology Letters 188: 112-118.

Kilbourn, B. 2003. Cerium and cerium compounds. Kirk-Othmer encyclopedia of chemical technology. John Wiley and Sons, Inc., New York, NY.

Kim, I.-S., M. Baek and S.-J. Choi. 2010. Comparative Cytotoxicity of Al2O3, CeO2, TiO2 and ZnO Nanoparticles to Human Lung Cells. J. Nanosci. Nanotechnol. 10: 3453-3458.

Kosmulski, M. 2001. Chemical Properties of Material Surfaces. CRC Press, New York.

Kuang, Y.S., X. He, Z.Y. Zhang, Y.Y. Li, H.F. Zhang, Y.H. Ma, et al. 2011. Comparison Study on the Antibacterial Activity of Nano- or Bulk-Cerium Oxide. J. Nanosci. Nanotechnol. 11: 4103-4108.

Lanone, S., F. Rogerieux, J. Geys, A. Dupont, E. Maillot-Marechal, J. Boczkowski, et al. 2009. Comparative toxicity of 24 manufactured nanoparticles in human alveolar epithelial and macrophage cell lines. Part. Fibre Toxicol. 6.

Lead, J.R. and E. Smith. 2009. Environmental and Human Health Impacts of Nanotechnology. John Wiley and Sons, Ltd.

Lide, D.R. 2005. Handbook of chemistry and physics. CRC Press.

Limbach, L.K., R. Bereiter, E. Mueller, R. Krebs, R. Gaelli and W.J. Stark. 2008. Removal of oxide nanoparticles in a model wastewater treatment plant: Influence of agglomeration and surfactants on clearing efficiency. Environmental Science & Technology 42: 5828-5833.

Liu, J., D.A. Sonshine, S. Shervani and R.H. Hurt. 2010. Controlled Release of Biologically Active Silver from Nanosilver Surfaces. ACS Nano 4: 6903-6913.

Lopez-Moreno, M.L., G. de la Rosa, J.A. Hernandez-Viezcas, J.R. Peralta-Videa and J.L. Gardea-Torresdey. 2010. X-ray Absorption Spectroscopy (XAS) Corroboration of the Uptake and Storage of CeO(2) Nanoparticles and Assessment of Their Differential Toxicity in Four Edible Plant Species. Journal of Agricultural and Food Chemistry 58: 3689-3693.

Lu, K., Z.Y. Zhang, X.A. He, Y.H. Ma, K.B. Zhou, H.F. Zhang, et al. 2010. Bioavailability and Distribution and of Ceria Nanoparticles in Simulated Aquatic Ecosystems, Quantification with a Radiotracer Technique. J. Nanosci. Nanotechnol. 10: 8658-8662.

Lubick, N. 2008. Nanosilver toxicity: ions, nanoparticles-or both? Environmental Science & Technology 42: 8617-8617.

Ma, Y.H., L.L. Kuang, X. He, W. Bai, Y.Y. Ding, Z.Y. Zhang, et al. 2010. Effects of rare earth oxide nanoparticles on root elongation of plants. Chemosphere 78: 273-279.

Mahendra, S., H. Zhu, V.L. Colvin and P.J. Alvarez. 2008. Quantum Dot Weathering Results in Microbial Toxicity. Environmental Science & Technology 42: 9424-9430.

Majdan, M. and K. Zdenek. 1993. Synergistic Extraction of Lanthanides(III) by Trioctylmethylammonium Nitrate and Tributyl Phosphate. Solvent Extraction and Ion Exchange 11: 331-348.

Marcus, Y. 1980. Ibid. 9.

Marcus, Y. 1980. A Compilation and Evaluation of Solubility Data in the Mercury (U) Chloride-Water System. Journal of Physical and Chemical Reference Data 9: 1307-1329.

Martin, T.L., N.K. Kaushik, J.T. Trevors and H.R. Whiteley. 1999. Review: Denitrification in temperate climate riparian zones. Water Air and Soil Pollution 111: 171-186.

Moller, P., G. Morteani and P. Dulski. 2003. Anomalous gadolinium, cerium, and yttrium contents in the adige and isarco river waters and in the water of their tributaries (Provinces Trento and Bolzano/Bozen, NE Italy). Acta Hydrochimica Et Hydrobiologica 31: 225-239.

Monafo, W.W., S.N. Tandon, V.H. Ayvazian, J. Tuchschmidt, A.M. Skinner and F. Deitz. 1976. Cerium nitrate: a new topical antiseptic for extensive burns. Surgery 80: 465-473.

Moore, K.T., L. Belhadi, F. Decremps, D.L. Farber, J.A. Bradley, F. Occelli, et al. 2011. Watching a metal collapse: Examining cerium's gamma <-> alpha transformation using X-ray diffraction of compressed single and polycrystals. Acta Mater. 59: 6007-6016.

Muljadi, D., A.M. Posner and J.P. Quirk. 1966. The Mechanism of Phosphate Adsorption by Kaolinite, Gibbsite, and Pseudoboehmite. Journal of Soil Science 17.

Mulvaney, R.L., S.A. Khan and C.S. Mulvaney. 1997. Nitrogen fertilizers promote denitrification. Biology and Fertility of Soils 24: 211-220.

Murphy, J. and J.P. Riley. 1986. A Modified Single Solution Method for the Determination of Phosphate in Natural-Waters. Current Contents/Agriculture Biology & Environmental Sciences: 16-16.

Nalabotu, S.K., M.B. Kolli, W.E. Triest, J.Y. Ma, N. Manne, A. Katta, et al. 2011. Intratracheal instillation of cerium oxide nanoparticles induces hepatic toxicity in male Sprague-Dawley rats. Int. J. Nanomed. 6: 2327-2335.

Napierska, D., L.C.J. Thomassen, V. Rabolli, D. Lison, L. Gonzalez, M. Kirsch-Volders, et al. 2009. Size-Dependent Cytotoxicity of Monodisperse Silica Nanoparticles in Human Endothelial Cells. Small 5: 846-853.

Nesse, W.D. 2000. Introduction to Mineralogy. Oxford University Press, Oxford, NY.

O'Neil, M. 2001. The Merck Index: an encyclopedia of chemicals, drugs, and biologicals. 13 ed. Merck and Co, Inc., Whitehouse Station, NJ.

Ogata, F., H. Tominaga, H. Yabutani and N. Kawasaki. 2011. Phosphate Adsorption Ability of Granular Gibbsite and Cerium Hydroxide. Journal of Oleo Science 60: 133-138.

Orge, C.A., J.J. Orfao, M.F. Pereira, A.M. de Farias, R.C. Neto and M.A. Fraga. 2011. Ozonation of model organic compounds catalysed by nanostructured cerium oxides. Appl. Catal. B-Environ. 103: 190-199.

Oxford, J.E. 2011. Nature's Building Blocks: An A-Z Guide to the Elements. 2 ed. Oxford University Press, Oxford, UK.

Palasz, A. and P. Czekaj. 2000. Toxicological and cytophysiological aspects of lanthanides action. Acta Biochimica Polonica 47: 1107-1114.

Palmberg, C. and N. Tuomo. 2006. Industrial renewal and growth through nanotechnology? An overview with focus on Finland. ETLA Discussion Papers, The Research Institute of the Finnish Economy.

Pan, Y., S. Neuss, A. Leifert, M. Fischler, F. Wen, U. Simon, et al. 2007. Size-dependent cytotoxicity of gold nanoparticles. Small 3: 1941-1949.

Paquette, L.C., RM; Denmark, SE. 1999. Handbook of Reagents for Organic Syntsyhesis: Reagents, Auxiliaries and Catalysts for C-C Bond FormationWiley, New York, NY.

Park, E., J. Choi, Y. Park and K. Park. 2008. Oxidative stress induced by cerium oxide nanoparticles in cultured BEAS-2B cells. Toxicology 245: 90-100.

Patnaik, P. 2003. Handbook of inorganic chemicals. McGraw-Hill.

Pearson, R.G. 1963. J. Am. Chem. Soc.: 3533-3543.

Pelletier, D.A., A.K. Suresh, G.A. Holton, C.K. McKeown, W. Wang, B.H. Gu, et al. 2010. Effects of Engineered Cerium Oxide Nanoparticles on Bacterial Growth and Viability. Appl. Environ. Microbiol. 76: 7981-7989.

Pirmohamed, T., J.M. Dowding, S. Singh, B. Wasserman, E. Heckert, A.S. Karakoti, et al. 2010. Nanoceria exhibit redox state-dependent catalase mimetic activity. Chem. Commun. 46: 2736-2738.

Rakicioglu, Y. and A. Akseli. 1998. New fluorimetric reagents, sodium pyrophosphate, sodium trimetaphosphate, and sodium tetrametaphosphate, for the determination of cerium(III). Journal of Fluorescence 8: 45-52.

Recillas, S., A. Garcia, E. Gonzalez, E. Casals, V. Puntes, A. Sanchez, et al. 2012. Preliminary study of phosphate adsorption onto cerium oxide nanoparticles for use in water purification; nanoparticles synthesis and characterization. Water Science and Technology 66: 503-509.

Reinhardt, K. and H. Winkler. 2002. Cerium mischmetal, cerium alloys, and cerium compounds. Ullmann's encyclopedia of industrial chemistry. Wiley-VCH, Weinheim, Germany. p. 285-300.

Rodea-Palomares, I., K. Boltes, F. Fernandez-Pinas, F. Leganes, E. Garcia-Calvo, J. Santiago, et al. 2011. Physicochemical Characterization and Ecotoxicological Assessment of CeO(2) Nanoparticles Using Two Aquatic Microorganisms. Toxicol. Sci. 119: 135-145.

Rogers, N.J., N.M. Franklin, S.C. Apte, G.E. Batley, B.M. Angel, J.R. Lead, et al. 2010. Physico-chemical behaviour and algal toxicity of nanoparticulate CeO(2) in freshwater. Environmental Chemistry 7: 50-60.

Roh, J., Y. Park, K. Park and J. Choi. 2010. Ecotoxicological investigation of CeO(2) and TiO(2) nanoparticles on the soil nematode Caenorhabditis elegans using gene expression, growth, fertility, and survival as endpoints. Environmental Toxicology and Pharmacology 29: 167-172.

Rubasinghege, G.K., PK; Scherer, MM; Grassian, VH. 2012. Proton-promoted dissolution of α-FeOOH nanorods and microrods: size dependence, anion effects (carbonate and phosphate), aggregation and surface adsorption. J Colloid Interface Sci. 385: 15-23.

Rzigalinski, B.A., D. Bailey, L. Chow, S.C. Kuiry, S. Patil, S. Merchant, et al. 2003. Cerium oxide nanoparticles increase the lifespan of cultured brain cells and protect against free radical and mechanical trauma. Faseb Journal 17: A606-A606.

Schubert, D., R. Dargusch, J. Raitano and S.W. Chan. 2006. Cerium and yttrium oxide nanoparticles are neuroprotective. Biochem. Biophys. Res. Commun. 342: 86-91.

Schwertmann, U. 1991. Solubility and Dissolution of Iron-Oxides. Plant and Soil 130: 1-25.

Sherry, A.D. 1997. MR imaging and spectroscopy applications of lanthanide complexes with macrocyclic phosphonate and phosphonate ester ligands. Journal of Alloys and Compounds 249: 153-157.

Snoeyink, V.L. and D. Jenkins. 1980. Precipitation and Dissolution. Water Chemistry. John Wiley & Sons, Inc., New York. p. 243-315.

Sparks, D.L. 2003. Environmental Soil Chemistry. 2 ed. Academic Press, San Diego, CA 92101.

Sposito, G. 1984. Surface Chemistry of SoilsOxford University Press, New York.

Stassis, C., T. Gould, O.D. McMasters, K.A. Gschneidner and R.M. Nicklow. 1979. Lattice and Spin Dynamics of Gamma-Ce. Physical Review B 19: 5746-5753.

Stumm, W. 1997. Reactivity at the mineral-water interface: Dissolution and inhibition. Colloids and Surfaces a-Physicochemical and Engineering Aspects 120: 143-166.

Thill, A., O. Zeyons, O. Spalla, F. Chauvat, J. Rose, M. Auffan, et al. 2006. Cytotoxicity of CeO2 nanoparticles for Escherichia coli. Physico-chemical insight of the cytotoxicity mechanism. Environmental Science & Technology 40: 6151-6156.

Torrent, J., V. Barron and U. Schwertmann. 1990. Phosphate Adsorption and Desorption by Goethites Differing in Crystal Morphology. Soil Sci. Soc. Am. J. 54: 1007-1012.

van Haandel, A.C., G.A. Ekama and G.v.R. Marais. 1981. The activated sludge process—3 single sludge denitrification. Water Res. 15: 1135-1152.

Van Hoecke, K., K.A.C. De Schamphelaere, P. Van der Meeren, G. Smagghe and C.R. Janssen. 2011. Aggregation and ecotoxicity of CeO2 nanoparticles in synthetic and natural waters with variable pH, organic matter concentration and ionic strength. Environmental Pollution 159: 970-976.

van Loef, E.V.D., P. Dorenbos, C.W.E. van Eijk, K. Kramer and H.U. Gudel. 2001. High-energy-resolution scintillator: Ce(3+) activated LaBr(3). Appl. Phys. Lett. 79: 1573-1575.

VandeVoort, A.R. and Y. Arai. 2012. Effect of Silver Nanoparticles on Soil Denitrification Kinetics. Industrial Biotechnology 8: 358-364.

Weeks, M.E. 1932. The discovery of the elements. XVI. The rare earth elements. Journal of Chemical Education 9: 1751.

Xia, T., M. Kovochich, M. Liong, L. Madler, B. Gilbert, H.B. Shi, et al. 2008. Comparison of the Mechanism of Toxicity of Zinc Oxide and Cerium Oxide Nanoparticles Based on Dissolution and Oxidative Stress Properties. ACS Nano 2: 2121-2134.

Yuan, Z.Y., V. Idakiev, A. Vantomme, T. Tabakova, T.Z. Ren and B.L. Su. 2008. Mesoporous and nanostructured CeO2 as supports of nano-sized gold catalysts for low-temperature water-gas shift reaction. Catalysis Today 131: 203-210.

Zhang, H., X. He, Z. Zhang, P. Zhang, Y. Li, Y. Ma, et al. 2011. Nano-CeO(2) Exhibits Adverse Effects at Environmental Relevant Concentrations. Environmental Science & Technology 45: 3725-3730.

Zhang, P., Y. Ma, Z. Zhang, X. He, Z. Guo, R. Tai, et al. 2012. Comparative toxicity of nanoparticulate/bulk Yb2O3 and YbCl3 to cucumber (Cucumis sativus). Environmental Science & Technology 46: 1834-1841.

Zhang, Z.Y., X. He, H.F. Zhang, Y.H. Ma, P. Zhang, Y.Y. Ding, et al. 2011. Uptake and distribution of ceria nanoparticles in cucumber plants. Metallomics 3: 816-822.

RESEARCH SUMMARY AND CONCLUSIONS

In the United States and other countries, widespread uses and applications exist for compounds of the lanthanide cerium. A cerium compound of particular interest is nanoparticulate ceria, also known as cerium oxide (CeO_2). A review of the literature in Chapter 1 revealed that, by far, cerium oxide nanoparticles (CeO_2 NPs) are the most widely commercially used cerium compound. Due to the rise of nanotechnology in industry, the concentrations of engineered metal oxide nanoparticles being released to the environment are increasing daily, posing questions about the fate of these NPs in the environment.

In Chapter 1, it was found that the application of wastewater treatment plant biosolids to agricultural lands serves as a significant source of CeO_2 NP exposure to the terrestrial environment. In the last decade, the scientific community has begun to uncover the effects of CeO_2 NPs on ecosystem health through toxicological studies of plants, bacteria, aquatic organisms, and mammals. However, the research findings are often difficult to extrapolate to natural aquatic and terrestrial systems since the majority of studies do not consider the effect of natural geochemical conditions on the reactivity of CeO_2 NPs (e.g., solubility and chemical speciation). This gap in the literature presented an opportunity for the studies detailed in this thesis. In low-temperature geochemical environments, CeO_2 NPs are likely to react with ligands (e.g., protons, inorganic and organic acids) and/or

partition into geomedia, resulting in changes in chemical speciation. It can be expected that these geochemical reactions may alter the toxicity of CeO_2 NPs as particulates or as dissolution products.

While many studies were available detailing the effects of CeO_2 NPs in *E. coli* and similar bacteria, the literature did not include any studies of the effects of CeO_2 NP exposure in denitrifying bacteria such as *Pseudomonas*, *Bacillus*, or *Alcaligenes*. The studies presented capitalize upon the importance of denitrification in soil systems as well as the widespread lack of consideration of geochemical effects in existing literature. Based on the review of the literature in Chapter 1, two main research tasks were formulated: 1) assessing the toxicity effects of CeO_2 NP exposure to soil denitrifying bacteria, and 2) investigating the effect of physicochemical properties and geochemical conditions (e.g., particle size, concentration, pH, ligand concentration) of CeO_2 NPs on the soil denitrifying process. These tasks were accomplished via geochemistry experiments including dissolution and sorption in Chapter 2 and denitrification experiments in Chapter 3.

In Chapter 2, the dissolution of small (10 – 30 nm) and large (50 – 105 nm) uncapped manufactured CeO_2 NPs was studied as a function of pH in the absence and presence of phosphate in order to understand the physicochemical interactions of CeO_2 nanoparticles post-environmental release. It was found that Ce dissolution was negligible at pH > 7 and was only significant at pH < 5; dissolution became far more pronounced as pH decreased.

When 100 µM phosphate was present, dissolution from CeO_2 NPs was significantly reduced. Via the studies in Chapter 2, phosphate-suppressed CeO_2 dissolution was linked to the chemisorption of PO_4^{3-}. It was postulated that the Ce(III) impurity metal-centered complexation with PO_4^{3-} ligands could facilitate the formation of Ce(III)PO_4 surface precipitates at the CeO_2-water interface. The pH dependent phosphate sorption was more pronounced in small NPs than in larger NPs. Adsorption isotherms showed that both NPs exhibited an L-type shaped isotherm curve, revealing a high affinity for phosphate. In conclusion, it was found in Chapter 2 that both pH and bioavailable phosphate ligands likely play an important role in controlling the release of Ce from CeO_2 NPs; thus, the dissolution properties of CeO_2 NPs affected by pH and phosphate should be considered in assessing the fate of CeO_2 NPs in the aquatic and terrestrial environment. Phosphate is one of most common oxyanions present in surface and subsurface waters; the interaction between PO_4^{3-} and Ce(III) impurities in manufactured CeO_2 NPs may be critical since it greatly affects both surface charge properties and structure.

The studies presented in Chapter 3 reveal the toxicity effects of multiple Ce species to the soil denitrifying bacteria community. To understand the impact of CeO_2 NPs on the microbially mediated nutrient cycles, a subchronic toxicity study of NPs on soil denitrification process was conducted as a function of particle size (10 and 50 nm), total Ce concentration (50 – 500 mg L^{-1}), and speciation (Ce(IV) vs. Ce(III)). Statistical analyses on the antimicrobial effect on soil denitrifiers were conducted using both steady-state evaluation and zero-order kinetic models in order to compare the toxicity effects. It

was found that soluble Ce(III) was far more toxic than Ce(IV)O_2 NPs when an equal total concentration of Ce was evaluated. Particle-size dependent toxicity, species-dependent toxicity, and concentration-dependent toxicity were all observed in this study for both the steady-state and the kinetic evaluations. It was found that both Ce(III) and CeO_2 NP species exhibited particularly strong sorption properties with soil; XANES analysis also revealed some chemical speciation changes in small NPs in soil. The analysis indicated predominance of Ce species that were similar to Ce(IV) references for the large NP, but indicated reductive transformation and thus species that were similar to both the Ce(IV) and Ce(III) references for the small NPs. It is clear that even among two differently sized nanoparticles of the same species, different physical and chemical factors may contribute to toxicity effects. This is supported by much of the data in Chapter 2. The strong sorption affinity for Ce(III) and CeO_2 NPs to soils was also demonstrated in Chapter 3, confirming the clear likelihood of physicochemical transformation of the Ce species via sorption mechanisms. Cerium species are already fairly insoluble and are even more insoluble when PO_4^{3-} ligand is present, as demonstrated in Chapter 2. This conclusion, coupled with the results from Chapter 3, support the possibility that Ce species have a large potential to build up in sediments over time; thus, toxicological studies such as these detailing the environmental fate and reactivity of CeO_2 NPs to soil bacterial communities are largely necessary.

In conclusion, the data from the studies presented in this thesis expand the scientific community's current knowledge of CeO_2 NP toxicity to heterogeneous systems by

determining the impact of geochemical factors on CeO_2 NP toxicity to the soil denitrification process. These studies revealed that not only do CeO_2 NPs exert toxicity effects to soil denitrifying bacteria, but also that this process is subject to be affected both by physicochemical characteristics of the NPs and the geochemical conditions in the environment, including pH and phosphate ligand availability. Thus, the results of these studies should be considered in future evaluations of possible implications following environmental exposures to CeO_2 NPs.